RELATIONSHIP BETWEEN SURFACE FREE ENERGY AND

TOTAL WORK OF FRACTURE OF ASPHALT BINDER AND

ASPHALT BINDER-AGGREGATE INTERFACES

A Dissertation

by

JONATHAN EMBREY HOWSON

Submitted to the Office of Graduate Studies of
Texas A&M University
in partial fulfillment of the requirements for the degree of

DOCTOR OF PHILOSOPHY

August 2011

Major Subject: Civil Engineering

Relationship Between Surface Free Energy and Total Work of Fracture of Asphalt

Binder and Asphalt Binder-Aggregate Interfaces

RELATIONSHIP BETWEEN SURFACE FREE ENERGY AND

TOTAL WORK OF FRACTURE OF ASPHALT BINDER AND

ASPHALT BINDER-AGGREGATE INTERFACES

A Dissertation

by

JONATHAN EMBREY HOWSON

Submitted to the Office of Graduate Studies of
Texas A&M University
in partial fulfillment of the requirements for the degree of

DOCTOR OF PHILOSOPHY

Approved by:

Chair of Committee,	Eyad Masad
Committee Members,	Dallas N. Little
	Robert Lytton
	Zachary Grasley
	Anastasia Muliana
Head of Department,	John Niedzwecki

August 2011

Major Subject: Civil Engineering

ABSTRACT

Relationship Between Surface Free Energy and Total Work of Fracture of Asphalt
Binder and Asphalt Binder-Aggregate Interfaces. (August 2011)
Jonathan Embrey Howson, B.S., Texas A&M University;
M.E., Texas A&M University
Chair of Advisory Committee: Dr. Eyad Masad

Performance of asphalt mixtures depends on the properties of its constituent
materials, mixture volumetrics, and external factors such as load and environment. An
important material property that influences the performance of an asphalt mixture is the
surface free energy of the asphalt binder and the aggregate. Surface free energy, which
is a thermodynamic material property, is directly related to the adhesive bond energy
between the asphalt binder and the aggregate as well as the cohesive bond energy of the
asphalt binder. This thermodynamic material property has been successfully used to
select asphalt binders and aggregates that have the necessary compatibility to form
strong bonds and resist fracture.

Surface free energy, being based on thermodynamics, assumes the asphalt binder
is a brittle elastic material. In reality, the asphalt binder is not brittle and dissipates
energy during loading and unloading.   The total work of fracture is the culmination of
all energy inputted into the sample to create two new surfaces of unit area and is
dependent on the test geometry and testing conditions (e.g., temperature, loading rate,
specimen size, etc.).   The magnitude of the bond energy (either adhesive or cohesive)
can be much smaller in magnitude when compared to the total work of fracture
measured using mechanical tests (i.e., peel test, pull-off test, etc.).   Despite the large
difference in magnitude, there exists evidence in the literature supporting the use of the
bond energy to characterize the resistance of composite systems to cohesive and/or
adhesive failures. If the bond energy is to be recognized as a useful screening tool by

the paving industry, the relationship between the bond energy and total work of fracture needs to be understood and verified.

The effect of different types of modifications (addition of polymers, addition of anti-strip agents, and aging) on the surface free energy components of various asphalt binders was explored in order to understand how changes in the surface free energy components are related to the performance of the asphalt mixtures. After the asphalt binder-aggregate combination was explored, the next step was to study how the surface free energy of water was affected by contact with the asphalt binder-aggregate interface. Aggregates, which have a pH of greater than seven, will cause the pH of water that contacts them to increase. A change in the pH of the contacting water could indicate a change in its overall surface free energy, which might subsequently increase or decrease the water's moisture damage potential. With surface free energy fully explored, the total work of fracture was measured using pull-off tests for asphalt binder-aggregate combinations with known surface free energy components. In order to fully explore the relationship between bond energy and total work of fracture, temperature, loading rate, specimen geometry, and moisture content were varied in the experiments. The results of this work found that modifications made to the asphalt binder can have significant positive or negative effects on its surface free energy components and bond energy. Moreover, the results from the pull-off tests demonstrated that a relationship exists between bond energy (from surface free energy) and total work of fracture (from pull-off tests), and that surface free energy can be used to estimate the performance of asphalt binder-aggregate combinations.

DEDICATION

To everyone who pursues knowledge for the betterment of themselves and society. May they excel in their efforts and forge a brighter future for mankind.

ACKNOWLEDGEMENTS

TABLE OF CONTENTS

LIST OF FIGURES

LIST OF TABLES

CHAPTER I

INTRODUCTION

Overview

Fatigue cracking and moisture induced damage are major forms of distresses in asphalt pavements. An important thermodynamic material property that is used to characterize fatigue cracking and moisture sensitivity of asphalt mixtures is the surface free energy of the asphalt binder and the aggregate. Surface free energy is used to calculate various energy parameters such as the cohesive bond energy of the asphalt binder, the adhesive bond energy between the asphalt binder and the aggregate in dry condition, and the energy potential for water to displace the asphalt binder from the surface of the aggregate. A combination of one or more of these energy parameters is related to the resistance of the asphalt mixture to fatigue cracking and moisture induced damage.

Griffith (1) demonstrated that the minimum amount of work required for a crack to propagate in an elastic material is a function of its surface free energy (numerically equal to the surface tension). Schapery (2) used an energy balance approach similar to the one by Griffith (1) to extend the fundamental principles of crack growth to viscoelastic materials. An important material property to determine the work required for a crack to propagate within a material using the energy balance approach is the cohesive bond energy of that specific material. Little et al. and Masad et al. (3, 4) demonstrated that the cohesive bond energy of asphalt binders can be used to predict the fatigue cracking characteristics for asphalt mastics and mixtures.

_____

This dissertation follows the style of *Transportation Research Record*.

Moisture damage in asphalt mixtures is related to the adhesive bond energy and the magnitude of reduction in this energy when the asphalt binder debonds from the aggregate surface in the presence of water. Cheng (5) pointed out that the affinity of the aggregates for water is far greater than it is for the asphalt binder. During the stripping process, water diffuses through the thin layer of asphalt binder or mastic and collects on the surface of the aggregate. It has been discovered that the aggregate surface will then influence the pH of the contacting water (6-9). In many cases the pH of the contacting water will increase (become more basic) due to the adsorption of hydrogen ions onto the surface of the aggregate from the water. This was observed by Yoon and Tarrer (9), who demonstrated that if different aggregate powders (chert gravel, quartz sand, quartz gravel, granite, limestone, and dolomite) were added to water and allowed to interact, the pH of the water-aggregate blend reached a steady asymptotic value.

The change in pH of water might affect its surface energy components that can in turn aggravate or retard the stripping process. Scott and Hughes et al. (8, 10) reported that adhesion between asphalt cement and aggregate in the presence of water became weakened when the pH of the buffer solution was increased from 7.0 to 9.0. A later study by Van Oss and Giese (11) measured the contact angles of normal reverse osmosis water, water with hydrochloric acid, and water with sodium chloride. The researchers found little change in the measured contact angles over the range of pH tested. No study has been found in the literature that measures influence of pH on the surface free energy components of water. Therefore, part of this study will focus on understanding this effect based on experiments with different aggregates and asphalt binders.

Most of the previous work related to the application of surface free energy to predict performance of asphalt mixtures is based on the use of neat (unmodified) asphalt binders. A pertinent question that has arisen from these studies regards the effect of modifications to the asphalt binder on its surface free energy and consequently on the predicted performance. The term 'modification' is used to imply the different natural and/or engineering processes that asphalt binders are subjected to during production and in service. The modifications that were addressed in this study are:

- Modifications made to the asphalt binder by the manufacturer to achieve a certain performance grade (PG) in accordance with the Superpave specifications. The original PG grade asphalt binder is referred to as the base asphalt.

- Modifications made to the binder by materials and/or design engineers to improve the performance of the asphalt mixture. A typical example of this is the addition of liquid anti-strip agents to improve moisture resistance of the asphalt mixture. These modifications can be made to either a base asphalt binder or an asphalt binder that is already modified by the manufacturer.

- Modifications due to environmental effects. An example of this modification is oxidative aging, which significantly alters the chemistry of the binder and consequently its mechanical properties.

Even though the bond energy between aggregates and asphalt binder or within the asphalt binder can be obtained from the individual surface free energies of the component materials, as mentioned earlier, there can be significant differences between this amount and the total work of fracture that is obtained from mechanical tests. The bond energy is based on fundamental material properties and, therefore, is independent of any external or experimental factors; however, the total work of fracture depends on various experimental factors such as specimen geometry and loading conditions (e.g., peel test versus pull-off test, loading rate for time dependent materials, etc.). As a consequence, it can be expected that different experimental tests, or test conditions, will provide different data regarding total work of fracture (12). Many studies have evaluated the differences between the bond energy and total work of fracture under this principle. The main finding is that total work of fracture can be much greater than the bond energy depending on material properties, geometry of the specimen, adhesive thickness, temperature, and loading rate for time-dependent materials. However, it has also been shown for different composite materials that the plastic and viscoelastic components of energy dissipation are correlated to the bond energy, and that any change in the measured bond energy is reflected in a significant change in total work of fracture (13). In other words, for a given set of experimental conditions and class of materials,

the total work of fracture is directly correlated to the bond energy. The relationship between the bond energy and total work of fracture hasn't been investigated before for asphalt-aggregates systems; therefore, part of this dissertation focuses on understanding the factors that influence this relationship.

Objectives and Scope of Study

Surface free energy has been shown to be a very important material property in past research studies and has the potential to be used as a screening tool for material selection. It is therefore critically important to understand the effect of modifications on the surface free energy of asphalt binders and to understand and evaluate the relationship between surface energy and cohesive and adhesive total work of fracture. In addition, the magnitude of the total work of fracture is dependent upon external factors such as loading rate, testing temperature, film thickness, and interfacial moisture; the effects of which need to be understood independently and with regard to the bond energy. The objectives of this research are to:

- Evaluate the effect of the different types of modifications on the surface free energy of asphalt binders and their effect on the moisture resistance of various asphalt-aggregate combinations.

- Determine if the change in pH of water in contact with different aggregate surfaces will significantly alter the total surface free energy and/or surface free energy components of the water.

- Develop a testing platform capable of measuring the cohesive and adhesive total work of fracture of thin asphalt films between both stainless steel and aggregate substrates.

- Investigate how changes in loading rate, testing temperature, film thickness, and moisture at the asphalt-aggregate affect the measured total work of fracture.

- Investigate the relationship between bond energy and the total work of fracture between different asphalt binders and aggregate substrates.

Outline of Dissertation

Chapter II of this dissertation presents a literature review on the principles of surface free energy and bond energy, an overview of total work of fracture as it relates to some engineering materials, and the types of tests used to measure the total work of fracture.

Surface free energy has been shown to be a good indicator of the moisture resistance of asphalt binder-aggregate combinations. Chapter III investigates how various modifications made to the asphalt binder affect its surface free energy, resulting bond energy, and resistance to moisture induced damage. During stripping, water (moisture) comes into contact with the aggregate surface, and the pH of the water has the potential to change after contacting the aggregate surface. Chapter IV investigates if a change in the pH of water will cause a change in its surface free energy.

The relationship of the bond energy to total work of fracture is explored in Chapters V and VI. Chapter V investigates whether or not a relationship exists between the bond energy and the total work of fracture using asphalt binder-stainless steel samples. Chapter VI further explores this relationship using asphalt binder-aggregate samples and investigates how experimental variations (i.e., asphalt film thickness, loading rate, testing temperature, and moisture content) affect the measured total work of fracture.

CHAPTER II

LITERATURE REVIEW

Introduction

This chapter begins with a brief review of surface free energy and its relationship to adhesive and/or cohesive bond energy. The subsequent section presents a review of the total work of fracture and its relationship to bond energy. The relationships between bond energy and total work of fracture presented in this section are for both inelastic materials (i.e., viscoelastic, plastic, etc.) and brittle. The last section explores the different experimental setups that have been used to measure the total work of fracture of various types of polymers and the advantages and disadvantages of each.

Principles of Surface Free Energy

Surface free energy (SFE) is defined as the work required to create a unit area of new surface of a material in a vacuum. According to the Good-van Oss-Chaudhury theory, or acid-base theory, the SFE of a material is divided into three components based on the origin of the intermolecular forces (14). These components are: Lifshitz-van der Waals, γ^{LW}; monopolar acid, γ^+; and a monopolar basic, γ^-. The total SFE of a material, γ^{Total}, is obtained from the three components as shown in Equation 1.

$$\gamma^{Total} = \gamma^{LW} + 2\sqrt{\gamma^+ \gamma^-} \tag{1}$$

There are two possible locations for crack initiation: through the bulk of an asphalt binder or along the interface between the asphalt binder and aggregate. The energy required for a crack to propagate through the bulk of a material is known as the

cohesive bond energy or work of cohesion, Equation 2, and is twice the total SFE of the material.

$$\Delta G_{coh} = 2\gamma^{Total} = 2\left(\gamma^{LW} + 2\sqrt{\gamma^{+}\gamma^{-}}\right)$$ (2)

The energy required for a crack to propagate along the interface of the asphalt binder and aggregate is known as the adhesive bond energy, or work of adhesion, and is a function of the SFE of both the asphalt binder and aggregate as shown in Equation 3.

$$\Delta G_{adh} = 2\sqrt{\gamma_1^{LW}\gamma_2^{LW}} + \sqrt{\gamma_1^{+}\gamma_2^{-}} + \sqrt{\gamma_1^{-}\gamma_2^{+}}$$ (3)

where, subscript 1 represents the asphalt binder and subscript 2 represents the substrate (aggregate). A higher value of the cohesive or adhesive bond energy indicates a greater amount of energy is required for a crack to propagate through the bulk of a material or along the interface between an asphalt binder and aggregate, respectively.

When water is present along the asphalt-aggregate interface, the energy required for the crack to propagate is a function of the SFE of the asphalt, aggregate, and water. The interaction is called a hydrophobic interaction because the energy required for water to displace asphalt binder from the aggregate surface is almost always less than zero (i.e., the displacement of asphalt binder on the aggregate surface by water is a thermodynamically favorable process). However, a recent study in which surface energy was measured using the universal sorption device on 22 minerals at Texas A&M University revealed that four of the 22 minerals tested demonstrated a thermodynamically favored bond with certain asphalt binders than with water (15). However, this finding should be considered in the context that the minerals with a thermodynamically stable bond with asphalt binder may make up a very small fraction of the total surface area of most aggregates. Therefore, it is realistic to continue to assume that total surface energy of most aggregate surfaces generally favor a bond with

water over a bond with asphalt binder. The magnitude of energy for water to displace asphalt binder is as follows:

$$\Delta G_{123}^{a} = \gamma_{13} + \gamma_{23} - \gamma_{12} \tag{4}$$

where, the subscripts 1, 2, and 3 represent the asphalt binder, substrate (aggregate), and water, respectively. On the right-hand side of Equation 4, γ_{ij} represents the energy of the interface between any two materials "i" and "j" and is computed from their SFE components as follows:

$$\gamma_{ij} = \gamma_i + \gamma_j - 2\sqrt{\gamma_i^{LW}\gamma_j^{LW}} - \sqrt{\gamma_i^+\gamma_j^-} - \sqrt{\gamma_i^-\gamma_j^+} \tag{5}$$

The SFE has been successfully used in previous studies to determine the cohesive strength of asphalt binders and the adhesive strength, both dry and in the presence of water, of asphalt-aggregate combinations (3, 16-18).

Little et al. (3) reported four different energy parameters (*ER*) that were correlated to the moisture sensitivity of asphalt mixtures. These parameters were computed using the surface free energy components of materials used in the asphalt mixtures. All four parameters were developed using similar hypotheses and demonstrated similar trends with the moisture sensitivity of asphalt mixtures. Little et al. (3) compared the results given by the energy parameters to actual field data. The energy parameter with the best observed correlation was used in this research to assess the change in moisture sensitivity of asphalt mixtures due to the modifications made to the asphalt binders. This parameter is a function of the surface free energy components of the asphalt binder and the aggregate and is expressed as:

$$ER = \left| \frac{\Delta G_{adh} - \Delta G_{coh}}{\Delta G_{123}^{a}} \right| \tag{6}$$

In Equation 6 the terms ΔG_{adh}, ΔG_{coh}, and ΔG_{123}^{a} represent the adhesive bond energy between the asphalt binder and the aggregate (Equation 3), cohesive bond energy of the asphalt binder (Equation 2), and work of debonding when water displaces asphalt binder from its interface with the aggregate (Equation 4), respectively. A higher value of ΔG_{adh} indicates that more work is required to break the adhesive bond between the asphalt binder and the aggregate and hence implies better resistance to moisture damage. The term, $\Delta G_{adh} - \Delta G_{coh}$, represents the ability of the asphalt binder to wet or coat the surface of the aggregate. Better coating of micro textural features on the surface of the aggregate by the asphalt binder enables better mechanical interlocking between the two materials. A lower magnitude of ΔG_{123}^{a} indicates a lower energy potential for water to displace asphalt binder from its interface with the aggregate and hence a higher resistance to moisture damage.

Total Work of Fracture

The thermodynamic criterion for unstable crack growth to occur is that the energy stored in the specimen should be sufficient to supply the energy needed for the increase in the area of the crack (i.e., to create new surfaces of the material). For the case of elastic materials, Griffith (1) showed that this criterion is satisfied when the critical strain energy release rate (G_c) is equal to the bond energy or work of fracture (2γ) as shown in Equation 7:

$$G_c = 2\gamma^{Total} \tag{7}$$

where γ^{Total} is as defined earlier. (SFE) of the material is defined as the work required to create a unit area of new surface of the material in vacuum.

For the case of adhesive fracture for purely elastic materials, the criterion for unstable crack becomes:

$$G_c = \gamma_1 + \gamma_2 - \gamma_{12} \qquad (8)$$

where, γ_1 and γ_2 are the surface free energies of the two materials, and γ_{12} is the SFE of the interface (Equation 5).

For a plane stress condition representing an infinitely long sheet with an elliptical crack that has a length of $2c$ and very small minor axis, and the plane of the crack is perpendicular to the applied load, the applied stress is related to material properties as follows:

$$\sigma \le \sigma_c = \left(\frac{2E\gamma}{\pi c} \right)^{1/2} \qquad (9)$$

where, σ_c is the critical stress at which the crack becomes unstable ($\sigma = \sigma_c$), E is the Young's modulus of the material, and γ is the SFE. As can be seen in Equation 9, the critical stress that causes an unstable cohesive crack is directly related to the magnitude of the SFE and elastic modulus of the material.

A noteworthy observation from Griffith's work is that the theoretical tensile strength, computed based on SFE, is 10 times or more than the measured tensile strength of the material. Griffith experimentally demonstrated that the presence of flaws (i.e., sites with high local stress intensity) were responsible for this difference. Also, the theoretical tensile strength computed from Equation 9 clearly indicates that even small and marginal changes in SFE can result in significantly different tensile strengths for materials with high modulus. While this result was derived for a purely brittle elastic

material, there are several reasons, as will be discussed later, why the total work of fracture is typically higher than the bond energy for brittle elastic and inelastic materials.

Inelastic materials experience irreversible energy dissipation during the fracture process that causes the total work of fracture to be much higher than the bond energy calculated using the right hand sides of Equations 7 and 8. The total work of fracture is composed of three different energies: the bond energy, calculated from the right-hand sides of Equations 7 and 8, the dissipated plastic energy, and the dissipated viscoelastic energy. Orowan (19) modified Griffith criterion for cohesive failure in order to account for plastic energy dissipation, W_{PL}, at the crack tip as shown in Equation 10:

$$G_c = 2\gamma + W_{PL} \tag{10}$$

Orowan (19) considered W_{PL} to be a material property that is independent of crack geometry and loading configuration. In order to account for W_{PL} during cohesive cracking, Orowan (19) modified Equation 9 to become as shown in Equation 11:

$$\sigma \leq \sigma_c = \left(\frac{E\left(2\gamma + W_{PL}\right)}{\pi c} \right)^{1/2} \tag{11}$$

Irwin (20) extended Griffith's theory for the case of elastic-plastic materials to account for crack and specimen geometry. Irwin's relation for plane stress is shown in Equation 12.

$$\sigma \leq \sigma_c = \frac{1}{\alpha}\left(\frac{E\left(2\gamma + W_{PL}\right)}{\pi c} \right)^{1/2} \tag{12}$$

where, α is a geometrical correction factor depending on the crack shape and specimen geometry.

Total Work of Fracture versus Bond Energy for Inelastic Materials

An important difference between the bond energy and the total work of fracture is that the former is based on fundamental material properties and, therefore, is independent of any external or experimental factors. However, the total work of fracture depends on various experimental factors such as specimen geometry and loading conditions (e.g., peel test versus pull-off test, loading rate for time dependent materials, etc.). As a consequence, it can be expected that different experimental tests, or test conditions, will provide different data regarding total work of fracture (12). Many studies have evaluated the differences between the bond energy and the total work of fracture under this principle. The main finding is that total work of fracture can be much higher than the bond energy depending on material properties, geometry of the specimen, adhesive thickness, temperature, and loading rate for time-dependent materials. However, it has also been shown that the plastic and viscoelastic components of energy dissipation are correlated to the bond energy, and that any change in the bond energy is reflected in a significant change in the total work of fracture (13). In other words, for a given set of experimental conditions and class of materials, the bond energy is directly correlated to the total work of fracture.

In the early 70s, Gent and Kinloch (21), Gent and Schultz (22), and Andrews and Kinloch (23) conducted experimental studies to measure fracture energy of rubber-to-polymer substrate systems, investigate the influence of loading rate on fracture energy, and evaluate the effect of a variety of wetting liquids on the resistance to peeling separation. Some of the findings from these studies were:

- The bond energy and total work of fracture are similar in magnitude when the joint failure is totally interfacial, but the total work is much higher than the bond energy when substantial cohesive failure occurs. A plausible explanation of this phenomenon is that the cohesive failure involves more material deformation, and consequently, more energy is dissipated due to the plastic and/or viscoelastic response of the material in comparison to the adhesive failure.

- The total work of fracture reaches a value equal to the bond energy (based on thermodynamically predicted values from SFE) only at small peel rates (Figure 1), and it increases with an increase in peel rate. Gent and Kinloch (21) stated that "…, both for cohesive rupture and adhesive failure, the failure energy at extremely low rates of failure is not much larger than would be expected on equilibrium thermodynamic grounds. As the rate of failure is increased, the measured failure energy increases by orders of magnitude, presumably reflecting energy dissipation when deformation takes place under non equilibrium conditions."

- The total work of fracture is a product of two terms: the bond energy and a numerical "inefficiency" factor. The term "inefficiency" was used to quantify deviation from the perfect elastic behavior. This factor was found to depend on peel rate and temperature for viscoelastic materials.

- The change in the bond energy due to the presence of some liquids at the interface is in good agreement with the reduction in the total work of fracture, although the latter is much higher than the former. This relationship can be seen clearly in Figure 2, which plots the ratio of total work of fracture in the presence of a liquid to the total work of fracture in air (W_l/W) versus the change in the bond energy due to the presence of the liquid (Δ).
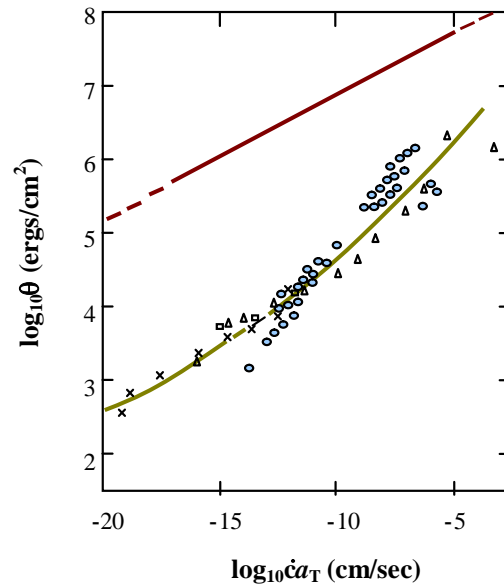
Figure 1. Relationship between Total Work of Fracture (θ) and Rate of Propagation of Crack Tip $\dot{c}$ (a_T is the Time Temperature Shift Factor for Viscoelastic Material, T_g is the Glassy Temperature and T is the Test Temperature) for Different Experimental Set-Ups. After Gent and Kinloch (21).
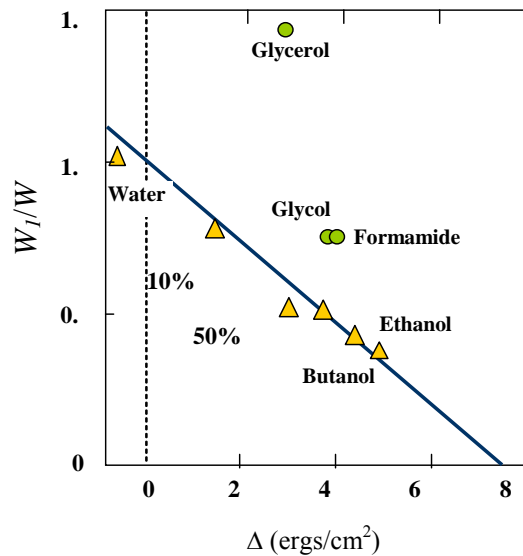
Figure 2. Ratio of Peeling Energy Versus Change in Bond Energy, W_1 is Peeling Energy in the Presence of Liquids, W is Peeling Energy in Air, and Δ is the Change in Bond Energy. Modified after Gent and Schultz (22).

In a more recent work, Okamatsu et al. (13) evaluated the relationship between the bond energy and total work of fracture of a polypropylene oxide (DMSi–PPO) / diglycidylether of bisphenol A (DGEBA) in contact with different polymeric substrates. It was found that the measured peel adhesion energy was in relatively good agreement with the bond energy (14.3 - 31.6 mJ/m^2) for the systems containing low surface energy substrates, but when high surface energy substrates were used, the peel adhesion energies were 10^3–10^4 times larger than the thermodynamic work of adhesion (50.4 - 64.6 mJ/m^2). The differences were attributed to the dissipated viscoelastic energy. The results from this study (Figure 3) are in agreement with the results in Figure 2 in demonstrating that small changes in the bond energies produce significant changes in the experimental or total work of fracture.
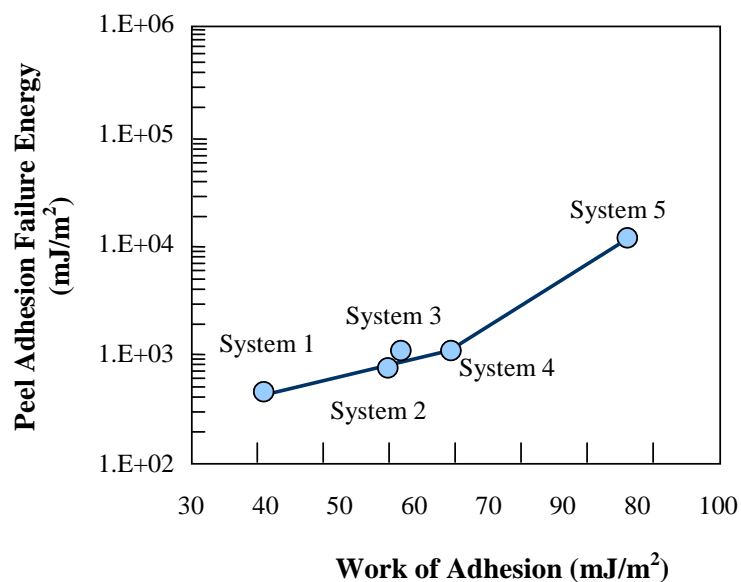
Figure 3. Relationship between Bond Energy (Work of Adhesion) and Total Work of Fracture for Adhesive Joints Systems with the Same Adhesive and Different Polymeric Substrates. Modified from Okamatsu et al. (13).

The fracture energy of the interface of two viscoelastic materials or a viscoelastic material bonded to rigid substrate was studied by Xu et al. (24). In agreement with the studies by Gent and Schultz (22), Gent and Kinloch (21), and Andrews and Kinloch (23), Xu et al. (24) stated that the crack propagation and energy dissipation are functions of loading history and loading rate. Xu et al. (24) derived an analytical relationship showing that the total work of fracture, W_T, of the interface between two viscoelastic materials is related to the bond energy, W_B, through the following relationship:

$$W_T = W_B\left[1 + f\left(a_T, \dot{a}, k\right)\right] \tag{13}$$

where a_T is the time-temperature shift factor for a viscoelastic material, $\dot{a}$ is crack growth velocity, and k is a factor that is a function of the micromechanical properties of the interface, mechanical properties of viscoelastic material and specimen geometry. The presence of a_T, and $\dot{a}$ in Equation 13 represents the influence of temperature and loading rate, respectively, on the response of viscoelastic materials.

The relationship derived by Xu et al. (24) was further studied by Shull et al. (25), who expanded the relationship to include interfacial effect as shown in Equation 10.

$$W_T = W_B\left\{1 + \Psi\left(\dot{a}\right)\right\}\left\{1 + f\left(a_T, \dot{a}\right)\right\} \tag{14}$$

where, $\Psi(\dot{a})$ accounts for the interfacial effects, and f accounts for energy dissipation in the crack tip region. Shull et al. (25) go on to explain that when the crack growth velocity is equal to zero, $f(a_T, \dot{a})$ is equal to zero, but Ψ can have a large value. Interfacial effects, as explained by Shull et al. (25), are effects which occur even when the crack velocity is zero. These interfacial effects include the thermodynamic work of adhesion, direct and indirect bonding across the interface, and contact electrification. The authors realized Ψ and f might not always be separable or linearly proportional to one another, as Equation 14 is empirical.

Seshadri et al. (26) investigated the relationship between total work of fracture and bond energy by analyzing a one-dimensional model for steady-state crack propagation between a rigid substrate and a thin viscoelastic film subjected to tensile loading. These authors reported that the total work of fracture is a function of crack-tip velocity. This observation is in agreement with the dependency between W_T and $\dot{a}$ established by Xu et al. (24) in Equation 13. Seshadri et al. (26) reported a relationship between total work of fracture and bond energy similar to that shown in Equation 13.

Kaelble (27) analyzed the effects of plasticity on the relationship between bond energy and total work of fracture. This study focused on the effects of different vapor and liquid phase immersion on the interfacial crack propagation (adhesive failure) of polymer-polymer interfaces. Based on experimental measurements obtained from peel-off tests, it was found that for the case where the plastic energy is much higher than the bond energy, there exists a relationship between the two quantities dictated by: $W_{PL} = K W_B$, with $K = 9700(\text{dyn/cm})^{1/2} \pm 20\%$ for all the immersion phases used in the study except for glycerol.

Jokl et al. (28) studied the relationships between plastic work and bond energy for deformable solids. They found that W_{PL} is a function of the bond energy. As such, they modified Orowan's criterion in Equation 10 to become:

$$G_c = 2\gamma^{Total} + W_{PL}(\gamma) \tag{15}$$

In 1998, Wei and Hutchinson (29) used peel-adhesion data and a cohesive zone model to numerically investigate the dependency of the total work of fracture and the plastic deformation in an adhesive film on the bond energy. They demonstrated that the interface strength, $\hat{\sigma}$, has the most influence on the difference between bond energy and total work of fracture. For values of normalized interface strength, ($\hat{\sigma}/\sigma_y$, σ_y yield stress), smaller than 2, the plastic energy dissipation is negligible compared to the bond energy. As a result, the total work of fracture is close to the bond energy and is independent of the film thickness. For values of normalized interface strength larger than

2, plastic deformation becomes an important contributor to the total work of fracture. In these cases, the proportion between total work of fracture and bond energy depends on the film thickness and the hardening index. The numerical work from Wei and Hutchinson (29) provided a computational tool to partition the total work of fracture into the bond energy and plastic dissipation.

Based on the review of previous studies, Volinsky et al. (30) also reported that plastic energy is a function of bond energy. They discussed that the type of failure at the interface is a function of the bond energy and the yield stress of a plastic material. If the yield stress is low and the bond energy is high, ductile failure is most likely to occur at the interface. However, when the yield stress is high and the bond energy is low, brittle failure is most likely to occur.

Total Work of Fracture versus Bond Energy for Brittle Elastic Materials

The difference between the thermodynamic bond energy and total works of fracture can also be observed in brittle elastic materials, albeit due to different reasons than those discussed in the previous section for elasto-plastic and viscoelastic materials. Sharon et al. (31) conducted experiments to study the fracture mechanism in PMMA (polymethyl-methacrylate), which is a brittle, amorphous material at low temperatures. The researchers found that the energy required for a crack to propagate at a given speed remained almost constant up to a certain threshold crack velocity. Beyond this threshold, it was found that fracture energy increased linearly as a function of crack velocity. This phenomenon was explained by experimental measurements, which show the formation of unstable micro-branching of the crack after the threshold crack velocity was reached. The presence of micro-branches resulted in up to an order of magnitude increase in the true fracture surface area. Figure 4 shows the relative surface area (surface area formed per unit crack extension) as a function of crack velocity. This study concluded that a significant portion of the apparent increase in fracture energy in brittle materials such as PMMA could be attributed to a "microbranching" instability in the crack propagation process.
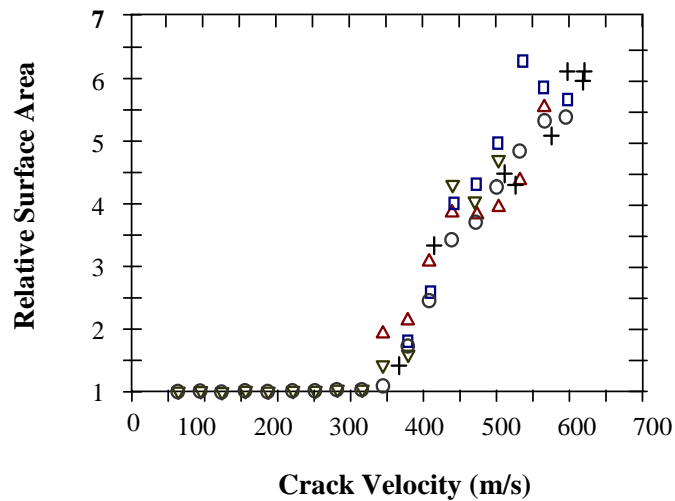
Figure 4. Relationship between Increase in Surface Area due to Microbranching and Crack Velocity. After Sharon et al. (31).

Miller et al. (32) conducted a numerical study to simulate the fracture process in brittle materials. This study reported a very strong correlation between the energy release rate and rate of formation of fracture surface, thereby confirming the experimental results by Sharon et al. (31). The main conclusion of the study by Miller et al. (32) was that "the observed increase in fracture energy can arise, even with a work of separation which is independent of rate, due to the increase in the surface area caused by extensive crack microbranching at high crack speeds."

The results of the studies by Sharon et al. (31) and Miller et al. (32) showed that the increase in fracture energy of materials that do not exhibit viscoelastic or plastic behavior can occur simply due to the increase in the true fracture surface area (as opposed to the nominal fracture area used to compute the total work of fracture). A detailed experimental study of the development of microbranching during crack propagation and a numerical implementation of microbranching instability for brittle materials can be found in Fineberg et al. (33) and Zhang et al. (34), respectively.

Penn and Defex (35) investigated the differences between bond energy and total work of adhesion fracture for selected low-molecular weight compounds. Joints were

constructed by the combination of six low-molecular weight adhesives and six solid plastic substrates that were tested under special conditions to eliminate contributions from irreversible and energy-consuming processes in the materials. Similar to the results obtained by Sharon et al. (31) and Miller et al. (32), the authors found that even under controlled conditions that prevent energy dissipations by viscous or plastic effects, there is a difference between the thermodynamic bond energy and the total work of adhesion. Based on these data, the authors concluded that there exists an exponential relationship between the bond energy and total work of fracture:

$$W_T = 91.3e^{0.033W_B} \tag{16}$$

Penn and Defex (35) stated that "even for the simplest and weakest interfaces, irreversible processes can occur within the interfacial region during loading and fracture, causing experimentally determined values for work of fracture to exceed the thermodynamic work of adhesion."

Influence of Deformation and Wetting on Fracture Energy

Zosel (36) conducted a comprehensive experimental study on the influence of deformation and wetting of polymers on fracture energy. In this study, Zosel (36) differentiated between "tack" and "maximum adhesive failure energy." Tack, as defined by Zosel (36), was the "the maximum adhesive failure energy of bonds formed under low contact pressure and with a short dwell time." As such, tack is not a material property as it is highly dependent on the conditions under which the bond is formed. The tack increases with an increase in contact pressure, increase in contact time between adhesive and adherent (substrate), and increase in compliance.

Zosel (36) stated that the maximum adhesive failure energy occurred "with optimum or fully developed interfacial contact between adhesive and adherent" and it was "a viscoelastic quantity of the adhesive insofar it fulfills the temperature rate superposition principle." Similar to many studies discussed earlier in this paper, Zosel

(36) showed that the maximum adhesive failure energy (or total work of fracture) was related to the bond energy as in Equation 13.

Based on the results by Zosel (36), the schematic in Figure 5 is proposed to represent the relationship between compliance and adhesive fracture energy. At low contact time and/or low contact pressure, an increase in the adhesive's compliance gives it more ability to flow and cover more contact area of the adherent or substrate. As a result, the non-equilibrium adhesive fracture energy or "tack" increases with an increase in compliance. This relationship is represented by the dashed lines in Figure 5. However, as the contact time and pressure increase, and the bond becomes more developed, the adhesive ability to deform will have very little influence on increasing contact area. Therefore, there would be no increase in fracture energy due to an increase in compliance. On the contrary, the increase in compliance, due to an increase in temperature or decrease in loading rate, would cause a decrease in the maximum adhesive fracture energy due to a decrease in the function (f) in Equation 13. This relationship between maximum adhesive fracture energy and compliance is represented by the solid line in Figure 5.
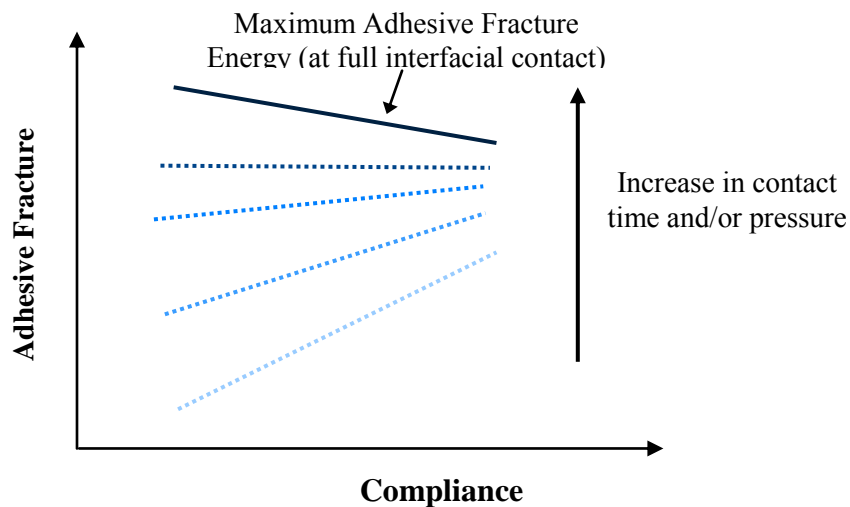
Figure 5. A schematic of the Relationship between Fracture Energy and Compliance at Different Contact Times and Pressure.

Wetting is the process during which the adherent comes into contact with the surface of the adhesive and develops an adhesive bond with it. The thermodynamic potential that drives wetting is the difference between the surface energy of the adherent and the surface energy of the adhesive (16). As this difference increases, the surface of the adherent would have greater affinity to the surface of the adhesive as compared to the bulk of the adherent. Zosel (36) presented experimental results supporting this phenomenon, and the authors developed the schematic in Figure 6 based on these results. In this figure, the tack is represented by the dashed lines. When surface energy of the material used as an adhesive decreases, the tack increases due to an increase in wetting. This phenomenon occurs until the surface energies of the adhesive and the adherent become equal as marked by the vertical dashed line. To the left of this line, the adherent surface energy is higher than that of the adhesive promoting wetting of the adherent surface; consequently, further decrease in surface energy of the adhesive material does not cause any more increase in wetting. The maximum adhesive fracture energy is associated with the complete wetting at high contact time and contact pressure as represented by the solid line.

Maximum Adhesive Fracture Energy (at full interfacial contact)

Adhesive Fracture Energy

Increase in contact time and/or pressure

Adhesive Surface Energy

Wetting increases

Surface Free Energy of the material used as an adhesive is less than adherent (substrate) surface energy, maximum wetting is being achieved
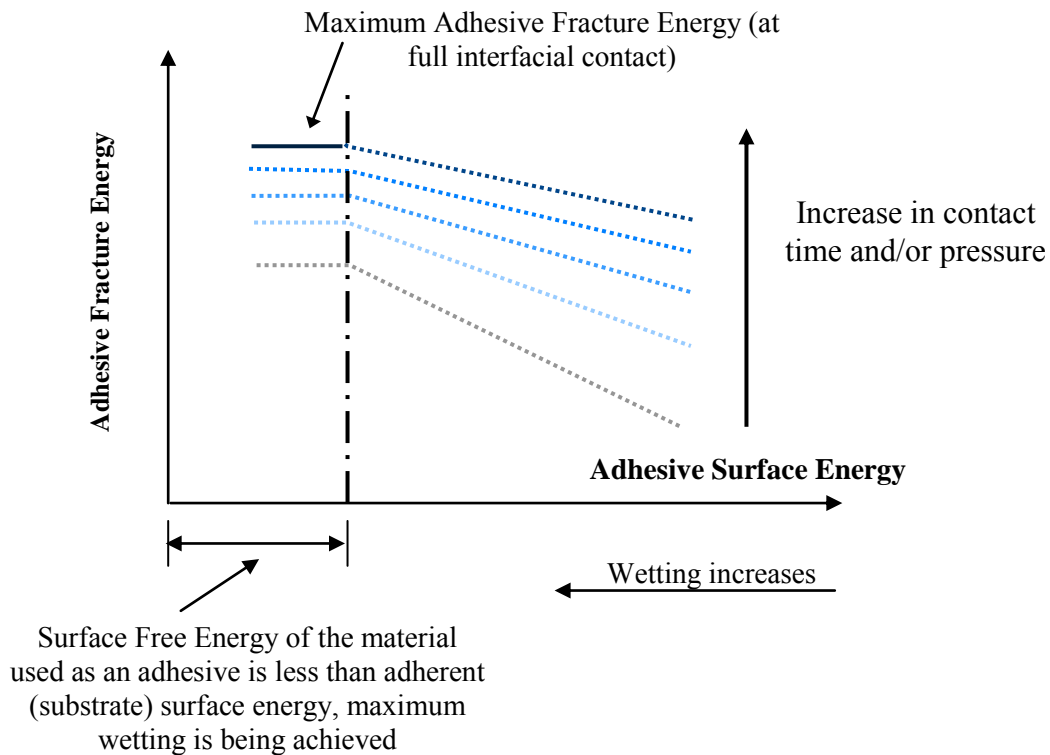
Figure 6. A Schematic of the Relationship between Fracture Energy and Wetting.

The phenomena described in Figures 5 and 6 can be used to evaluate the influence of compliance and contact pressure on the fracture characteristics of binder-aggregate systems. Binder-aggregate systems are mixed and prepared at high temperatures and under very high shear stresses. At these mixing conditions, asphalt binders are characterized as Newtonian viscous fluids. Therefore, it is reasonable to state that binders have the ability to reach equilibrium wetting over aggregate surfaces in relatively short durations of time. Consequently, binder deformation properties (viscosity or compliance at the mixing temperature), contact time, and contact pressure during mixing or formation of the bond would have negligible influence, if any, on the strength of the bond. As such, the authors of this study believe that the measured fracture energy for asphalt-aggregate systems corresponds to the maximum value of total work of fracture, and it is not the tack value. In addition, it is well known that the

surface free energy of the aggregate (adherent) is several times higher than that of the asphalt binder (adhesive). Therefore, according to the concept illustrated in Figure 6, it is reasonable to expect complete wetting between the aggregate and the asphalt binder irrespective of the asphalt binder's surface free energy. In other words, the asphalt binder-aggregate systems belong to the left side of the vertical dashed line in Figure 6 in which the magnitude of the asphalt binder's surface free energy is not expected to be an important factor in affecting the wettability of the asphalt binder to the aggregate.

Tests for Measuring Total Work of Fracture

There are three basic types of tests for measuring the total work of adhesion that have been used primarily for polymers: peel test, hemispherical probe tack test, and uniaxial flat pull-off test. Each test has its advantages and disadvantages, and is suitable for different applications. A brief description and background of each test is presented herein.

The peel test has been utilized heavily in the packaging and electronic industries to determine the adhesive strength of their products. There are three main types of peel test setups: fixed arm, T-peel, and Mandrel (37, 38). For all peel setups the measured peel energy needs to be divided into several components for analysis: strain energy, dissipated tensile energy, dissipated bending energy, and the plastic work done in bending the peel arm (38-40). In addition, researchers found that peel energy needed to separate the substrate from the adhesive was up to 100 times higher than the actual adhesion strength (39). A later study found that up to 85% of the peel energy came from energy required to plastically deform the system, and the assumptions made to separate this energy from the actual adhesion strength resulted in a significant loss of details (41).

The analysis of the peel test can further be complicated when failure is not uniform. Stick-slip (saw tooth) failure has been seen in many studies involving thin film peel tests (39, 42, 43). This intermittent failure motion occurs due to repeated cycles of unstable crack growth followed by an arrest period (44). Another phenomenon which

can complicate the analysis of the peel force is the transition between adhesive and cohesive failure mechanisms during the peel test (38). The failure mechanisms will generate a peel force that fluctuates between a high (cohesive failure) and low (adhesive failure) value.

Hemispherical probe tack testers have the advantage of being insensitive to slight misalignments between the probe and film, giving the experiment very reproducible results (45, 46). The shape of the indenter causes the stress field to be highly inhomogeneous within the adhesive layer, causing different parts of the adhesive film to be subjected to very dissimilar strain rates (46). Also, if a softer adhesive is used, large inhomogeneous deformations occur along with possible viscoelastic flow (47). With this known, Lakrout et al. (46) came to the conclusion that despite the reproducibility of the hemispherical probe, it is ill-suited to a more systematic investigation of the molecular parameters controlling adhesion.

The main downside of the flat probe is the difficulty in properly aligning the flat punch to the adhesive layer. Despite this problem, the flat probe configuration provides a much more uniform stress distribution and strain rate beneath the probe. Because of this uniformity, it is much more applicable for systems in which failure occurs due to the formation of cavities and fibrils (46, 48).

Creton and Lakrout (49) state that a typical flat punch test for soft viscoelastic polymers has a layer thickness of 10 – 100 μm and a punch diameter of 2 mm – 1 cm. With these dimensions, the adhesive layer will be highly constrained, and cavitation will occur in the adhesive layer during application of a negative hydrostatic pressure (49). Lakrout et al. (46) discovered that thin films of soft adhesives confined between parallel plates do not observe crack propagation from the edge, but rather experience the formation of multiple cracks with cavitations as their starting locations. They also discovered that the cavities nucleate at random over the entire plate surface, implying a homogenous negative hydrostatic stress across the plate. After formation, the cavities grow laterally on the surface of the plate, perpendicular to the applied tensile force (46, 49). The next step in the growth of the cavities depends on the mode of failure of the

sample. If adhesive failure occurs, the cavities do not interact prior to sample failure, and no fibrils form (50). If cohesive failure occurs, the distance between the cavities stabilizes, and the walls begin to grow in the direction of the applied tensile stress to form fibrils (46).

CHAPTER III

EFFECT OF MODIFICATION PROCESSES ON BOND ENERGY OF ASPHALT BINDERS*

Introduction

The overall performance of an asphalt mixture depends on the combined positive or negative impact of several different material properties such as bond strength within the mixture, viscoelasticity of the asphalt binder, and internal structure distribution. Previous research studies have shown that bond energy (cohesive or adhesive) is an important material property that has significant impact on performance (3, 18). Consequently, the focus on this study will be on using the bond energy and the parameter *ER* to estimate the positive or negative impact of different types of modifications to the asphalt binder. The modifications that were considered were those made by manufacturers to improve performance by adding polymers and antistrip agents and modification due to the environment (i.e., short- and long-term aging). This chapter includes three sections:

- Brief description of the materials used in this study.
- Comparison of the changes in the energy parameters due to modifications made to the asphalt binders and its implication on the performance of asphalt mixtures.
- Statistical analysis to rank the moisture resistance of asphalt binders and asphalt-aggregate combinations, respectively.

The parameter *ER* is a function of the surface free energy components of both the asphalt binder and the aggregate. As such, the study involved measuring the surface free

---

energy of 37 neat and polymer modified asphalt binders and 11 aggregates. In addition, the surface free energy was measured for three asphalt binders after two anti-strip agents were added separately (six binder-anti-strip agent combinations) and for nine asphalt binders that were both short- and long-term aged. It was found that anti-strip agents, in general reduced the cohesive bond energy of asphalt binder, allowing better wetting and adhesion to aggregates and increase in resistance to moisture damage. Aging of the asphalt either increased or decreased the cohesive bond depending upon the chemical composition of the unaged asphalt binder.

Materials

Table 1 includes a list of asphalt binders tested in this project. The asphalt binders were obtained from 16 different sources and labeled as *A*, *B*, *C*, etc. Base asphalt binders from sources *A* through *J* were modified by their respective manufacturer to produce a total of 21 modified asphalt binders. These modifications were achieved by introducing additives to the base asphalt binder. The additives included materials such as SBS (styrene-butadiene-styrene), SBR (styrene-butadiene-rubber), and tire rubber. The exact nature, amount, and process of modification varied from one manufacturer to another; the details of which were not disclosed to the authors. The asphalt binders are labeled by the source followed by the PG grade followed by the type of modifier. For example, binder A 64-22 B indicates source *A*, PG 64-22 binder, and a base (*B*) or unmodified binder. A binder with the label A 70-22 S indicates source *A*, grade PG 70-22, and modified using SBS. A shaded cell in Table 1 indicates that surface energy was measured for this binder at the listed condition.

Table 1. Matrix of Asphalt Binders Tested for Surface Free Energies.

Source	PG Grade and Modifier	Unaged	SAFT Aged	PAV Aged	Anti-Strip Agent 1	Anti-Strip Agent 2
Asphalt A	64-22 B	▓			▓	▓
	70-22 S	▓			▓	▓
	76-22 S	▓			▓	▓
Asphalt B	64-22 B	▓	▓	▓		
	70-22 S	▓	▓	▓		
	76-22 TRS	▓	▓	▓		
	76-22 S	▓	▓	▓		
Asphalt C	64-22 B	▓	▓	▓		
	70-22 S	▓	▓	▓		
	76-22 TRS	▓	▓	▓		
Asphalt D	58-22 B	▓	▓	▓		
	70-28 S	▓	▓	▓		
Asphalt E	64-22 B	▓				
	70-22 S	▓				
	76-22 S	▓				
	70-28 S	▓				
	76-28 S	▓				
Asphalt F	58-28 B	▓				
	58-34 S	▓				
	58-40 S	▓				
Asphalt G	64-22 B	▓				
	70-22 S	▓				
	76-22 S	▓				
Asphalt H	64-22 B	▓				
	70-22 S	▓				
	76-22 S	▓				
Asphalt I	64-22 B	▓				
	70-22 S	▓				
	76-22 S	▓				
Asphalt J	64-22 B	▓				
	76-22 SR	▓				
Asphalt K	76-22 S	▓				
Asphalt L	76-22 S	▓				
Asphalt M	76-22 S	▓				
Asphalt N	76-22 S	▓				
Asphalt O	76-22 S	▓				
Asphalt P	76-22 S	▓				

Note: Descriptions provided by binder suppliers: B = Base asphalt binder; S = SBS modifier; TRS = Tire rubber & SBS modifiers. ▓ Indicates surface energy measurements were made on that specific binder.

Eleven different aggregates were also utilized in this study. Table 2 includes a list of these aggregates. Similar aggregates with a different suffix (e.g., Limestone 1, Limestone 2, Limestone 3) indicate that the generic aggregate type was obtained from different sources with a unique suffix assigned to each source.

Table 2. Aggregates Used in the Measurements of Surface Free Energy.

Aggregate
Granite
Gravel 1
Gravel 2
Gravel 3
Gravel 4
Limestone 1
Limestone 2
Limestone 3
Quartzite
Sandstone 1
Sandstone 2

The base and manufacturer-modified asphalt binders from sources *B*, *C*, and *D* were used to evaluate the effect of aging on their surface free energy components and concomitant energy parameters. Two aging methods were used in this research. The first type was the stirred airflow test (SAFT), and the second type was the pressurized aging vessel (PAV). According to the literature, SAFT is a suitable simulation of short-term aging, especially for polymer modified asphalt binders (51). PAV, on the other hand, simulates long-term aging, representing about 5 to 10 years of aging in asphalt pavements.

The base and manufacturer-modified asphalt binders from source *A* were used to evaluate the effect of liquid anti-strip agents on their surface free energy components. Two different types of liquid anti-strip agents, commonly used by the Texas Department

of Transportation (TxDOT) in various field mixtures, were included in this project. The manufacturer's recommended amount of anti-strip agent was added to the asphalt binder.

The surface free energy of the asphalt binders was measured using the Wilhelmy Plate device. The Wilhelmy Plate works by measuring the contact angles between asphalt coated slides and probe liquids with known surface free energy values. The surface free energy values of the aggregates were measured using the USD. The USD measures the increase in mass of aggregate particles at different vapor pressures of liquids with known surface free energy values. Detailed methodologies to measure the surface free energy components of asphalt using the Wilhelmy Plate method and the surface free energy components of aggregates using the USD can be found in publications by Hefer et al. (52) and Bhasin and Little (53), respectively.

Results

Surface Free Energy Components

The values of the surface free energy components of the asphalt binders were then arranged in an ascending order, and the quartiles of the distribution were determined. The first, second (median), and third quartiles refer to the values at which 25 percent, 50 percent, and 75 percent of the measurements are less, respectively. Figures 7 – 9 display these quartiles for the LW, acid, and base components of the surface free energy of unaged binders, respectively. The LW component (Figure 7) is generally the largest among the three components, usually followed by the base component (Figure 8), with the acid component (Figure 9) being the smallest. It is important to have as high an acid component as possible since the acid component of the asphalt bonds with the base component of the aggregate, as seen in Equation 3. Aggregates have much larger values of surface free energy compared to asphalt binders and also have very large base components, as shown in Table 3. The acid and base values are computed using a relative scale based on the assumption that the acid and base components for water are equal. This assumption was made by van Oss et al. (14)

and was necessary in order to establish a reference point for the calculation of acid and base components for other liquids and solids. Therefore, the absolute values for the acid and base component for the same material are not known, only the relative values. Because of this, the magnitude of the acid and base components within a single material should not be compared to conclude if that material is basic or acidic. However, the same component (acid or base) of different materials can be compared to conclude that one material is more acidic (or basic) than the other.
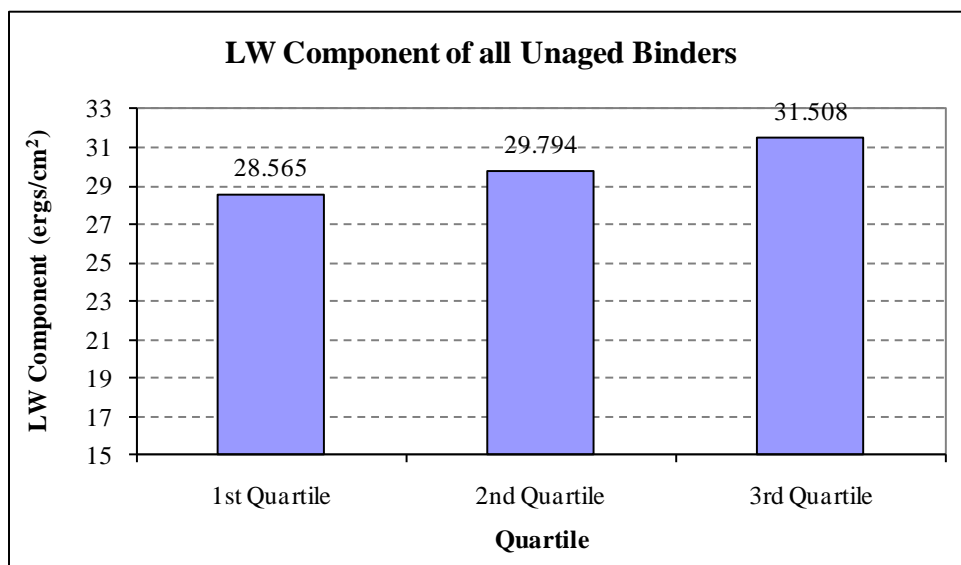
Figure 7. Quartiles of the Lifshitz-van der Waals Component of All Unaged Binders.
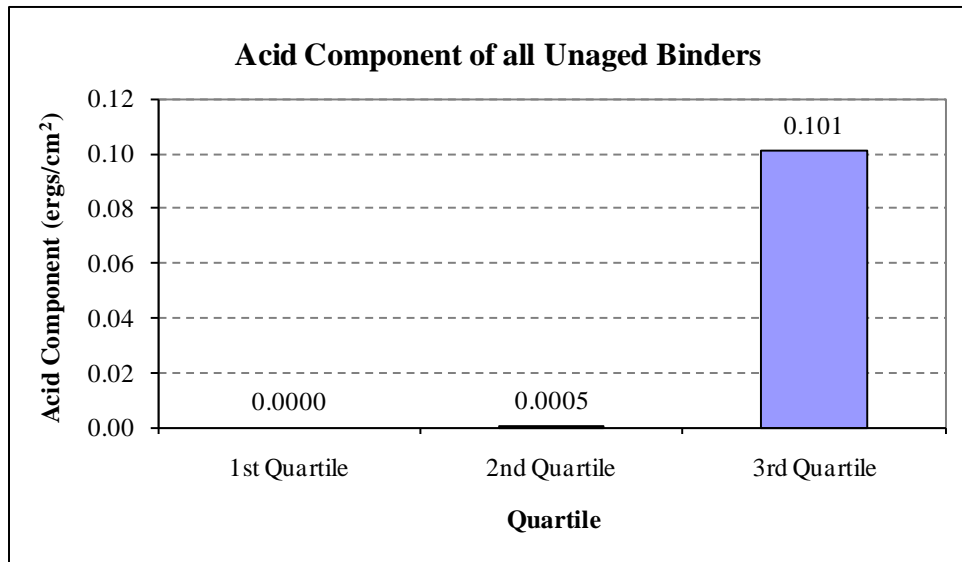
Figure 8. Quartiles of the Acid Component of All Unaged Binders.
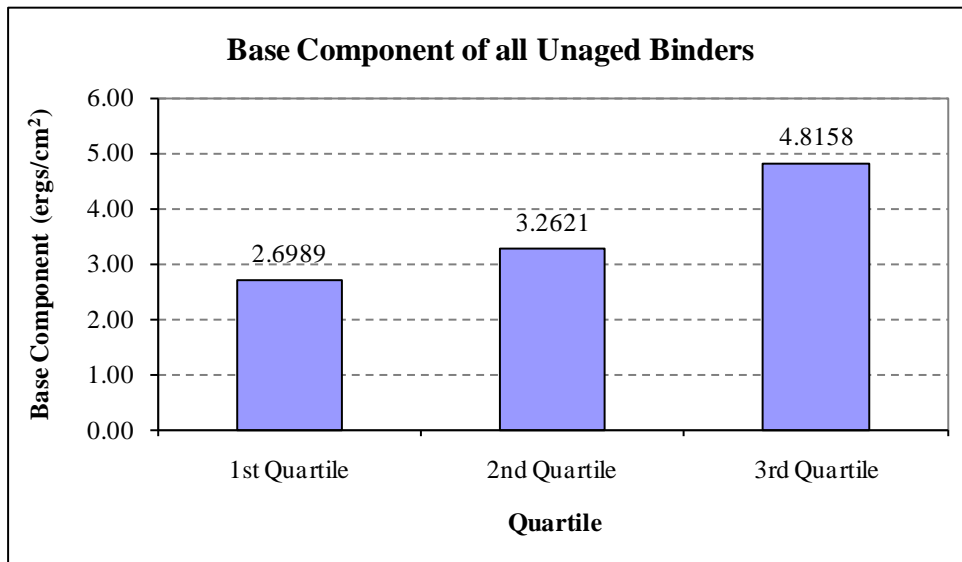
Figure 9. Quartiles of the Base Component of All Unaged Binders.

Table 3. Aggregate Surface Free Energy Components (ergs/cm^2).

Aggregate	Γ^{LW}	Γ^+	Γ^-
Granite	56.35	43.45	782.70
Gravel 1	59.49	1.20	285.98
Gravel 2	63.48	7.70	546.26
Gravel 3	81.34	1.10	426.85
Gravel 4	57.50	23.00	973.00
Limestone 1	59.89	18.82	561.11
Limestone 2	58.01	1.76	401.07
Limestone 3	57.70	5.50	340.40
Quartzite	60.86	8.89	544.98
Sandstone 1	62.46	2.03	222.61
Sandstone 2	63.97	8.51	316.90

Table 4 displays the change in the surface free energy components caused by the addition of anti-strip agents. It can be seen that all asphalt binders except one had an increase in either the acid or base component of surface free energy due to the addition of liquid anti-strip agents, and some had increases in both. As shown later, the asphalt binder that did not have an increase, Asphalt A 70-22 S with Anti-strip 2, is also the asphalt binder that showed the greatest decrease in *ER*. This decrease in *ER* indicates that the acid and base components of an asphalt binder are very important to moisture resistance. The non-polar component of surface free energy, γ^{LW}, decreased for all binders when a liquid anti-strip agent was added.

Table 4. Surface Free Energy Components due to Addition of Anti-Strip Agents.

Asphalt	Anti-Strip	Γ^{LW}	Γ^{+}	Γ^{-}	Γ^{Total}
Asphalt A 64-22 B	None	29.79	0.000	1.42	29.80
	1	29.10	0.000	1.78	29.11
	2	29.72	0.000	5.12	29.75
Asphalt A 70-22 S	None	27.34	0.000	2.77	27.34
	1	18.89	0.055	3.81	19.80
	2	24.79	0.000	1.67	24.80
Asphalt A 76-22 S	None	33.22	0.000	2.30	33.22
	1	22.66	0.000	2.49	22.66
	2	25.91	0.001	2.91	26.00

Table 5 displays the change in the surface free energy components caused by aging of the asphalt binders. The results are much more varied than those from the anti-strip study. Asphalt binders from source *B* showed mixed results after being SAFT aged. Three of the four asphalt binders from source *B* exhibited a decrease in the γ^{LW} component of surface free energy, one of the four asphalts showed a decrease in the γ^{+} component of surface free energy, and two of them showed a decrease in the γ^{-} component of surface free energy. After PAV aging, two of the asphalts from source *B* showed a decrease in the γ^{LW} component of surface free energy, and all asphalt binders from source *B* showed a decrease in the polar components of surface free energy. All asphalt binders from source *C* showed a decrease in the γ^{LW} component of surface free energy and an increase in either the γ^{+} or γ^{-} component of surface free energy or both. Asphalt D 58-28 B showed an increase in the γ^{LW} component of surface free energy after being short- and long-term aged, but Asphalt D 70-28 S showed a decrease in the γ^{LW} component of surface free energy after being short- and long-term aged. The only change to the γ^{+} component occurred after long-term aging of Asphalt D 70-28 S. The basic component of Asphalt D decreased in all cases except 58-28 B after PAV aging.

Table 5. Surface Free Energy Components of Asphalt Binders before and after Aging.

Asphalt	Aging	γ^{LW}	γ^+	γ^-	γ^{Total}
Asphalt B 64-22 B	Unaged	20.16	0.033	3.75	20.87
	SAFT	16.91	0.137	4.51	18.48
	PAV	26.2	0.000	3.2	26.23
Asphalt B 70-22 S	Unaged	22.50	0.001	6.79	22.66
	SAFT	21.72	0.036	3.74	22.45
	PAV	21.3	0.000	4.1	21.29
Asphalt B 76-22 TRS	Unaged	18.75	0.663	4.57	22.23
	SAFT	21.4	0.083	4.8	22.67
	PAV	17.8	0.219	4.4	19.73
Asphalt B 76-22 S	Unaged	22.67	0.003	7.86	22.96
	SAFT	21.72	0.006	5.35	22.06
	PAV	24.1	0.000	6.4	24.10
Asphalt C 64-22 B	Unaged	32.17	0.000	0.92	32.17
	SAFT	28.1	0.000	1.4	28.12
	PAV	26.0	0.000	5.1	25.97
Asphalt C 70-22 S	Unaged	35.78	0.000	0.44	35.78
	SAFT	28.6	0.004	2.5	28.80
	PAV	20.5	0.137	5.4	22.25
Asphalt C 76-22 TRS	Unaged	34.55	0.000	1.85	34.55
	SAFT	27.0	0.000	4.6	26.99
	PAV	24.8	0.027	8.5	25.78
Asphalt D 58-28 B	Unaged	18.96	0.000	3.26	18.96
	SAFT	21.3	0.000	2.9	21.28
	PAV	24.6	0.000	3.3	24.63
Asphalt D 70-28 S	Unaged	23.01	0.000	5.44	23.01
	SAFT	20.3	0.000	2.9	20.26
	PAV	17.7	0.441	4.7	20.57

The lack of trend in the surface energy components of short- and long-term aged asphalt binders can be explained on the basis of asphalt chemistry. Researchers at the Western Research Institute (WRI) have extensively investigated the aging phenomenon in asphalt binders and determined that the properties of short- and long-term aged asphalt binders depend on the chemistry of the unaged binder (54). Two important compounds that are formed during the oxidative aging of asphalt binders are sulfoxides and ketones. An asphalt binder with low sulfur is unlikely to produce a high concentration of sulfoxides after short-term aging. Therefore, depending on the initial

chemistry, each unaged asphalt binder reacts differently to aging. Since the physiochemical surface properties of the asphalt binder are dictated by its chemistry, it is reasonable to expect that different asphalt binders exhibit different trends due to aging.

For any given asphalt binder, the difference in trends between short-term and long-term aging are explained on the basis of kinetics of the oxidation reaction. For example, sulfoxides (weak bases) form at a much faster rate compared to ketones (weak acids) (55). As a result, it is not possible to extrapolate the effect of short-term oxidation on surface energy to predict surface energy components that may be formed after long-term aging. The net impact of aging on the chemical and physio-chemical properties of asphalt binders can be different depending on the duration of aging and chemical nature of individual asphalt binders.

The different trends in surface energy components exhibited by the asphalt binders due to short- and long-term aging ultimately translate into different values of the energy ratio and, hence, different expected trends in moisture resistance of the asphalt binders due to aging. Researchers at WRI have conducted freeze thaw tests on asphalt mixtures using several different aged and unaged asphalt binders (54). They have demonstrated that the moisture resistance of asphalt mixtures either decreased or increased after oxidative aging of the binder, depending on the type of binder.

Cohesive Bond Energy

Figure 10 displays the quartiles for the cohesive bond energy for all the tested unaged binders. The cohesive bond energy values range from 26 ergs/cm^2 to 71.5 ergs/cm^2. These values can determine the relative ranking of a binder with respect to a comprehensive list of binders such as those used in this project.
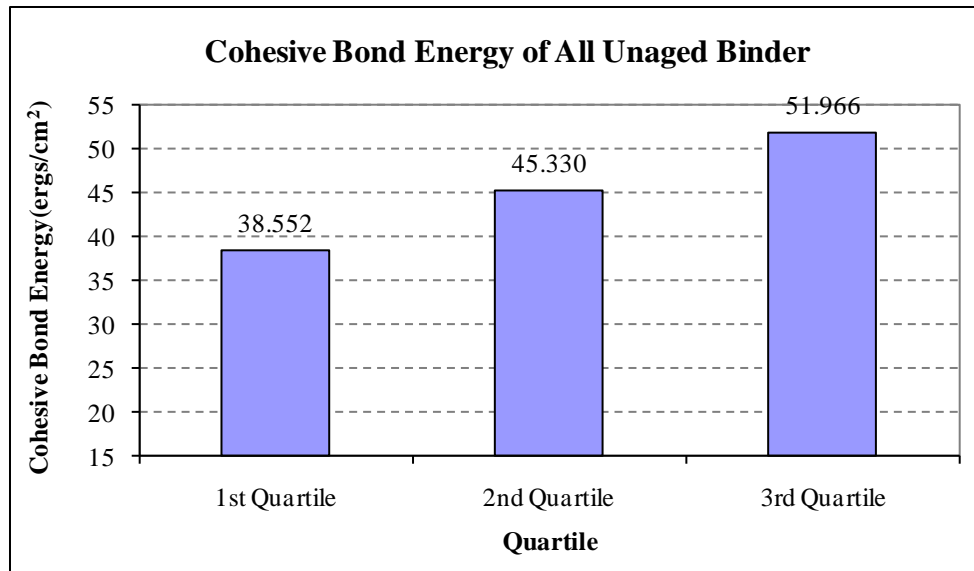
Figure 10. Quartiles of Cohesive Bond Energy of All Unaged Binders.

Table 6 displays the percent change in cohesive bond energy caused by the addition of anti-strip agents. It can be seen that the addition of anti-strip agents to the asphalt binder caused an overall decrease in the cohesive bond energy. There are two main implications from a decrease in the cohesive bond energy of an asphalt binder. The first is a reduction in the amount of work, or intrinsic fracture energy, needed for a crack to propagate through the asphalt binder. The second implication of a reduction in the surface free energy or surface tension of the asphalt binder is that it enables better coating of the aggregate by the asphalt binder. However, the reduction in the intrinsic fracture energy is offset by the improved adhesion between the binder and the aggregate. This observation is supported by Lucic et al. (56) who found that the fracture resistance of a matrix increases due to improved adhesion between a polymer phase (asphalt binder) and filler particles (aggregate fines). Therefore, a reduction in the cohesive bond energy due to the addition of liquid anti-strip agents can be indirectly correlated to improved fracture resistance of the asphalt-aggregate matrix.

Table 6. Percent Change in Cohesive Bond Energy due to Addition of Anti-Strip Agents.

Asphalt	Anti-Strip	Γ Cohesive	% Change in Cohesive Bond Energy (Increase Positive)
Asphalt A 64-22 B	None	59.59	
	1	58.21	-2.32
	2	59.50	-0.15
Asphalt A 70-22 S	None	54.67	
	1	39.60	-27.56
	2	49.59	-9.30
Asphalt A 76-22 S	None	66.44	
	1	45.31	-31.80
	2	52.00	-21.74

B = Base asphalt binder; S = SBS modifier

In terms of the effects of aging, Table 7 shows that the percent change in the cohesive bond energy due to aging of the asphalt binder is more variable than the change due to the addition of anti-strip agents; however, the overall trend is a decrease in cohesive bond energy due to aging. Seven of the nine asphalt binders that were short-term aged showed a decrease in their cohesive bond energy, and six of the nine asphalt binders that were long-term aged showed a decrease in their cohesive energy. Of the five asphalt binders that showed an increase in the cohesive bond energy after aging, three were base (unmodified) binders. By evaluating the surface free energy components of the asphalt binders, it can be seen that the increase or decrease of the cohesive bond energy is mainly due to an increase or decrease in the γ^{LW} component of surface free energy, respectively.

Table 7. Percent Change in Cohesive Bond Energy due to Aging of the Asphalt Binder.

Asphalt	Aging	$\Gamma^{Cohesive}$	% Change in Cohesive Bond Energy (Increase Positive)
Asphalt B 64-22 B	Unaged	41.73	
	SAFT	36.96	-11.45
	PAV	52.46	25.70
Asphalt B 70-22 S	Unaged	45.33	
	SAFT	44.90	-0.95
	PAV	42.57	-6.08
Asphalt B 76-22 TRS	Unaged	44.46	
	SAFT	45.34	1.97
	PAV	39.45	-11.26
Asphalt B 76-22 S	Unaged	45.92	
	SAFT	44.12	-3.92
	PAV	48.19	4.95
Asphalt C 64-22 B	Unaged	64.34	
	SAFT	56.24	-12.58
	PAV	51.93	-19.28
Asphalt C 70-22 S	Unaged	71.56	
	SAFT	57.59	-19.52
	PAV	44.50	-37.81
Asphalt C 76-22 TRS	Unaged	69.09	
	SAFT	53.97	-21.89
	PAV	51.56	-25.37
Asphalt D 58-28 B	Unaged	37.92	
	SAFT	42.56	12.23
	PAV	49.25	29.88
Asphalt D 70-28 S	Unaged	46.02	
	SAFT	40.52	-11.94
	PAV	41.14	-10.60

B = Base asphalt binder; S = SBS modifier; TRS = Tire rubber.

As stated earlier, a decrease in the cohesive bond energy of an asphalt binder implies that less work is needed for a crack to propagate through an asphalt binder. In the case of the anti-strip agents, which were added prior to mixing, this was counteracted by the increase in the coating of the asphalt binder to the aggregate. However, with aging, the reduction in the cohesive bond energy occurs after mixing has occurred, therefore, there is no benefit of better coating due to the reduction in cohesive bond energy.

Energy Parameter

Figure 11 displays quartiles for the *ER* of all the unaged asphalt binders in combination with the aggregates listed in Table 2. From the previous studies, researchers know that a higher value of *ER* is desirable for better resistance to moisture damage (3, 57). The range of *ER* values determined by this study had a minimum of 0.10 and a maximum of 0.92. The range of *ER* values reported by Bhasin et al. (57), which had a minimum value of 0.15 and a maximum value of 1.15, is in good agreement to the values reported in this study. The *ER* can be used to determine the ranking of an asphalt binder-aggregate combination with respect to other choices in order to ascertain the compatibility of the asphalt binder and aggregates in terms of its resistance to moisture damage. Using this method the best asphalt binder-aggregate combination, with respect to moisture resistance, can be found.
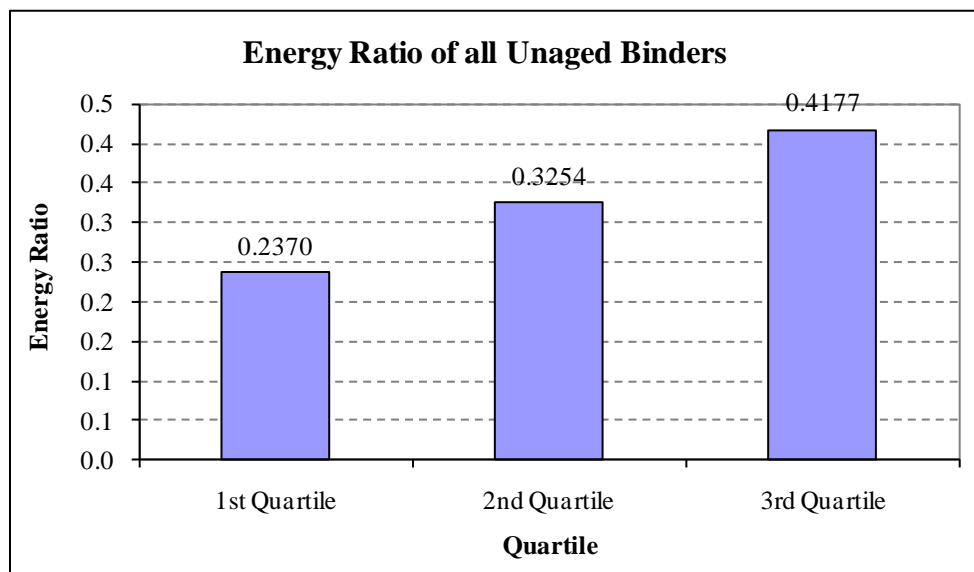
**Figure 11. Quartiles of the Energy Ratio of All Unaged Binders.**

Table 8 displays the percent change in the *ER* caused by the addition of anti-strip agents. The energy ratio is a function of the surface free energy of both the asphalt

binder and the aggregate as explained earlier. For this reason, an asphalt binder might show an improvement in *ER* with one aggregate, but a decrease in *ER* with another aggregate. From Table 8, it can be observed that the addition of anti-strip agents increased the *ER* in the majority of the cases. Only 10 out of the 66 cases showed a decrease in the *ER*, and only three had a decrease greater than 5 percent. This implies that the addition of anti-strip agents, in the majority of cases, will increase an asphalt mixture's resistance to moisture induced damage.

Table 8. **Percent Change in the Energy Ratio (*ER*) due to Addition of Anti-Strip Agents.**

Asphalt	Anti-Strip	GR	G1	G2	G3	G4	L1	L2	L3	Q	S1	S2
Asphalt A 64-22 B	1	6	1	3	0	5	4	2	3	3	0	2
	2	40	-1	15	-1	31	26	5	12	17	-1	14
Asphalt A 70-22 S	1	45	31	37	19	51	39	40	35	39	22	27
	2	-9	3	-2	0	-6	-5	2	-1	-3	2	-3
Asphalt A 76-22 S	1	14	14	11	0	16	13	17	15	13	8	9
	2	20	14	15	4	20	17	18	17	16	9	12

Q = Quartzite; S1 – S2 = Sandstone 1 - Sandstone 2; G1 – G4 = Gravel 1 – Gravel 4; L1 – L3 = Limestone 1 – Limestone 3, GR = Granite

There are three factors that determine the effectiveness of the anti-strip agents: the source of anti-strip agent, the type and mineralogy of the aggregate, and the chemical composition of the asphalt binder. Looking at Asphalt A 70-22 S in Table 8, Anti-strip 1 increased *ER* by at least 20 percent in every case, whereas Anti-strip 2 decreased *ER* in seven of the 11 cases. The effect of aggregate mineralogy can best be seen by looking at the case of Asphalt A 64-22 B with Anti-strip 2 in Table 8. Gravel 1 and Gravel 3 decreased *ER*; however, Gravel 2 and Gravel 4 increase *ER*. This effect can be seen in several other cases and shows that aggregate mineralogy plays a large role in resisting moisture related damage in asphalt concrete. This also implies that not all limestone, river gravel, or granite aggregates can be treated as the same; there are differences in the mineralogical makeup that will manifest themselves as differences in the moisture

resistance of the mixture. The effect of the chemical composition of the asphalt binder used can be seen by looking at Asphalt A 64-22 B with Anti-strip 1 and Asphalt A 70-22 S with Anti-strip 1 in Table 8. The unmodified base asphalt binder shows little or no improvement in *ER* when coupled with Anti-strip 1; however, when Anti-strip 1 is used with the modified asphalt binder, 70-22 S, a much greater improvement in *ER* is observed.

From Table 9, it can be seen that the percent change in the *ER* due to aging varies among the different binder-aggregate combinations. Upon closer inspection, it can be seen that the changes can be correlated with modifications made by the manufacturer. Asphalts B 64-22 B and 70-22 S both showed increases in *ER* after SAFT aging; however, Asphalt B 76-22 TRS showed a decrease in *ER* after SAFT aging and Asphalt B 76-22 S displayed both increases and decreases in *ER* (all minor) after SAFT aging. Moreover, Asphalt D 58-28 B showed a general decrease in *ER* after PAV aging, but Asphalt D 70-28 S showed a large increase in *ER* after PAV aging. This shows that modifications made by the manufacturer can have an effect, positive or negative, on the moisture susceptibility of an asphalt pavement once the asphalt binder has been aged.

Asphalt C from Table 9 showed an increase in *ER* for all PG grades, aggregates, and aging except for one case, Asphalt C 64-22 B with aggregate Gravel 3 after being PAV aged. Upon inspection of the surface free energy components of the aged binders, researchers noted that the increase or decrease of the polar components of surface free energy, γ^+ and γ^-, was directly proportional to the increase or decrease of an asphalt mix's moisture resistance, respectively; measured in terms of *ER*. The acid and/or base components of surface free energy increased for both types of aging for Asphalt C. Looking at another asphalt binder, Asphalt B 64-22 B from Table 9, it can be seen that an increase in *ER* occurred after SAFT aging, and a decrease in *ER* occurred after PAV aging. After inspection of surface free energy components, it was noted that SAFT aging increased the polar components, and PAV aging decreased the polar components; see Table 5.

Table 9. Percent Change in the Energy Ratio (*ER*) due to Aging of the Asphalt Binder.

Asphalt	Aging	GR	G1	G2	G3	G4	L1	L2	L3	Q	S1	S2
Asphalt B 64-22 B	SAFT	23	16	20	13	26	21	20	18	21	12	15
	PAV	-23	-19	-21	-13	-26	-21	-23	-20	-22	-15	-16
Asphalt B 70-22 S	SAFT	1	19	11	17	8	5	19	11	11	16	8
	PAV	-15	-2	-8	-3	-13	-12	-4	-7	-9	-2	-7
Asphalt B 76-22 TRS	SAFT	-34	-35	-35	-32	-38	-34	-37	-34	-36	-31	-30
	PAV	-24	-24	-25	-24	-26	-24	-25	-23	-25	-22	-22
Asphalt B 76-22 S	SAFT	-8	4	-2	3	-5	-5	2	-1	-2	3	-2
	PAV	-11	-5	-8	-4	-11	-9	-7	-7	-8	-4	-6
Asphalt C 64-22 B	SAFT	17	6	9	0	15	13	9	10	10	4	8
	PAV	63	7	26	-1	50	42	16	25	30	4	23
Asphalt C 70-22 S	SAFT	76	23	38	8	66	54	33	40	44	16	32
	PAV	195	66	106	35	184	140	96	103	120	46	82
Asphalt C 76-22 TRS	SAFT	40	12	21	1	35	30	18	22	24	7	18
	PAV	97	30	54	14	90	72	46	52	61	20	44
Asphalt D 58-28 B	SAFT	-4	0	-1	2	-3	-3	-1	-2	-2	1	-1
	PAV	-2	-2	-1	3	-3	-2	-3	-3	-2	0	0
Asphalt D 70-28 S	SAFT	-14	2	-6	-1	-11	-10	0	-4	-6	1	-6
	PAV	74	79	81	68	96	73	92	74	83	62	60

Q = Quartzite; S1 – S2 = Sandstone 1 - Sandstone 2; G1 – G4 = Gravel 1 – Gravel 4; L1 – L3 = Limestone 1 – Limestone 3, GR = Granite

Summary of Findings

Three types of modifications were investigated in this study. These included, modifications made to the binder by the manufacturer, modification due to addition of liquid anti-strip agents, and modification due to in-service oxidative aging of the binder. Important conclusions related to the effect of each type of modification on the fracture properties and moisture sensitivity of asphalt mixtures based on the changes observed in the energy parameters are as follows:

- Asphalt binders can be ranked based on their cohesive bond energy or any of its surface free energy components. This ranking can be used as a screening tool to

compare binders against each other and determine the ones that have the best resistance to fracture and moisture damage when used with aggregates.

- Modifications made to a base asphalt binder by the manufacturer to produce an asphalt binder with a higher PG grade typically increased the work of cohesion indicating better fracture resistance of the modified mixes. These modifications did not change the moisture sensitivity of the asphalt mixture significantly except when TRS was used as a modifier. In this case the acid component of the asphalt binder increased providing a potential improvement in the adhesive bond strength with most types of aggregates. For one of the asphalt binders, addition of SBS also showed improvement in the moisture resistance after aging.

- Addition of liquid anti-strip agents typically reduced the surface free energy and consequently the work of cohesion of the asphalt binders. Upon further examination, it was found that the decrease in the cohesive bond energy of the asphalt binder resulted from a decrease in the non-polar γ^{LW} component of the surface free energy. A reduction in the γ^{LW} component of the surface free energy allows better coating of the aggregate by the asphalt, improving interfacial adhesion and, thus, improving the fracture resistance of the mixture matrix. This can indirectly improve the fracture resistance by promoting better adhesion between the fines and the binder during the mixing and compaction process.

- Use of liquid anti-strip agents either improved or did not significantly change the moisture resistance of the asphalt binder with the selected aggregates (gauged using the parameter *ER*). The liquid anti-strip agents from the two different sources demonstrated different levels of changes in the moisture resistance even with the same asphalt binder and aggregate.

- Aging can have different impacts on different asphalt binders depending on the initial chemistry of the asphalt binder. Furthermore, differences in kinetics of different compounds formed during oxidative aging also influence the chemistry

and, consequently, the surface free energy components and performance of different asphalt binders after short- and long-term aging.

- In most cases long-term aging reduced the work of cohesion indicating lower fracture resistance of the aged binder. In the case of one neat binder and one modified binder the work of cohesion increased after long-term aging. After long-term aging, asphalt binders from one source demonstrated a decrease in the moisture sensitivity, while asphalt binders from the other source demonstrated an increase or no change with the moisture sensitivity with both the aggregates used in this study. Authors speculate that the differences in the polar functional groups between the two unaged asphalt binders resulted in different surface properties due to aging.

CHAPTER IV

THE EFFECTS OF CHANGES IN pH ON THE SURFACE FREE ENERGY COMPONENTS OF WATER*

Introduction

Water (moisture) is extremely detrimental to pavement performance. Moisture damage can occur within the asphalt binder or at the asphalt binder-aggregate interface. Moisture, which arrives at the aggregate surface will interact with the aggregate particle, causing properties of the water to change. The easiest change to measure is an increase or decrease in the pH of the water. A more difficult to measure, but equally important change that can occur in the water, is a change in its surface free energy and/or surface free energy components. A change in the surface free energy components of the water has the possibility of retarding or aggravating the moisture damage process. The results showed that the pH of the water increased slightly in all cases due to contact with the aggregates; however, no significant change was found in the total surface tension or surface free energy components of the water at the tested pH levels.

Materials

Four asphalt binders (Table 10) and four aggregates (Table 11) were employed to assess the influence of water's pH on its surface free energy and surface free energy components. All asphalt binders used in this study were PG 76-22 S with no aging and no anti-strip agents added, albeit from different sources. These asphalt binders were

chosen for their variable surface free energy components, measured using the Wilhelmy Plate method. Asphalt *O* had a very high acid component, Asphalts *K* and *P* had a higher basic component, and Asphalt L was almost completely non-polar. The rationale for selecting these four binders with different surface energy characteristics is described in the sections that follow.

Table 10. Surface Free Energy of Asphalt Binders.

Asphalt	γ^+	γ^-	γ^{LW}	γ^{Total}
O	1.50	1.27	10.24	13.00
K	0.19	1.18	17.20	18.14
P	0.00	0.88	22.68	22.77
L	0.00	0.07	19.24	19.24

The four aggregates used for the pH study were granite, sandstone, granite-sandstone mix, and river gravel. Table 11 displays the labeling scheme used for the aggregates. Aggregate *GR* was a granite with a low concentration of quartz, a high concentration of albite and anorthite, and appeared to be quartz monzodiorite. Aggregate *S* was a quartz rich sandstone. Aggregate *GRS* was a mixture of granite and sandstone, and aggregate *G* was a river gravel.

Table 11. Aggregate Labeling Scheme.

Aggregate Label	Aggregate Lithology
GR	Granite
S	Sandstone
GRS	Granite-Sandstone Mix
G	Gravel

Methodology

Using a similar process to the one utilized by Yoon and Tarrer (9), the pH of different water samples were altered. Various crushed aggregates passing sieve #16 (1.18 mm) retained on sieve #30 (0.6 mm) were placed in separate glass beakers filled with distilled water, and the pH was allowed to come to equilibrium. Distilled water with no aggregate was placed in another beaker, and its pH was also measured. The distilled water was used as a control to evaluate the change in pH of the water in contact with aggregates.

Two properties were measured after the pH of the different water with aggregate immersed in them reached equilibrium. The first property is the total surface tension of the water using the sessile drop method (which is equivalent to the total surface free energy), and the second is the surface free energy components of the water using the Wilhelmy Plate method.

The total surface tension, or surface free energy, of the water was measured using the pendant drop volume method using an image analysis software that accompanied the goniometer (sessile drop device) (58, 59). A high resolution digital camera was used to take pictures of the suspended drop of water every 3 seconds in order to calculate the corresponding surface tension in real time as the volume of the drop increased, Figure 12. As seen in Figure 13, the volume of the drop was increased until the equilibrium surface tension was achieved. The volume of the drop was then increased and decreased several times to ensure the equilibrium surface tension was, in fact, stable. Once a stable surface tension value was achieved, a best fit line was drawn through the points corresponding to the equilibrium surface tension, and the average surface tension value was recorded.
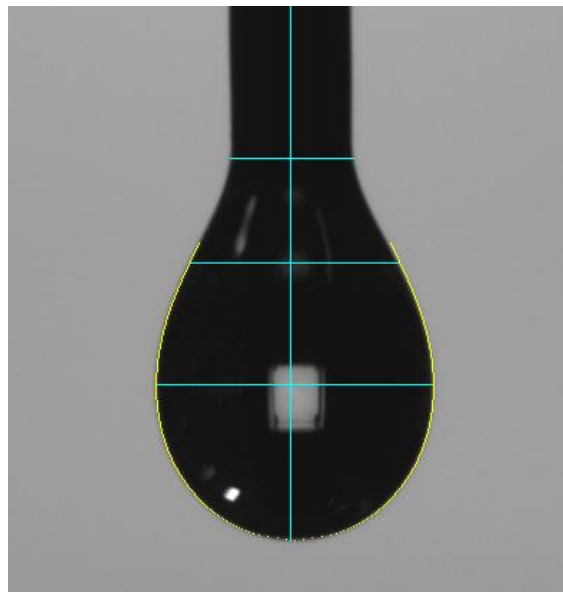
Figure 12. Image of Water Drop Used to Calculate Total Surface Tension by Pendant Volume Method.
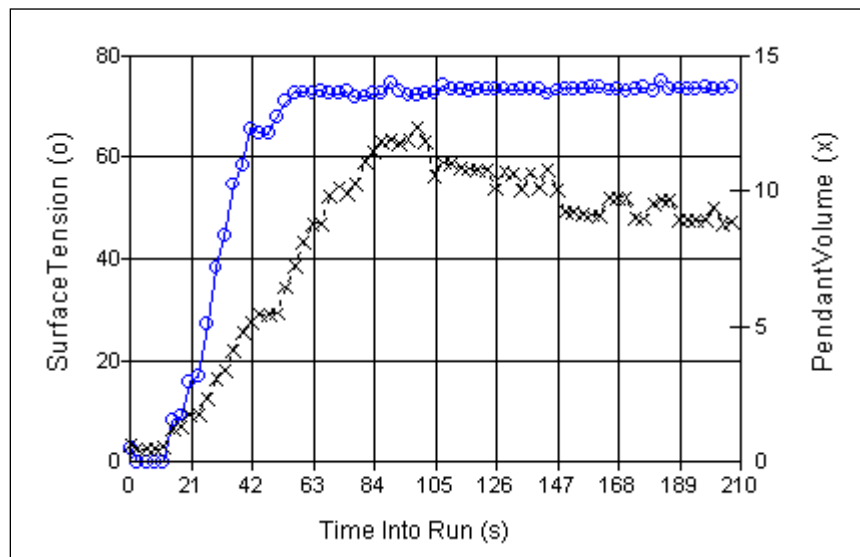
Figure 13. Surface Tension Versus Pendant Volume (Sessile Drop).

O – Surface Tension;   X – Pendant Volume

However, Equations 4 and 6 can only be used if all three surface energy components of the water with an altered pH are known. The surface free energy components of the pH altered and control sample of distilled water were determined using the Wilhelmy Plate method in a new fashion. The conventional methodology for using the Wilhelmy Plate device is that the contact angle of the material with unknown surface energy components (e.g., asphalt binder) is measured with three to five different probe liquids with known surface free energy components. In this study, the process was reversed and three to four different asphalt binders with known surface free energy components were used to back calculate the unknown surface free energy of the liquid, i.e., the pH modified water. The required analytical expressions to carry out this approach are discussed below.

The Wilhelmy Plate device measures the weight of a slide coated with the asphalt binder suspended in a probe liquid. The contact angle between the binder and the probe liquid is computed from the equation below:

$$\cos\theta_i^{pH} = \frac{\Delta F + V_{im}\left(\rho_L - \rho_{air}\right)g}{P_t \ \gamma_{LpH}^{Total}} \qquad (17)$$

where θ_i^{pH} is the contact angle, ΔF is the change in force measured by the balance, V_{im} is the volume of the immersed plate, ρ_L is the density of the probe liquid, ρ_{air} is the density of the air, g is the local acceleration of gravity, P_t is the perimeter of the asphalt coated plate, and γ_{LpH}^{Total} is the total surface tension of the water with an altered pH determined using the sessile drop method.

It is assumed that the change in density of water due to the change in pH is negligible because it is caused by the absorption of hydrogen ions, which have very little mass, onto the surface of the aggregate particles. Therefore, for a given combination of binder, liquid, and depth of immersion, ΔF, V_{im}, ρ_L, ρ_{air}, g, and P_t are all constants. By using Equation 17 and the Young-Dupre equation, with the assumption

that equilibrium film pressure is neglected for asphalt, Equation 18 can be obtained as follows:

$$\gamma_{Lph}^{Total}\left(1+\cos\theta_i^{pH}\right)=2\sqrt{\gamma_i^{LW}\gamma_{LpH}^{LW}}+2\sqrt{\gamma_i^{+}\gamma_{LpH}^{-}}+2\sqrt{\gamma_i^{-}\gamma_{LpH}^{+}} \qquad (18)$$

where γ_{LpH}^{Total} is the surface tension of the water with an altered pH or the control sample of distilled water determined using the sessile drop device, θ_i^{pH} is the contact angle determined from the Wilhelmy Plate device using the ith binder, subscript i denotes the ith binder, subscript *LpH* denotes the pH altered water or the control sample of distilled water as the case may be, and superscripts Total, LW, +, and – denote the total, Lifshitz-van der Waals, acid, and base components, respectively. Equation 18 can be rewritten as follows:

$$\gamma_{Lph}^{LW}+2\sqrt{\gamma_{LpH}^{+}\gamma_{LpH}^{-}}+\gamma_{Lph}^{Total}\left(\cos\theta_i^{pH}\right)=$$
$$2\sqrt{\gamma_i^{LW}\gamma_{LpH}^{LW}}+2\sqrt{\gamma_i^{+}\gamma_{LpH}^{-}}+2\sqrt{\gamma_i^{-}\gamma_{LpH}^{+}} \qquad (19)$$

Equation 19 is used to determine the surface free energy components of the pH altered water using asphalt binders with known surface free energy values.

As discussed earlier, the typical procedure to determine the surface free energy components of an asphalt binder is to measure its contact angle with at least three different probe liquids with known surface free energy components and then back calculate the surface free energy components of the binder. In this case, it is of interest to determine the surface free energy components of the liquid (pH altered and control sample of distilled water). Therefore, contact angles of at least three asphalt binders with known surface free energy components were measured with each of the liquids, and the unknown surface energy components of the liquid were back calculated. In this research four asphalt binders were used to introduce redundancy and improve the robustness of the back calculated values. The four asphalt binders, for which the surface

energy components were measured previously, were dipped into each pH altered water sample as well as the control distilled water, and the contact angle was recorded. The sum of square of error (SSE) for the four asphalt binders was determined using Equation 20 as follows:

$$SSE = \sum\nolimits_{i=1}^{4} \left(\begin{array}{c} \gamma_{Lph}^{LW} + 2\sqrt{\gamma_{LpH}^{+}\gamma_{LpH}^{-}} + \gamma_{Lph}^{Total}\left(\cos\theta_i^{pH}\right) - \\ 2\sqrt{\gamma_i^{LW}\gamma_{LpH}^{LW}} - 2\sqrt{\gamma_i^{+}\gamma_{LpH}^{-}} - 2\sqrt{\gamma_i^{-}\gamma_{LpH}^{+}} \end{array} \right) \qquad (20)$$

Microsoft Excel© Solver was used to minimize the SSE by changing the Lifshitz-van der Waals, acid, and base components of the surface free energy of the pH altered water or the control sample of distilled water using an iterative procedure. Equation 20 is nonlinear; therefore, the possibility of multiple false solutions exists. In order to minimize this error, the nonpolar, or γ^{LW}, component of surface free energy was fixed at its theoretical value of 21.8 ergs/cm^2 in this study because a change in pH is caused by an increase or decrease in the positively or negatively charged ions in a solution, and therefore, theoretically, should not affect the γ^{LW} component of surface free energy.

Results

Table 12 below displays the results of the tests of total surface tensions of the pH altered water that were obtained using the sessile drop method. The total surface tension of the five measured liquids does not change significantly, as is clearly shown in Table 12. The highest percent change between the total surface tension of the theoretical water and one of the measured waters occurred in water modified with aggregate *GR*. This percent change was only 0.824 percent (or 0.6 ergs/cm^2) and is not large enough to warrant a change in the total surface free energy. If distilled water is used as a basis, then the maximum percent change occurs with water modified with aggregate *S*. This percent change was less than 1 percent (or 0.7 ergs/cm^2). The differences in the total

surface tension of the various waters are not great enough to assert that there is any change in the total surface tension of the waters due to a change in the pH.

Table 12. Surface Tensions of Water with Different Aggregates Measured Using Sessile Drop Method.

Water with Aggregate	Total Surface Tension
GR	73.4
S	72.3
GRS	72.9
G	73
(No Aggregate Contact) Control Distilled Water	73

While the total surface tension or surface free energy of the pH altered water did not change significantly, the Wilhelmy Plate device was used to assess if there are any differences in the surface energy components of the pH altered water. Figure 14 displays the surface free energy components and total surface free energy of the water, measured using the Wilhelmy Plate device, which had the different aggregates submerged in it.

Effect of pH on Surface Free Energy Components
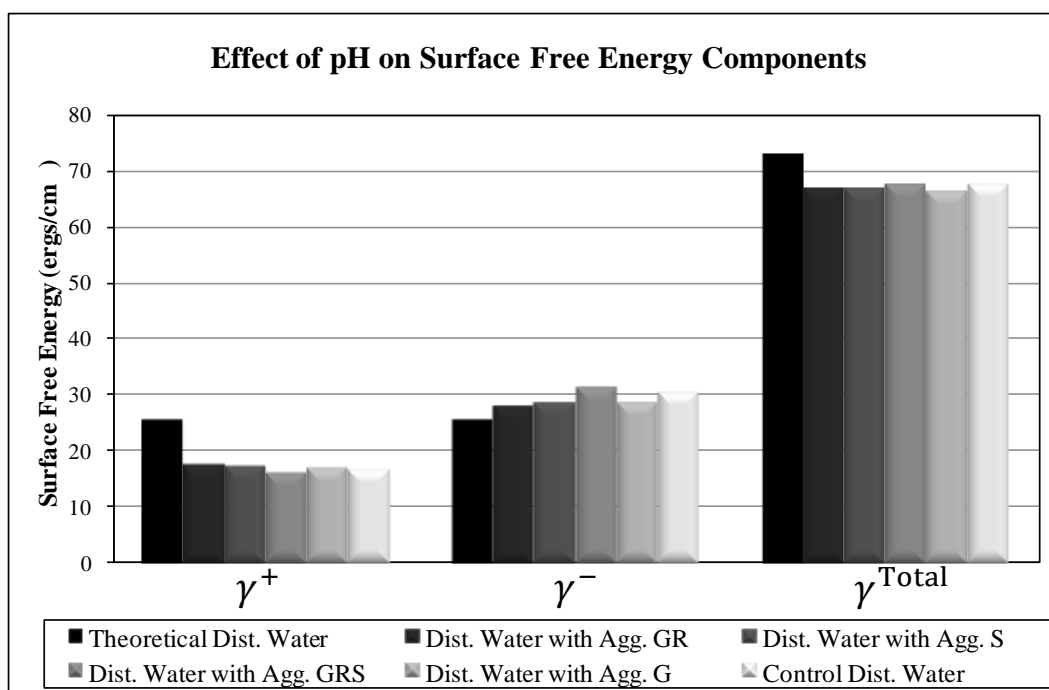
Figure 14. Surface Free Energy Components of Water Modified with Different Aggregates.

There was an inherent systematic error involved in this methodology because theory and lab measurements were used twice consecutively to arrive at the final values. Intrinsic theoretical and measurement errors were propagated when the surface free energy components of the four asphalt binders were determined using measurements with four probe liquids. These errors were further propagated when the four asphalt binders were used to calculate the surface free energy components of the pH altered water. For distilled water, the back calculated components demonstrated that the acid component was apparently lower as compared to the base component. This was most likely an artifact of error propagations. Not-withstanding these limitations in the back calculation approach, a comparison between the respective surface energy components for the pH altered water and the control sample of distilled water was still made.

Using the values from the control sample of distilled water as a reference, the total surface tension or surface free energy of the pH altered waters varied from -1.03 to 0 ergs/cm^2 with no specific trend with respect to the pH value. Similarly, the variation

in acid and base components with reference to the distilled water was -0.50 to +1.07 and -2.42 to +0.92 ergs/cm^2, respectively. In general, the variations in the surface energy components were small compared to the reference values and showed no specific trend with respect to the pH of the water. Within the range of pH that was achieved by exposing distilled water to aggregates in this project, there is no significant correlation between the change in surface free energy components and the pH of the water.

Summary of Findings

This chapter evaluated the effect of pH on the surface free energy components of water due to contact with aggregate particles was studied. The main findings and conclusions from the results discussed in this paper are:

- The sessile drop and Wilhelmy Plate were successfully used to capture the total surface tension of water and the surface free energy components of the same water, respectively.

- While the methodology used with the Wilhelmy Plate was able obtain the relative changes in surface free energy components of pH modified waters, it would not be a viable option if the absolute values were required due to error propagation.

- No significant changes in the total surface free energy or the acid and base components of surface free energy were observed when compared to values obtained using a control sample of distilled water. Within the range of pH that was achieved by exposing distilled water to aggregates in this project, there is no significant correlation between the change in surface free energy components and the pH of the water.

CHAPTER V

BOND ENERGY VERSUS TOTAL WORK OF FRACTURE OF ASPHALT BINDER ON STAINLESS STEEL SUBSTRATE*

Introduction

The results in the previous chapters have demonstrated that surface free energy and its associated energy indices have been successfully used to determine the resistance of asphalt binders to cohesive failure and the resistance of asphalt-aggregate systems to adhesive failure in both dry and wet conditions. Given the strong correlation of surface free energy with observed damage in the field, this property has been proposed as a screening tool for selecting materials that can be used to produce durable asphalt mixtures. It is recognized that the magnitude of the cohesive or adhesive bond energy calculated based on surface free energy measurements can be much smaller in magnitude compared to the total work of fracture measured using mechanical tests, such as the pull-off or peel-off tests. However, evidence in the literature indicates that, despite the large difference in magnitude, there exists a relationship between these two quantities that justifies the use of bond energy to characterize resistance of composite systems to cohesive or adhesive failures. The information from the literature was very useful in understanding some mechanisms that govern the fracture behavior of asphalt binders and asphalt mixtures, and to develop an experimental setup for conducting pull-off tests on asphalt binders that allow recording the force and displacement throughout the test. This chapter presents experimental data regarding cohesive and adhesive failures in asphalt-metal systems obtained from the pull-off test demonstrating the relationship between bond energy and total work of fracture.

Total Work of Fracture of Asphalt Binder and Asphalt Binder-Aggregate Interfaces

Chapter II of this dissertation has provided significant literature review on methods for measuring the total work of fracture and its relationship to the bond energy of various adhesive materials. This section reviews the limited studies that focused on measuring the total work of fracture of asphalt binders. One of the earlier studies was by Marek and Herrin (50) who evaluated the effects of loading rate, temperature, film thickness, asphalt consistency, and asphalt source on the tensile behavior and failure characteristics of thin asphalt films. The researchers varied film thickness and noted three failure modes: brittle failure, mixed mode failure, and flow failure. The failure mode was observed to depend on temperature, loading rate, and film thickness. They reported that an increase in loading rate caused an increase in the tensile strength when the temperature and film thickness were held constant. Conversely, they reported that an increase in temperature caused a decrease in tensile strength when loading rate and film thickness were held constant.

Harvey and Cebon (60, 61) evaluated the brittle and ductile failure of asphalt binder using aluminum pull-off and double cantilever beam. The researchers found that under brittle fracture conditions, the peak stress was rate independent; however, the peak stress was rate dependent when ductile failure occurred. They also reported that the strain at failure was rate independent for both ductile and brittle fracture. In order to achieve brittle failure, the researchers tested the samples below the glass transition temperature of the asphalt and used time-temperature superposition to calculate a temperature compensated strain rate in order to compare tests performed at different temperatures.

Cho et al. (62) used a pull-off test known as the pneumatic adhesion tensile testing instrument (PATTI) to measure the moisture susceptibility of different base and polymer modified asphalt binders adhered between a porous ceramic disc and aggregate surface. The researchers were interested in determining the correlation between the pull-off strength ratio of moisture conditioned and unconditioned asphalt specimens to the

tensile strength ratio of moisture conditioned and unconditioned mixture specimens. In a different study, Kanitpong and Bahia (63) also used the PATTI test to evaluate the effect of the addition of anti-strip additives and polymers on the moisture susceptibility of the asphalt-aggregate interface. The researchers reported that water reduced the pull-off strength, and the failure mode transitioned from cohesive to partly or fully adhesive after moisture conditioning. Copeland et al. (64) used the PATTI test to investigate the effects of different types of binder modifications and aging on pull-off tensile strength between the asphalt binder and the ceramic substrate. Similar to the results from Kanitpong and Bahia (63), the authors found that moisture decreased the pull-off tensile strength between the two materials. The authors concluded that not all modification procedures increased the moisture resistance of the adhesive bond (64).

Most studies that used the pull-off test for evaluating asphalt binders and asphalt-aggregate systems were concerned with measuring only the ultimate bond strength. Since information on both loading and deformation is required to calculate the total work of fracture of a composite system, the test setup developed in this study was instrumented to measure not only the strength but also the complete load and deformation history. The following sections include a description of the measurement setup, the protocols for preparing and testing samples, and the analysis and discussion of the results from the test.

Experimental Measurements of Bond Energy

As mentioned previously, the bond energy is a thermodynamic material property. The computation of the cohesive bond energy of an asphalt binder is achieved by means of its surface free energy (Equation 2), while the computation of the adhesive bond energy requires surface free energy component information for both binder (adhesive) and substrate (adherent) materials (Equation 3).

The fracture experiments discussed in the following section were conducted on three asphalt binders (designated as AAB, AAD, and ABD) with sample holders

(substrate) made of stainless steel. The asphalt binders were procured from the Strategic Highway Research Program Materials Reference Library. They were specifically chosen because of their range of surface free energy values as determined from previous research at Texas A&M University (65). The three asphalt binders were tested using the Wilhelmy Plate device to determine their SFE values (Table 13). Details on the measurement of surface free energy of these materials can be found in Little et al. (3). The surface free energy terms in Table 13 stand for the following:

- LW stands for the Lifhsitz - van der Waals component of surface energy, which corresponds to dipole interaction,
- Acid stands for the Lewis acid component of surface interaction, and
- Base stands for the Lewis base component of surface interaction.

In terms of the metallic sample holders, Hallab et al. (66) measured the surface free energy of a 316L stainless steel using a sessile drop apparatus and reported the values shown in Table 14.

Table 13. Surface Free Energy Values of Asphalt Binders.

Asphalt	Surface Free Energy Components (mJ/m^2)			Total (mJ/m^2)	Standard Deviation (mJ/m^2)		
	LW	Acid	Base		LW	Acid	Base
AAB	13.8	0.3	2.3	15.5	0.8	0.1	0.3
AAD	19.5	0.0	0.7	19.5	0.4	0.0	0.2
ABD	34.0	0.0	0.1	34.0	0.6	0.0	0.1

Table 14. Surface Free Energy Components of Stainless Steel.

Material	W (mJ/m^2)	Polar (mJ/m^2)	Total (mJ/m^2)
316L	33.40	96.24	129.65

Surface free energy values in Tables 13 and 14 were used in Equations 2 and 3 to obtain the cohesive and adhesive bond energy values displayed in Table 15.

Table 15. Adhesive Bond Energy between Asphalt and Stainless Steel and Cohesive Bond Energy of Asphalt Binders.

Failure Type	Bond Energy (mJ/m^2)		
	AAB	**AAD**	**ABD**
Cohesive	30.92	39.04	68.07
Adhesive (with stainless steel Substrate)	213.29	243.55	259.91

Experimental Measurements of Total Work of Fracture

The experimental setup used in this research consisted of testing an axisymmetric flat metallic punch containing a thin layer of asphalt binder in a displacement controlled direct tension apparatus. The purpose of this system was to measure the force and displacement of asphalt binders with different film thicknesses in order to compute the fracture energy (i.e., total work of fracture, W_T) of the metal-binder systems. The three neat asphalt binders (i.e., AAB, AAD and ABD) were tested with asphalt film thicknesses ranging from 5 to 50 μm. The displacement rate was held constant at 0.01 mm/sec. The force was recorded using a 5 kip load cell, and displacement of the thin asphalt film was measured using a high-resolution digital camera with image correlation software.

Sample Preparation

     The sample holders were constructed from 300 Series 18/8 stainless steel. A schematic of the dimensions of a sample holder is shown in Figure 15a, with a tested sample displayed in Figure 15b. The testing surface is a flat axisymmetric 10-mm diameter surface. The 12 x 2 x 6-mm portion of the sample holder is used to lock the sample into the testing frame.

     The sample holders were initially polished using fine grit wet/dry sandpaper (ANSI Grit Number 1200) with water to remove the larger texture left by the manufacturing process. Following sanding, the samples were cleaned in a sonic water bath to remove all metal particles from the surfaces. After drying, the testing surface was polished on a rotating platen with a short nap nylon polishing cloth attached. A 3-μm diamond spray was applied to the surface of the polishing cloth along with a lubricant. The testing face of each sample holder was polished to a mirror finish and then submersed in a sonic bath of alcohol to remove the lubricant and metal particles. After being removed from the sonic bath, the sample holders were rinsed with distilled water to remove any traces of the alcohol. This procedure was initially repeated for each sample holder, with the fine polishing repeated periodically when scratches appeared on the testing face.
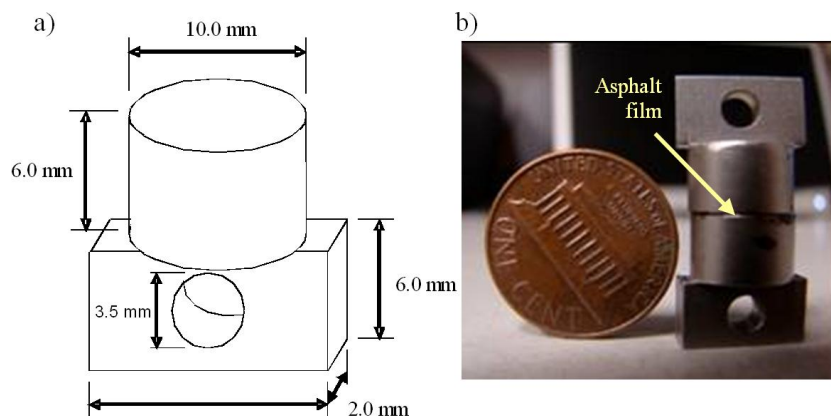
Figure 15. a) Sample Holder Dimensions, and b) Picture of a Tested Sample.

Asphalt binder samples were prepared between the two stainless steel substrates using an AR 2000 rheometer manufactured by TA Instruments, with a gap resolution of 1-μm. The end of the sample, which is attached to the loading frame, was designed to fit into grips supplied by the manufacturer. After alignment of the sample holders was checked, a propane torch was used to heat the substrate surface of the sample holders to remove water vapor and organic matter. A small drop of asphalt binder, heated to 130°C was applied to the substrate surface of the bottom sample holder. The gap was reduced to the desired film thickness and the sample was allowed to cool for 15 minutes before the excess asphalt binder was removed by means of a heated razor blade.

The prepared samples were conditioned for 24 hours at 10°C to guarantee the formation of a full adhesive bond. After conditioning, the samples were moved to the enclosed testing chamber, which was maintained at a constant temperature of 23°C. Three layers of flat white acrylic paint were applied to the outside of the sample holders. Painting the samples was a necessary step to provide the conditions required for the digital camera and correlation software to compute the displacement of the specimen during the test. Following painting, a light speckle coating of black flat spray paint was applied. Figure 16 shows a representative sample. The samples were returned to the temperature chamber and allowed 2 hours to equilibrate to the testing temperature.
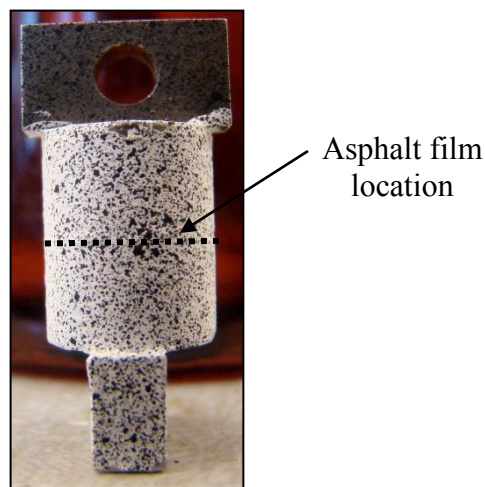
Figure 16. Prepared Sample for Use with Image Correlation Software.

Testing and Data Acquisition Systems

Testing of the samples was performed using a UTM-5P pneumatic testing machine produced by IPC Global. The program Stress/Strain from IPC Global controlled the operation of the pneumatic testing machine and recorded force, loading rate, and stress. The entire testing apparatus was contained inside an environmental chamber that controlled the test temperature at 23°C. The load applied to the sample was measured by means of a 5-kip load cell. A diagram of the experimental setup is shown in Figure 17.

The stainless steel grips were custom designed to hold the sample holders. The upper grip was attached directly into the load cell, and the lower grip was attached to the floor of the testing chamber by means of a locking silicone-stainless steel joint. The locking silicone-stainless steel joint served the purpose of aligning the top and lower grips. A prepared asphalt sample was inserted into the bottom grip, Figure 18, and locked in using a compression joint. The inside of the bottom grip was textured to provide a better hold and prevent the sample from moving during testing. The upper grip was lowered and attached to the sample through bearing force on a screw.
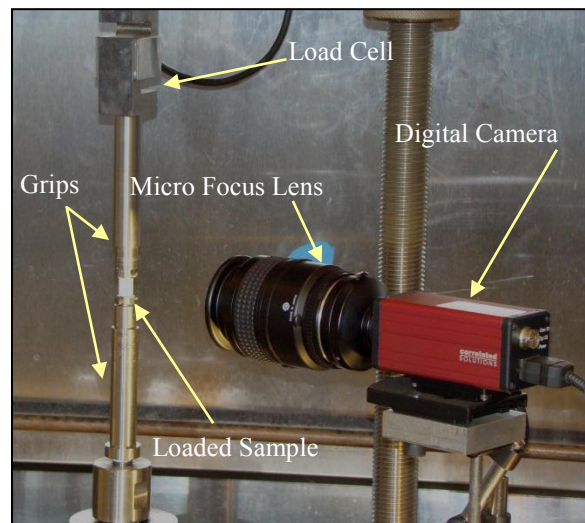
Figure 17. Schematic of the Experimental Setup.
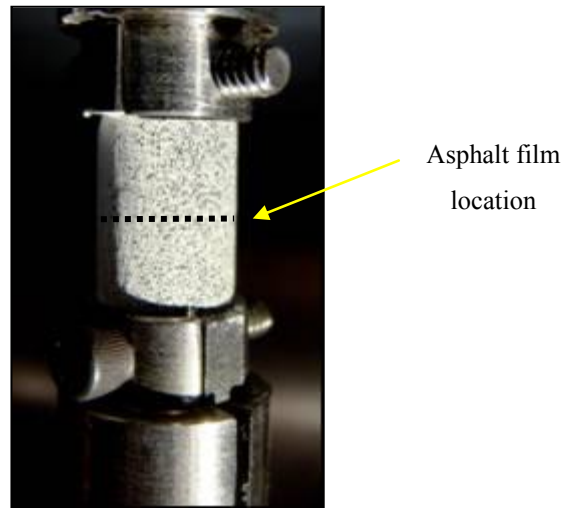
Figure 18. Prepared Sample Loaded into Testing Fixture.

As mentioned previously, the deformation data acquisition system used during the experiment consisted of a 3 megapixel digital camera, which captured images of the sample every 0.10 seconds. The digital camera and software operating it were produced by Correlated Solutions. The camera was mounted on a magnetic holder located inside the testing chamber. Two benefits of this configuration were a clearer image (not looking through glass door of environmental chamber) and increased resolution (camera closer to sample). The image analysis system has a resolution of (1/50,000)*(dimension of one side of image seen by camera). To maximize the resolution, a micro-focus lens from Nikon was used to magnify the image to 1-cm by 1-cm. The micro-focus lens produced a maximum resolution of 0.20-μm. A manually operated light increased illumination of the sample, which increased the contrast between the white paint and black speckle pattern.

The digital image correlation software divided the area of interest (AOI) into small cells and gave each cell a value for horizontal, vertical, and shear strain along with a value of vertical and horizontal deformation. Each test was comprised of roughly 300 images, of which 20 were chosen and used to calculate the evolution of strain and deformation in the sample. Figure 19 illustrates the strain data extracted from one image

of the test mapped onto the sample with the AOI. Σ_{xx}, Σ_{yy}, and Σ_{xy} represent the horizontal, vertical, and shear strain, respectively. The failure plane occurred where the strain was a maximum.
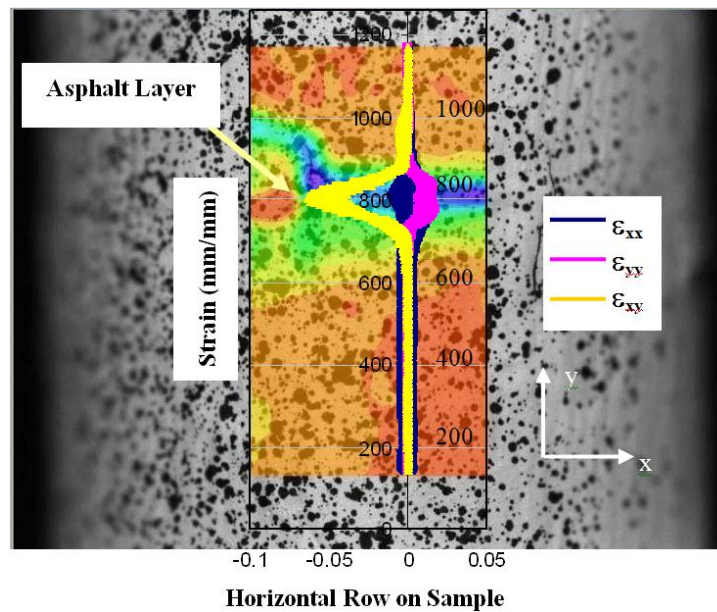
Figure 19. Shear, Vertical, and Horizontal Strain Distributions Measured Using Image Correlation Technique prior to Alignment Correction.

It is noteworthy that one of the main benefits offered by the digital image correlation system is that it provided information about the dynamics of the sample motion and deformation during testing. This information was very useful in improving the testing conditions and reducing variability. For example, deformation data during the test were used to identify misalignment problems, in the form of shear strain (Figure 19) and horizontal deformation that were corrected prior to executing the experiments. Figure 20 displays a visual representation of the shear strain in a sample before and after alignment correction. The reduction in shear strain was achieved by better alignment of the testing fixture.
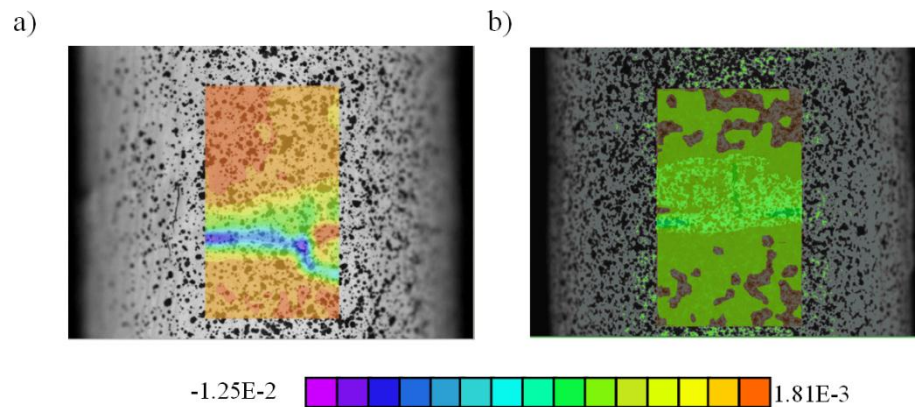
Figure 20. Example of Shear Strain (a) before Misalignment Correction, and (b) after Alignment Correction.

Displacement information from each image file was extracted for the area within which all the strain and deformation occurred. The program calculated the displacement of the upper sample holder at row 950 and the displacement of the lower sample holder at row 600 shown in Figure 19. The displacement of the thin asphalt film was calculated as the difference between the displacement of the upper and lower sample holders. Although the loading rate of the system was controlled by the built-in actuator LVDT and maintained at a constant rate of 0.01 mm/sec during the test, it was found that the actual displacement rate of asphalt film, measured with image correlation, was not constant throughout the test. The displacement rate was low initially and increased as the test proceeded. This shape of displacement curve occurred regardless of failure mode or asphalt source. This information was later used to compute the total work of fracture of the test specimens.

The shear, vertical, and horizontal strains were calculated between the same rows of interest. The row with the highest value of a respective strain was considered the plane of failure for that respective type of strain. The respective strain was reported as the maximum for the image being analyzed.

Analysis of Failure Mode

As explained earlier, three different neat asphalt types were used in this research: AAD, AAB, and ABD. A film thickness sweep was conducted on the three asphalts. Figure 21 displays representative images of different failure surfaces. Similar to the results reported by Marek and Herrin (50), cavitation formation and growth were noted in all samples regardless of thickness.

Transition from adhesive to cohesive failure
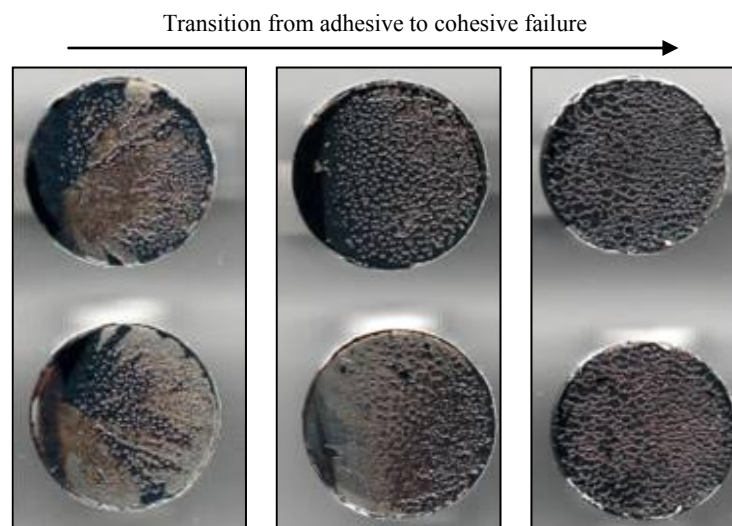
Figure 21. Examples of Adhesive Failure (Left), Mixed Mode Failure (Center), and Cohesive Failure (Right).

Immediately after completion of the test, the specimen was removed, and each sample holder was scanned using a flat-bed scanner in order to investigate the predominant type of failure (i.e., adhesive or cohesive). The resolution used to scan the sample holders was 16-μm/pixel. The image analysis software ImageJ was used to calculate the gray intensity of the surface. The gray level rises as more of the sample holder substrate becomes exposed, indicating more adhesive or less cohesive failure. The results in Figure 22 clearly show that the gray level is higher at lower film thicknesses indicating a more adhesive-type failure, independent of the source of asphalt binder. In addition, the failure surface images were analyzed to estimate the percent of substrate exposed after failure and the percent substrate covered by the asphalt binder. These values were used to estimate the percent of adhesive (P_a) and cohesive (P_c) failure within the specimen, respectively. The higher variability in the gray level at 15-μm is attributed to the transition between cohesive and adhesive failure, which occurs at this film thickness. Because of the transition in the failure mode, slight variations in the film thickness or defects on the surface of the metal substrate would cause the percent adhesive/cohesive failure to deviate, consequently causing increased variation in the measured gray level.
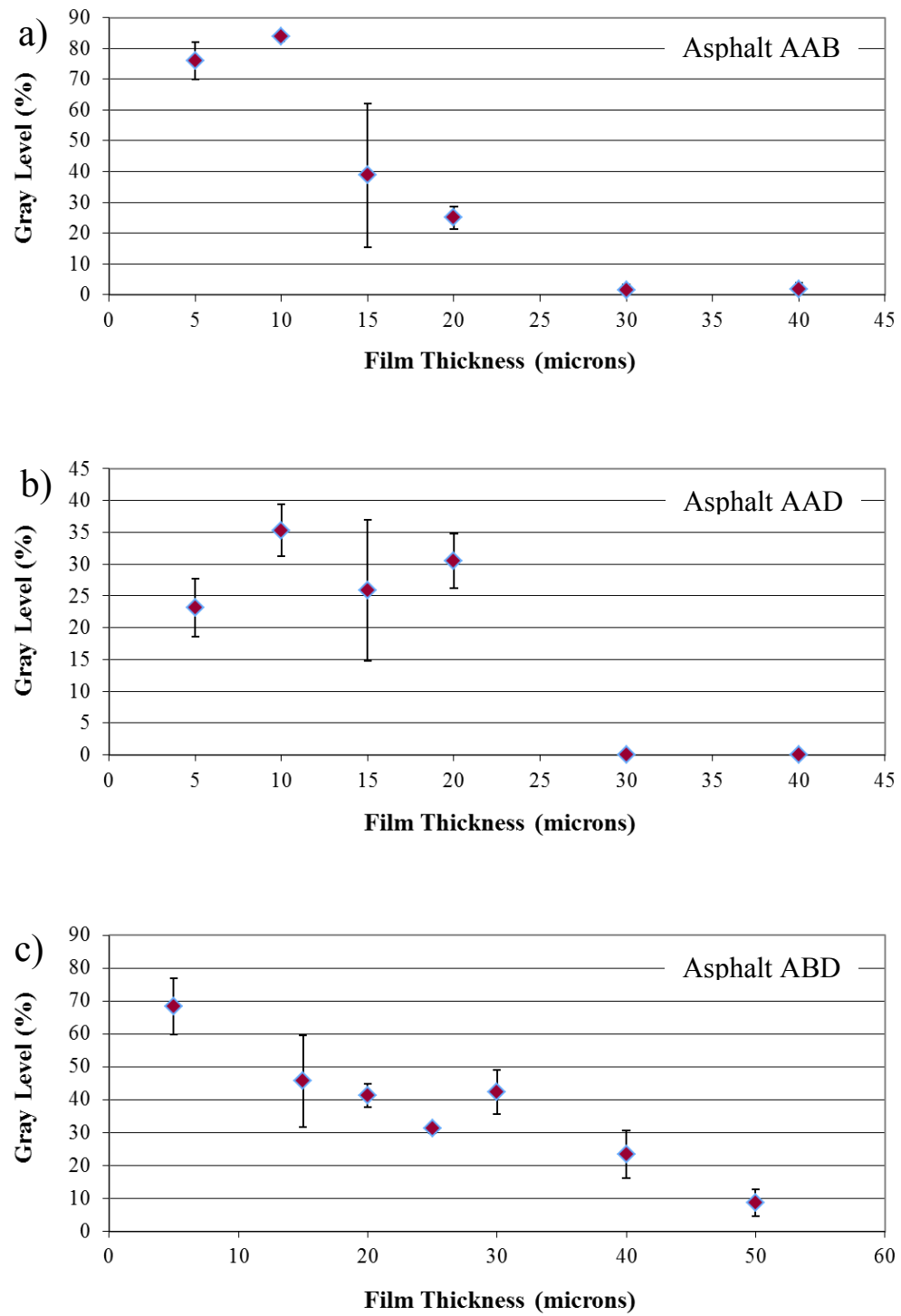
Figure 22. Gray Level Intensities of Sample Holder Surface at Different Asphalt Film Thicknesses.

Effect of Film Thickness on Strength and Displacement at Failure

The maximum force and displacement resulting from the direct tension tests in the three types of asphalt binder are shown in Figure 23. Error bars representing plus or minus 1.25 standard deviations are included for both force and displacement measurements. There are several conclusions that can be drawn from this figure. First, it is observed that there is a decrease in the maximum force at failure as the film thickness increases. Asphalt AAD, from thinnest (5-μm) to thickest film (40-μm), showed 54.1% decrease in the maximum load at failure, asphalt AAB showed 46.5% decrease in the maximum load at failure, and asphalt ABD showed 42.7% decrease in the maximum load at failure. The displacement at failure increased with an increase in the film thickness. When the failure mode transitioned to cohesive failure at a film thickness of 40-μm, there was a large increase in the displacement until failure.

ABD has about twice the cohesive bond energy of AAD or AAB (Table 15). As a result, ABD experienced a less cohesive (more adhesive) type of failure at thicker film thicknesses than the other two binders. This behavior is reflected in the higher gray level for ABD at film thicknesses of 40-μm and 50-μm (Figure 22) and the higher failure loads (Figure 23) in comparison with AAB and AAD.
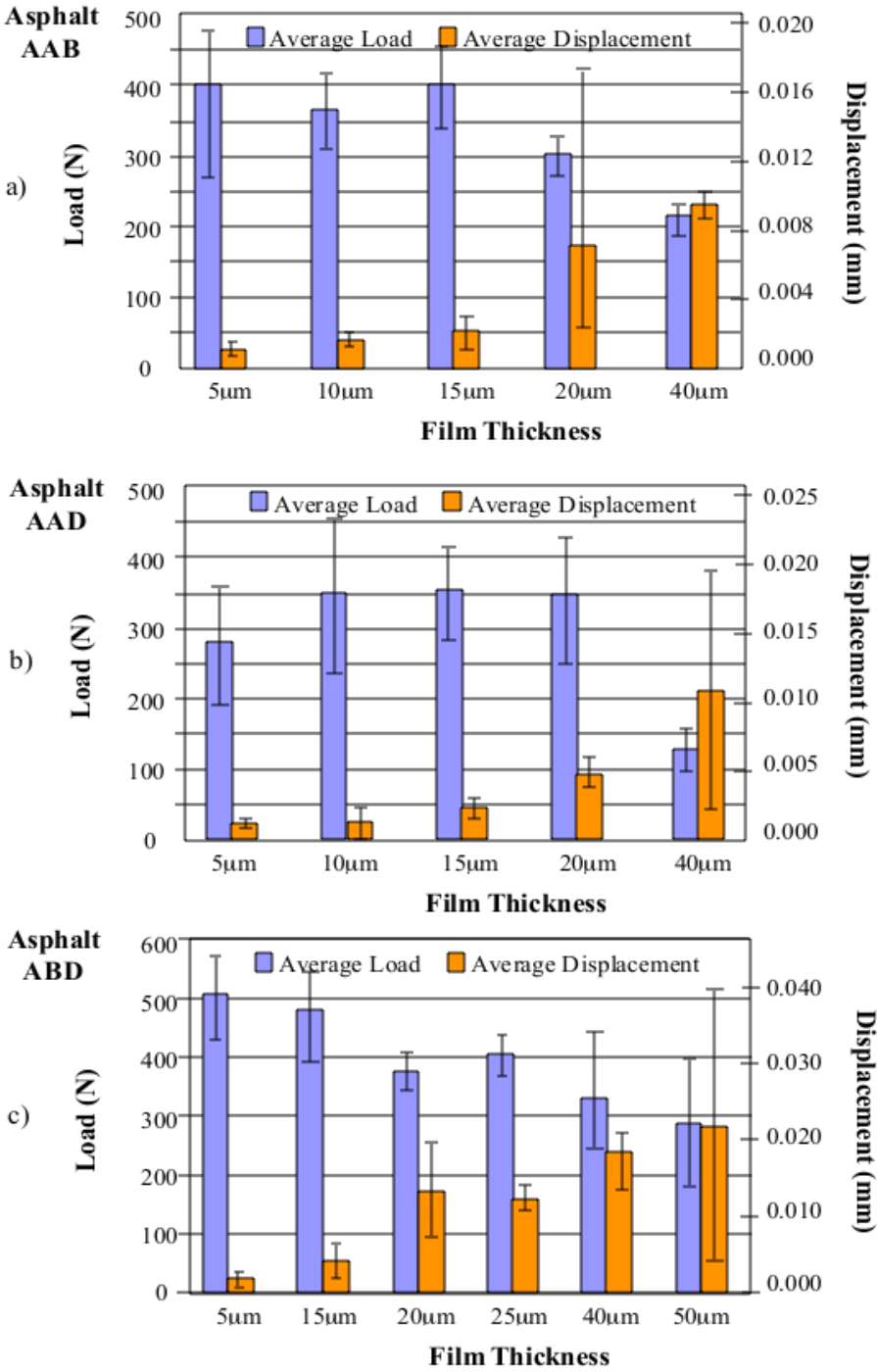
Figure 23. Load and Displacement at Peak Force of Samples with Asphalt a) AAB, b) AAD, and c) ABD.

Comparison between Bond Energy and Total Work of Fracture

The force and displacement history data were combined in order to plot force-displacement curves and calculate the total work of fracture (W_T). The total work of fracture included all stored and dissipated components of energy (elastic, viscoelastic, and plastic) that are associated with the deformation process. Therefore, W_T was calculated as the area under the force-displacement curve until failure. Figure 24 displays a representative force-displacement curve obtained from a tensile experiment of an asphalt binder.
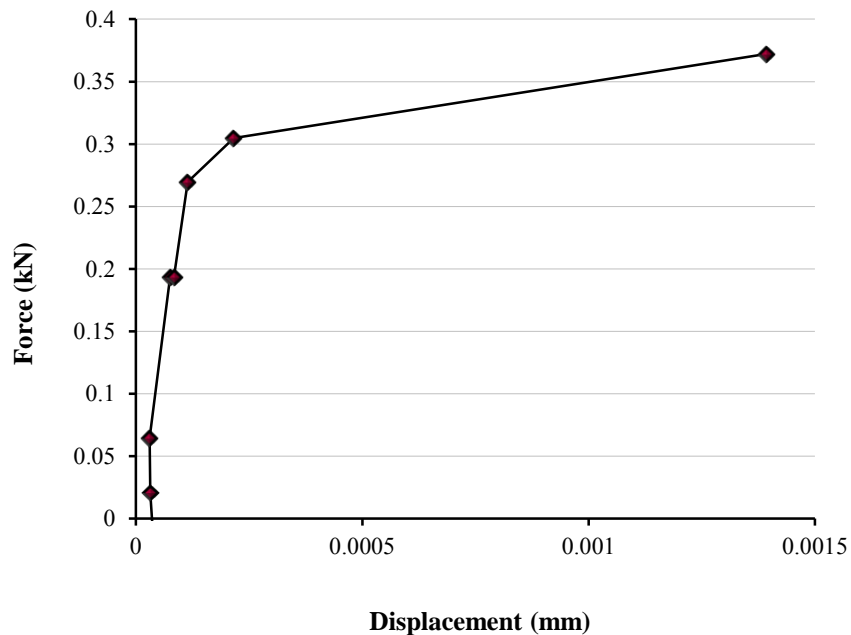
Figure 24. Example of a Force-Displacement Curve.

Table 16 presents the results of total work of fracture for the different types of asphalt binder and film thickness. The variability in the results is also reported in the table. Data from this table demonstrate that an increase in film thickness is related to an increase in the total work of fracture.

Table 16. Average and Standard Deviation of Total Work of Fracture.

Film Thickness (μm)	AAB		AAD		ABD	
	W_T^*	σ^*	W_T	σ	W_T	σ
	(J/m²)		(J/m²)		(J/m²)	
5	3.57	1.32	3.21	1.89	14.76	3.31
15	9.38	3.19	8.27	4.26	22.97	13.30
20	26.32	11.91	11.21	8.32	59.36	29.88
40	24.27	4.15	16.41	9.67	78.68	0.00

$^*W_T$ = Total work of fracture, σ standard deviation of total work of fracture.

With the total work of fracture known, the relationship between bond energy and total work of fracture can be determined. As discussed earlier, it was difficult to classify the failure as being cohesive or adhesive especially for binders with intermediate film thickness. Therefore, it was decided to calculate an effective bond energy that combines the cohesive bond energy and adhesive bond energy values reported in Table 15 using the following equation:

$$Effective\ Bond\ Energy = \left(\begin{array}{l} P_a \times Adhesive\ Energy + \\ P_c \times Cohesive\ Energy \end{array} \right) \tag{21}$$

where P_a is the percent of adhesive failure, and P_c is the percent of the cohesive failure determined using analysis of images of failure surfaces.

Figure 25 displays the relationship between the effective bond energy and total work of fracture for the three asphalt binders and for four different film thicknesses. Figure 26 displays the same relationship; however, in this case the effective bond energy is replaced with the adhesive bond energy. There are three data points for each film thickness; representing the three asphalt binders.

Data in these figures show that for every film thickness, asphalt ABD had a higher effective bond energy and total work of fracture than AAD and AAB. When the adhesive bond energy is used in place of the effective bond energy (Figure 26), there is still good correspondence between bond energy and total work of fracture.
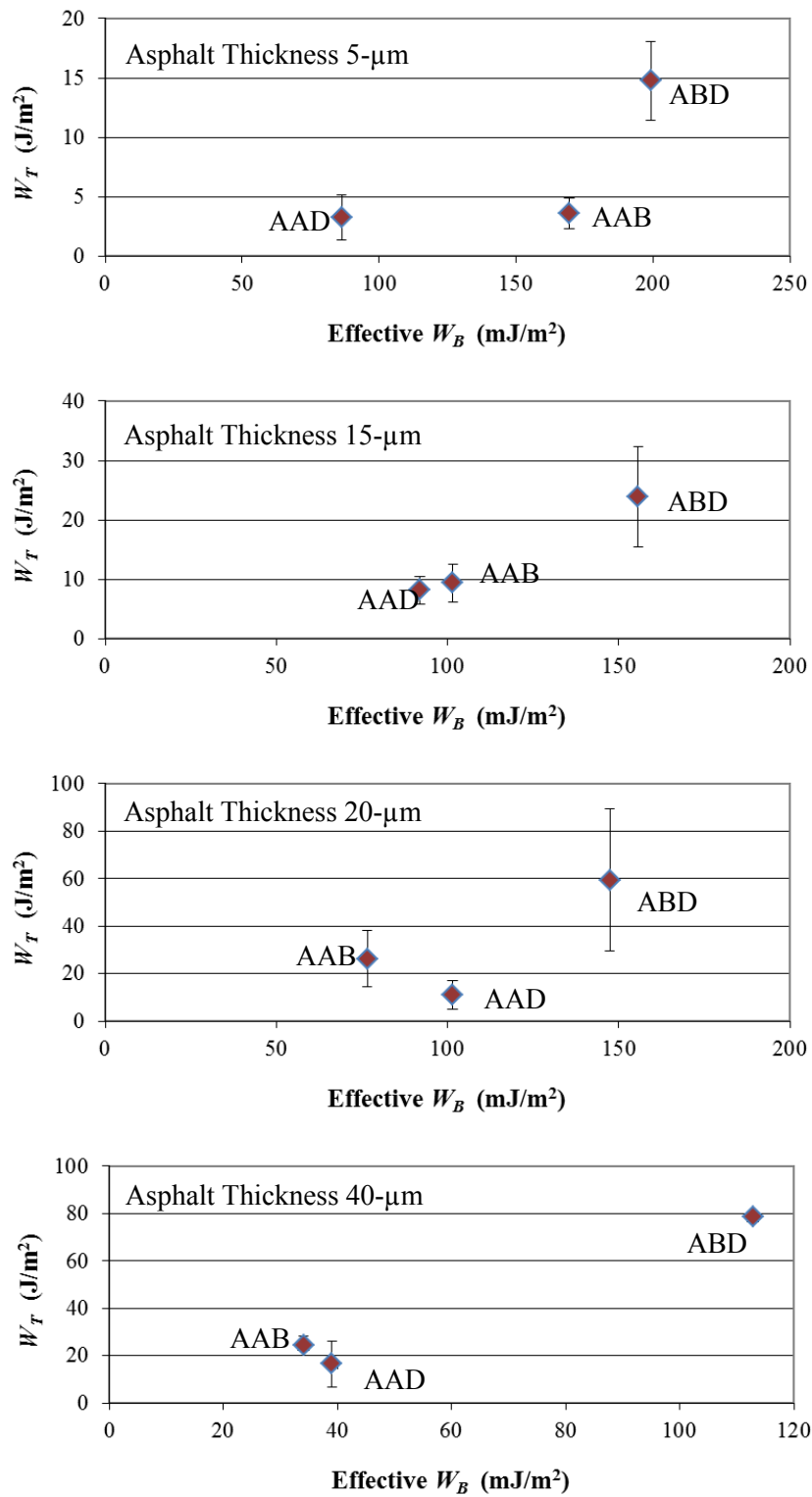
Figure 25. Relationship between Fracture Energy (Total Work of Fracture) and Effective Bond Energy at Different Film Thicknesses.
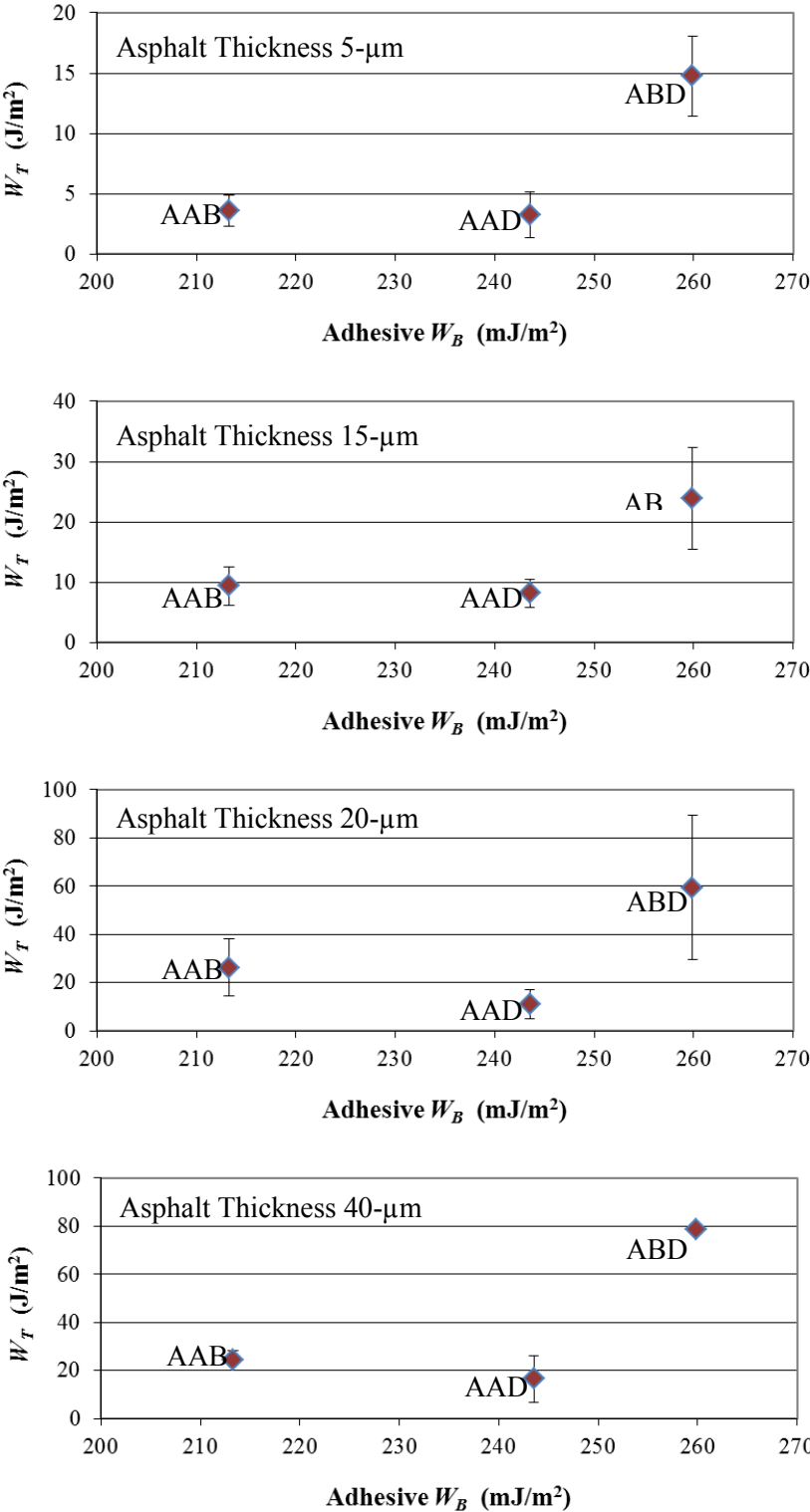
Figure 26. Relationship between Total Work of Fracture (W_T) and Adhesive Bond Energy (Adhesive W_B) for Different Film Thicknesses.

It is interesting to note that in some cases the total work of fracture for AAB is slightly higher than that of AAD, although asphalt AAD has a greater bond energy. A plausible explanation for this result is the difference in stiffness or compliance between the two materials. As shown in Figures 27 and 28, asphalt AAD has a lower dynamic modulus (or higher compliance) than asphalt AAB. Dynamic modulus data was obtained from (67). As discussed by Zosel (36), an increase in compliance causes a decrease in the total work of fracture when a full bond exists between the binder (adhesive) and substrate (adherent).
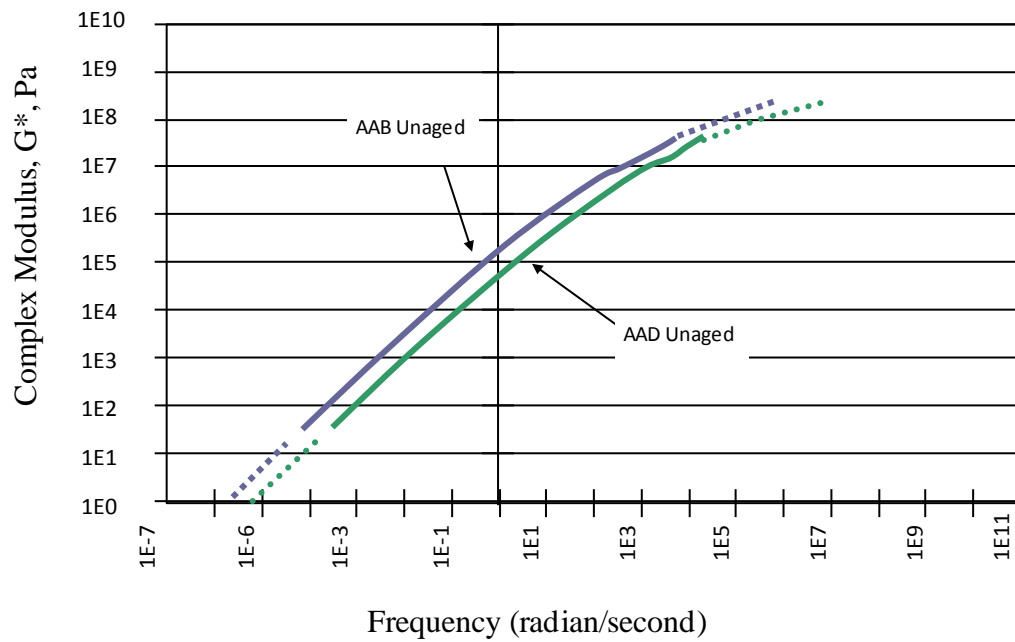
Figure 27. Complex Modulii of Unaged AAB and AAD Binders. After (67).
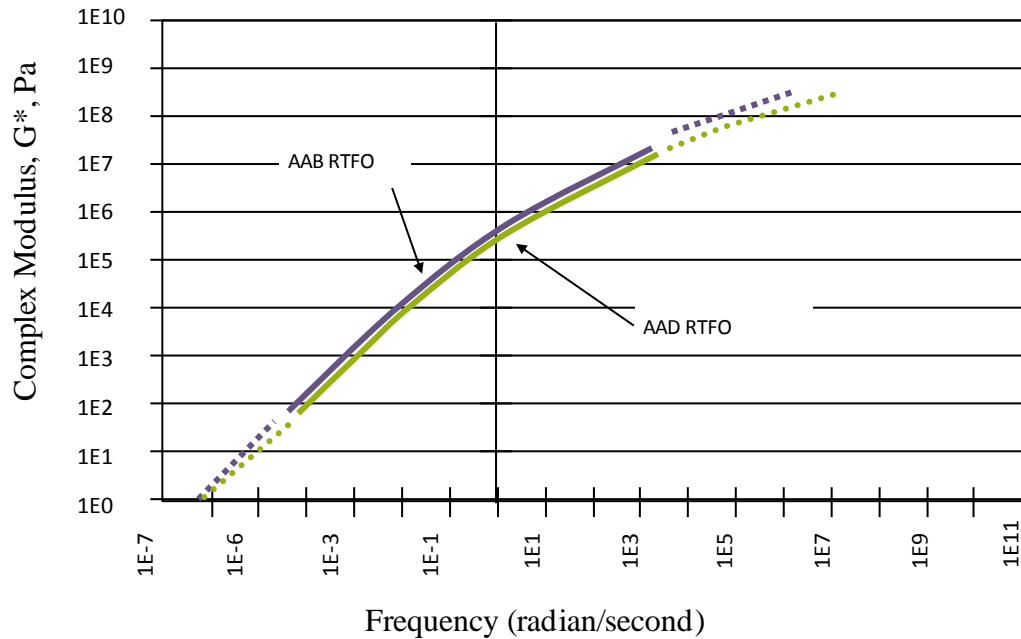
Figure 28. Complex Modulii of Aged AAB and AAD Binders. After (67).

Summary of Findings

Bond energy, W_B, computed using surface free energy measurements and the total work of fracture, W_T, determined from mechanical tests, are never equal. In fact, the latter can be several orders of magnitude larger than the former, independently of the type of failure (i.e., cohesive failure within the material or adhesive failure at the interface of adhesive joints). The factors contributing to such differences were explored using the experimental setup described in the chapter and are summarized below.

- Surface free energies of the substrate and adhesive (i.e., metal and asphalt binder, respectively) were used to compute the cohesive bond energy of three different types of asphalt binders and the adhesive bond energy corresponding to the asphalt binders-metal interface (W_B). Measurements of the total work of fracture (W_T) for the metal-asphalt binder specimens were obtained by means of a pull-off test. The test setup was designed to measure the tensile force and displacement for different film thicknesses of asphalt binders.

- The experimental results showed that as the thickness of the asphalt layer increased, the failure mode transitioned from adhesive to cohesive. Experimental data also showed that an increase in film thickness of the asphalt layer resulted in a decrease in the maximum tensile force at failure, an increase in the total displacement until failure, and an increase in the total work of fracture. In general, the experimental results support the hypothesis that for a given test configuration larger values of bond energy are associated with larger values of total work of fracture.

- The most important conclusion that can be extracted from the experimental results and available literature is that even though W_B is not equal in magnitude to W_T, these two values are strongly related. This means that any small modification in the bond energy will have a significant impact on the total work of fracture. In other words, materials with larger values of W_B will naturally show larger values of W_T during mechanical testing.

CHAPTER VI

BOND ENERGY VERSUS TOTAL WORK OF FRACTURE ON AGGREGATE SUBSTRATE

Introduction

The work documented in this chapter explores the relationship between the bond energy and the total work of fracture on samples composed of asphalt binder (adhesive) and aggregate substrate. In order to explore the relationship, several variables were considered: film thickness, interfacial moisture content, loading rate, and testing temperature. Equation 13 contains a relationship between bond energy and total work of fracture as determined by several researchers for a number of viscoelastic materials. The goals of this study are to determine the effect the testing variables have on the measured total work of fracture and to discover if asphalt binder adheres to the relationship in Equation 13.

The same basic experimental setup and analysis methods were employed in this work as documented in the previous chapter. Slight modifications were necessary to the preparation and testing protocols and experimental setup to accommodate the use of aggregate substrate. In addition, several challenges arose due to the use of aggregate substrate. These challenges included modification of the experimental setup, preparation of aggregate substrate for use in experimental setup, effect of aggregate surface roughness, and uniformity of the asphalt film.

Materials

Tables 17 and 18 display the materials used to determine the total work of fracture for the pull-off tests between asphalt binder and aggregate and the surface free

energy components of these materials. The surface free energy terms used are presented and defined for Equation 1 in Chapter II. The asphalt binders shown in Table 17 are the same asphalt binders used and described in Chapter V.

Two carefully chosen aggregates were selected to act as the substrate (Table 18). The first aggregate, limestone, is a sedimentary rock and had good performance in the field in terms of resistance to moisture damage. The second aggregate, andesite, is an igneous rock and had poor observed performance in the field.

Table 17. Surface Free Energy Values of Asphalt Binders.

Asphalt	Surface Free Energy Components (mJ/m^2)			Total (mJ/m^2)	Standard Deviation (mJ/m^2)		
	γ^{LW}	γ^+	γ^-		γ^{LW}	γ^+	γ^-
AAB	13.8	0.3	2.3	15.5	0.8	0.1	0.3
AAD	19.5	0.0	0.7	19.5	0.4	0.0	0.2
ABD	34.0	0.0	0.1	34.0	0.6	0.0	0.1

Table 18. Surface Free Energy Values of Aggregates.

Aggregate	Surface Free Energy Components (mJ/m^2)			Total (mJ/m^2)
	γ^{LW}	γ^+	γ^-	
Limestone	45.9	1.6	343.8	93.1
Andesite	56.7	2.5	1946.1	195.6

Surface free energy values in Tables 17 and 18 were used in Equations 2 and 3 to obtain the cohesive and adhesive bond energy values displayed in Table 19. Table 20 displays the values of the Energy Ratio (*ER*), computed using Equation 6, for each asphalt-aggregate combination. The material combination with a higher value of *ER* should display a greater resistance to moisture induced damage.

Table 19. Adhesive Bond Energy between Asphalt Binders and Aggregates and Cohesive Bond Energy of Asphalt Binders.

Aggregate	Failure Type	Bond Energy (mJ/m^2)					
		Dry (Asphalt)			Wet (Asphalt)		
		AAB	AAD	ABD	AAB	AAD	ABD
Limestone	Cohesive	30.92	39.04	68.07	65.56	85.48	97.07
	Adhesive	74.93	61.97	80.03	-98.35	-105.40	-96.07
Andesite	Cohesive	30.92	39.04	68.07	65.56	85.48	97.07
	Adhesive	110.14	89.08	97.68	-331.51	-355.39	-369.04

Table 20. Energy Ratio (*ER*) of Asphalt-Aggregate Combinations.

Aggregate	*ER* (Asphalt)		
	AAB	AAD	ABD
Limestone	0.45	0.22	0.12
Andesite	0.24	0.14	0.08

Methodology

The experimental setup used in this research is similar to the setup used in Chapter V to measure the force and displacement of asphalt-stainless steel samples with different film thicknesses. In summary, the force was recorded using a 5 kip load cell and displacement of the thin asphalt film was measured using a high-resolution digital camera with an image correlation software. The following factors were varied in testing each asphalt binder-aggregate combination:

- Film thickness: The asphalt film thickness was set at one of the following levels: 5-μm, 10- μm, 30-μm, 50-μm, and 100-μm. The testing temperature and loading rate were kept constant at 23°C and 0.01-mm/s, respectively, for all tests with different film thicknesses.

- Loading rate: Specimens were tested using loading rates of: 0.005-mm/s, 0.01-mm/s, and 0.02-mm/s. When the loading rate was varied, asphalt film thickness was kept constant at 30-μm.

- Temperature: Specimens were tested at temperatures of 10°C, 23°C, and 36°C. Asphalt film thickness was kept constant at 30-μm for specimens with varied testing temperatures.

- Moisture Content: Specimens were moisture conditioned after preparation for 12 hrs, 24 hrs, and 48 hrs. Asphalt film thickness, testing temperature, and loading rate were kept constant at 30-μm, 23°C, and 0.01-mm/s, respectively for specimens tested at different moisture contents.

A brief description of the sample preparation process is discussed below as well as some of the challenges faced. The testing and data acquisition systems were almost identical to the setup described in Chapter V, with the only change being a slight modification in the grips to accommodate the different sample holder geometry.

Sample Preparation

Aggregate particles with sizes between 15-cm and 30-cm in diameter were obtained from the appropriate quarry. The top and bottom of the aggregate particle was removed using a diamond saw to produce a flat and stable surface in which a core was taken from the aggregate. A 1.91-cm. diameter diamond core bit was used to extract the cores. A low speed saw, using distilled water as a lubricant, was used to cut the aggregate cores into 1-cm cylindrical stubs. The cylindrical aggregate stubs were then lightly polished on each flat face using 6-μm aluminum oxide polishing powder. Following the polishing process, the aggregate stubs were thoroughly rinsed by hand using distilled water, succeeded by submersion in a sonic bath of high purity distilled water to remove residual fine aggregate particles or polishing powder. The finished aggregate stubs were placed in an oven for 12 hours at 150°C to remove all moisture from the sample.

Asphalt binder samples were prepared between the aggregate substrates using an AR 2000 rheometer manufactured by TA Instruments, with a gap resolution of 1-µm. Custom designed grips were manufactured for the AR 2000 rheometer that allowed preparation of the asphalt-aggregate samples. The end of the sample holder, both upper and lower, which fits into the grip, was cylindrical. This design virtually reduces any chance of misalignments between the upper and lower sample holders.

The aggregate stubs were glued into the sample holders using a fast drying epoxy. After the epoxy had cured, a propane torch was used to heat the aggregate surfaces of the upper and lower sample holders to remove water vapor and organic matter. A small drop of asphalt binder, heated to 130°C was applied to the aggregate surface of the bottom sample holder. The gap was reduced to the desired film thickness, and the sample was allowed to cool for 15 minutes before the excess asphalt binder was removed by means of a heated razor blade. Holders were designed to allow the samples to rest horizontally, while maintaining perfect alignment, in order to minimize any creep within the asphalt film induced by the weight of the upper sample holder.

The samples were conditioned for 24 hours at 10°C to guarantee the formation of a full adhesive bond. After conditioning, the samples were moved to the enclosed testing chamber, which was maintained at a constant temperature of 23°C. Three layers of flat white acrylic paint were applied to the outside of the sample holders. Painting the samples was a necessary step to provide the conditions required for the digital camera and correlation software to compute the displacement of the specimen during the test. Following painting, a light speckle coating of black flat spray paint was applied. The samples were returned to the temperature chamber and allowed to equilibrate to the test temperature for two hours.

Aggregate, as opposed to stainless steel, is a naturally occurring raw material. Its properties and composition can vary due to small changes in position or depth. As a result the upmost care was needed when selecting aggregate particles, including sampling from the same geologic strata and position to ensure uniform aggregate composition. In addition, aggregate particles can contain cracks, voids, or inclusions

that can affect the structural integrity, surface texture or roughness, or surface free energy, respectively. The micro-cracks can cause the substrate to fail in tension prior to failure of the interface or adhesive. To reduce the possibility of micro-cracks, the largest possible samples were obtained directly from the quarry. Care was taken to minimize the content of voids and inclusions on the aggregate testing surface to minimize variability between replicates. Many samples were discarded for the above reasons; however, variability between replicates was still high. Possible causes for the variability include absorption of the asphalt binder into the aggregate substrate, differences in texture, and non-uniform surface free energy between aggregate particles.

Results

The results of this study are presented in four sections. The first section discusses the relationship of total work of fracture to asphalt film thickness. The second section examines how the total work of fracture changes due to moisture conditioning. The third section discusses the effect of loading rate and testing temperature on the total work of fracture. The final section examines the relationship between bond energy and total work of fracture.

Effect of Change in Film Thickness

Film thickness of the asphalt binder was varied from 5-μm to 100-μm in five steps: 5-μm, 10-μm, 30-μm, 50-μm, and 100-μm. All samples were tested at 23°C with a loading rate of 0.01-mm/s. Figure 2 (a – c) displays the total work of fracture for asphalt binders AAB, AAD, and ABD with the limestone and andesite substrate, respectively.

Figure 2 illustrates the increase in the total work of fracture due to an increase in the asphalt film thickness. Three primary observations were made in regard to the effect of film thickness of the asphalt binder on the measured total work of fracture. As the asphalt film thickness was increased, more energy was dissipated in the bulk of the

viscoelastic asphalt binder prior to failure. This was caused by increased viscous flow or yielding of the asphalt binder and the formation of larger cavitations and fibrils at the aggregate surface.

The second observation was related to the differences in the total work of fracture between asphalt binders.   As shown in Figure 2, large differences in the magnitude of the total work of fracture were measured among the three asphalt binders. All asphalt binders used in this study were unmodified and graded as PG64-22. Asphalt binders AAB and AAD exhibited very similar magnitudes of total work of fracture for both limestone and andesite substrates. The magnitude of the total work of fracture for asphalt binder ABD exceeded that of the other two asphalt binders for every film thickness and aggregate substrate. This was in good agreement with the measured surface free energy of the asphalt binders. The cohesive bond energy for asphalts AAB and AAD were similar (30.92 and 39.04 mJ/m^2, respectively) and lower than the cohesive bond energy of asphalt ABD (68.07 mJ/m^2). The difference in total work of fracture between the three asphalt binders was more pronounced with andesite substrate. The total work of fracture of asphalt ABD was at least 200% greater than the total work of fracture of asphalts AAB and AAD. The reason for this difference could be caused by surface texture, porosity, or chemical composition of the aggregate.

The third observation was the difference in the magnitude of the total work of fracture due to changes in aggregate substrate. Figure 2 displays the difference in magnitude of the total work of fracture when the aggregate substrate was changed. The limestone aggregate resulted in a higher magnitude of total work of fracture when asphalt AAB (Figure 2a) and asphalt AAD (Figure 2b) were used. Substrate mineralogy; however, did not impact the total work of fracture for asphalt ABD (Figure 2c). These findings were counterintuitive when the bond energy was considered (Table 3). According to the bond energies, the magnitudes of total work of fracture should have been identical for the two aggregate substrates when paired with each of the three asphalt binders if purely cohesive failure occurred, and the total work of fracture should have been greater for the andesite substrate for each of the three asphalt binders if any

adhesive failure occurred. This finding suggests that another mechanism besides physical adhesion influenced the total work of fracture. Work by Lesueur and Little (68), Little and Petersen (69), and Little and Epps (70) found that the addition of hydrated lime to asphalt binders has the possibility of improving the rheology of the binder at high temperatures and increasing the fracture toughening at low temperatures. In addition, the effectiveness of hydrated lime was found to be dependent on the chemical composition of the asphalt binder (71). While it was not feasible that free lime was formed from limestone, it was possible that calcium ions on the surface of the limestone aggregate could have developed stronger and more durable bonds with carboxylic acids or other functional groups in the asphalt binder, forming stronger and more durable bonds at the bitumen-aggregate interface. As described by Little and Petersen (69), this interaction could be reflected through the binder by amphoteric compounds.

Effect of Moisture Conditioning

The asphalt binder-aggregate samples were submerged in distilled water for time periods of 0-hrs, 12-hrs, 24-hrs, and 48-hrs. All samples were prepared with a film thickness of 30-μm and were tested at 23°C with a loading rate of 0.01-mm/s.
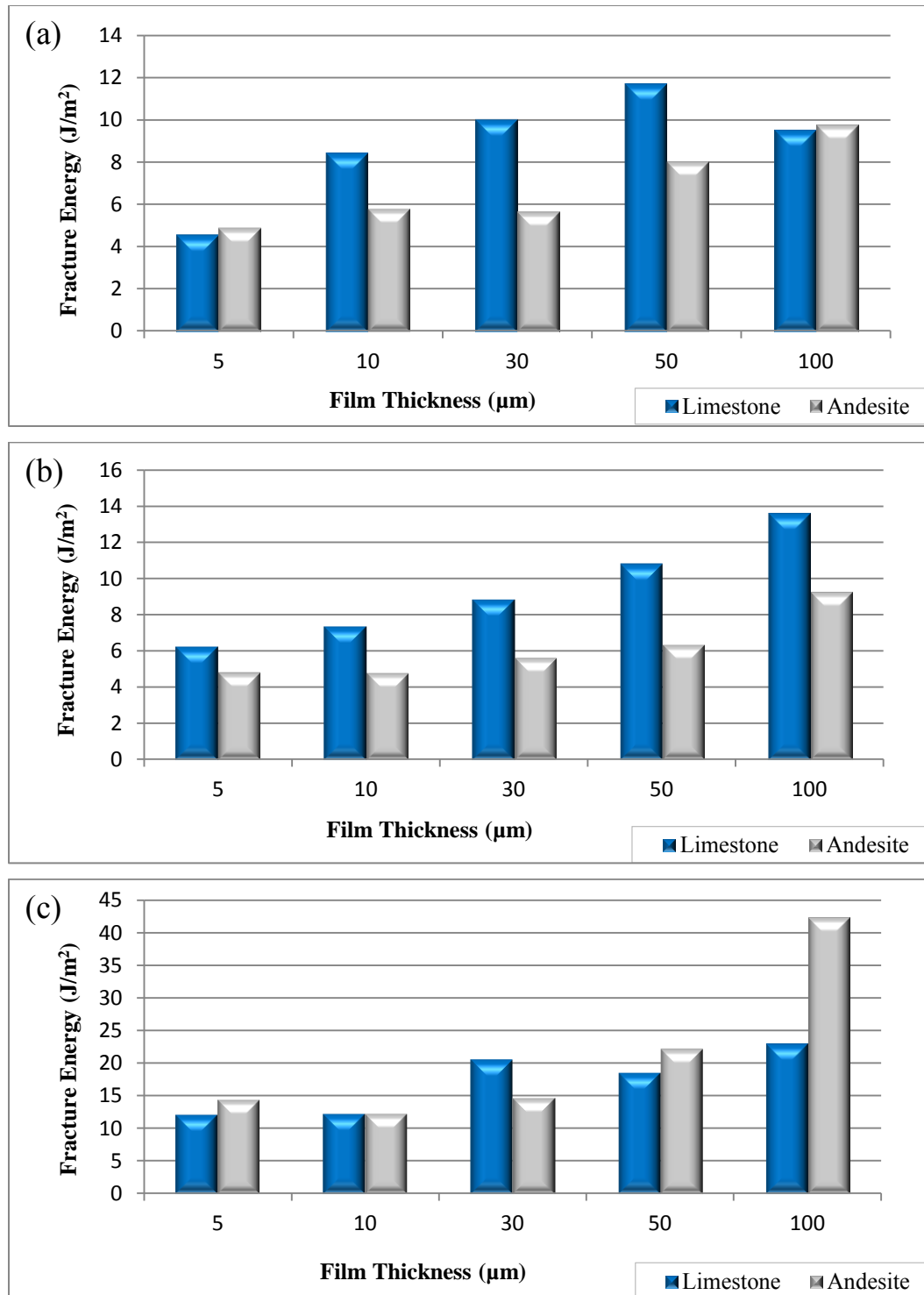
Figure 29. Comparison of Total Work of Fracture for Asphalt Binders (a) AAB, (b) AAD, and (c) ABD with both Limestone and Andesite Substrate.

Several interesting findings can be extracted from the moisture conditioning experiments. The first is related to the effect of moisture conditioning on the asphalt film. The asphalt film bonded to both limestone and andesite substrates displayed an increased ability to flow as the conditioning time was increased. Figure 3 displays the failed surfaces of samples of asphalt binder ABD with limestone and andesite substrate for moisture conditioning times of 0-hrs, 12-hrs, 24-hrs, and 48-hrs, respectively. The surface above the dotted line was the upper sample surface, with the lower sample surface being mirrored below the dotted line. As seen in Figure 3, all samples failed cohesively, but the cavitations became much larger, and visible fibrils appeared after the samples were conditioned for at least 12 hrs. The fibrils began as cavitations, but the asphalt binder's increased ability to flow, caused the pattern seen in the 12-hr, 24-hr, and 48-hr images. The lighter (brown) parts of the images are the center of the cavitations and were influenced by the coloration of the underlying aggregate substrate because of the very thin film of asphalt binder at these locations. The black (or gray due to light reflection) areas had more substantial film thicknesses and marked the ridges where the fibrils were formed and finally failed.
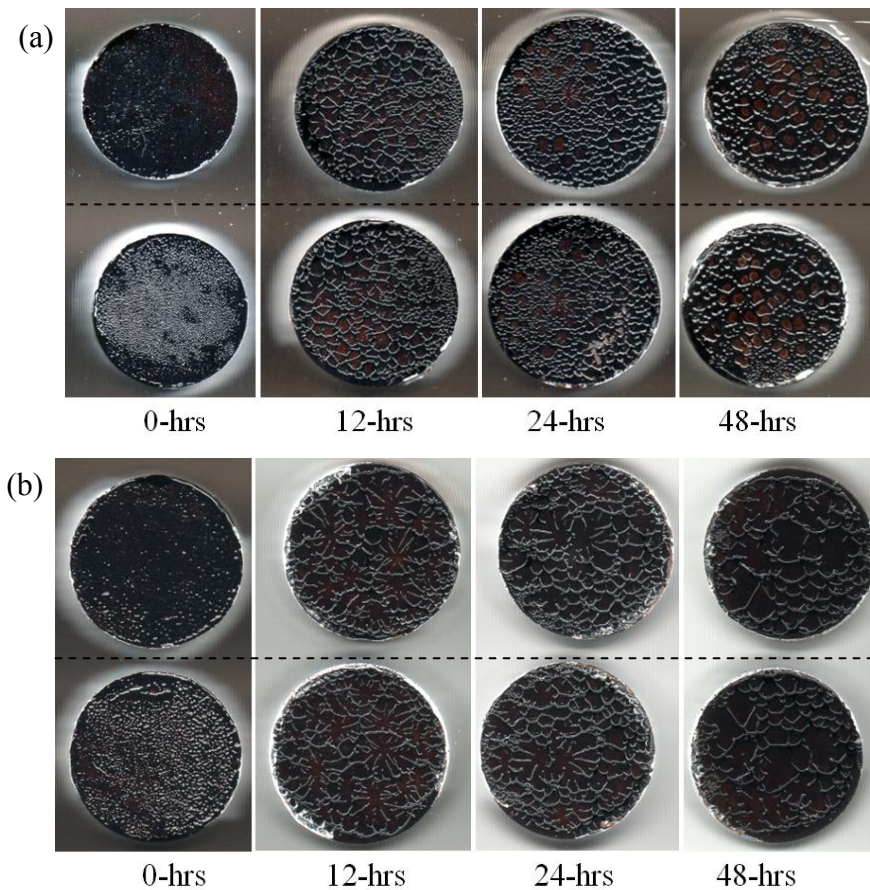
Figure 30. Effect of Moisture Conditioning on Thin Asphalt Film for Asphalt Binder ABD with (a) Limestone and (b) Andesite.

The force-displacement graph for asphalt binder ABD with both limestone and andesite substrate is shown in Figure 31. Observing Figure 31, it was clear that the aggregate substrate had a substantial effect on the measured total work of fracture. The increased flow of asphalt binder ABD after moisture conditioning resulted in a decrease in the measured force for both aggregate substrates. With the limestone substrate, the decreased failure force was countered by an increase in displacement until failure; however, this increase in displacement was not present when andesite was used as the substrate.
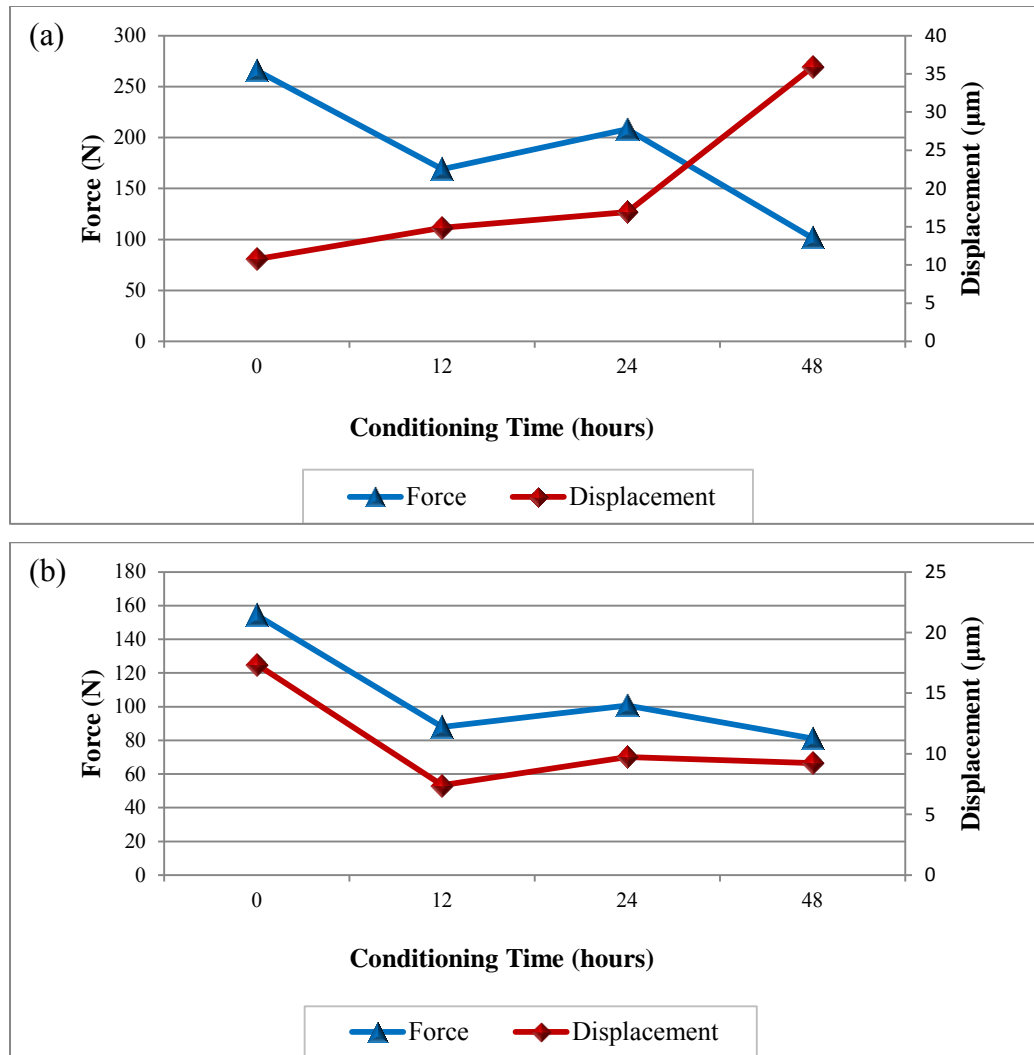
Figure 31. Force and Displacement for Asphalt Binder ABD with (a) Limestone and (b) Andesite Substrate.

When considering the impact of moisture conditioning, it was apparent that the increased displacement experienced by the asphalt binders bonded to the limestone substrate after moisture conditioning offset the accompanied decrease in force in most cases. In general, the total work of fracture increased upon moisture conditioning for asphalt binder AAB (Figure 32a), remained relatively constant asphalt binder AAD (Figure 32b), and decreased for asphalt binder ABD (Figure 32c) with limestone

substrate. When andesite was used as a substrate, the total work of fracture decreased for the majority of tests. Only asphalt binder AAB exhibited any increase in the total work of fracture after moisture conditioning for andesite substrate. These results were in good agreement with the observed field performance, which showed limestone and andesite having good and poor moisture resistance, respectively.

Each asphalt binder responded uniquely to moisture conditioning. As stated above, asphalt binder ABD displayed the greatest decrease in the magnitude of the total work of fracture after moisture conditioning. Prior to moisture conditioning the magnitude of the total work of fracture for asphalt binder ABD was at least 200% greater than the next highest asphalt binder for both substrates. After moisture conditioning; however, the difference in magnitude of the total work of fracture was greatly reduced.

The aggregate substrate had a substantial effect on the total work of fracture during the moisture tests. Moisture conditioning the specimens revealed the influence of aggregate substrate on the moisture resistance of an asphalt binder-aggregate combination. Looking at Figure 32, the limestone substrate resulted in a substantially higher total work of fracture compared to the andesite substrate for all three asphalt binders. The difference in the magnitude of total work of fracture between aggregate substrates was much greater for moisture conditioned specimens (Figure 32) as compared to non-moisture conditioned specimens (Figure 29).
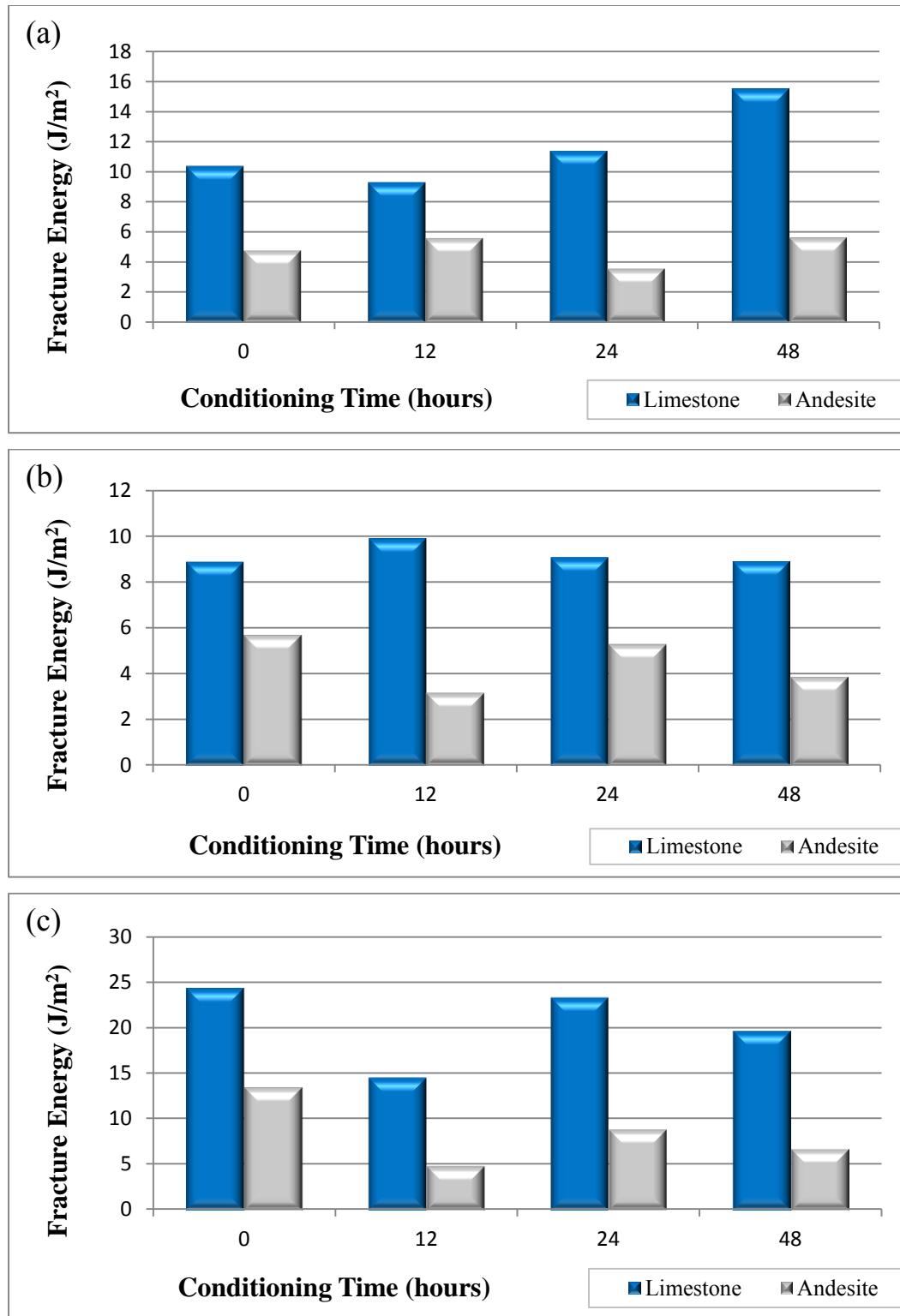
Figure 32. Comparison in Total Work of Fracture for Asphalt Binders (a) AAB, (b) AAD, and (c) ABD with Both Limestone and Andesite Substrate.

The results of the total work of fracture were in agreement with the values given by the energy parameter (*ER*). Table 21 displays the percent change of each asphalt binder-aggregate combination for a given moisture conditioning period, and the *ER* for that combination. A higher value of *ER* indicates that an asphalt binder-aggregate combination will be less susceptible to moisture induced damage and will have a smaller decrease in total work of fracture. *ER* was highest for asphalt binder AAB and lowest for asphalt binder ABD for both limestone and andesite aggregates. The relationship between *ER* and the average percent change in W_T for these experiments is shown in Figure 33. In addition, the relative percent changes in the total work of fracture of the asphalt binder-aggregate combinations with similar values of *ER* were comparable. Asphalt binder AAD with limestone exhibited an *ER* very close to that of asphalt binder AAB with andesite. The resulting percent changes in the total work of fracture due to moisture conditioning were very similar (Table 21 and Figure 33). The observation was the same for asphalt binder ABD with limestone and asphalt binder AAD with andesite. There was very good agreement between *ER* and the average percent change in W_T, demonstrating surface free energy can be used as a screening tool to select moisture resistant asphalt binder-aggregate combinations.

Table 21. Percent Change in Total Work of Fracture due to Moisture Conditioning.

Conditioning Time (hrs)	Percent Change					
	Limestone			Andesite		
	AAB	AAD	ABD	AAB	AAD	ABD
12	-10	12	-40	17	-44	-64
24	10	2	-4	-25	-7	-34
48	49	0	-19	17	-32	-50
Average	16	5	-21	3	-28	-49
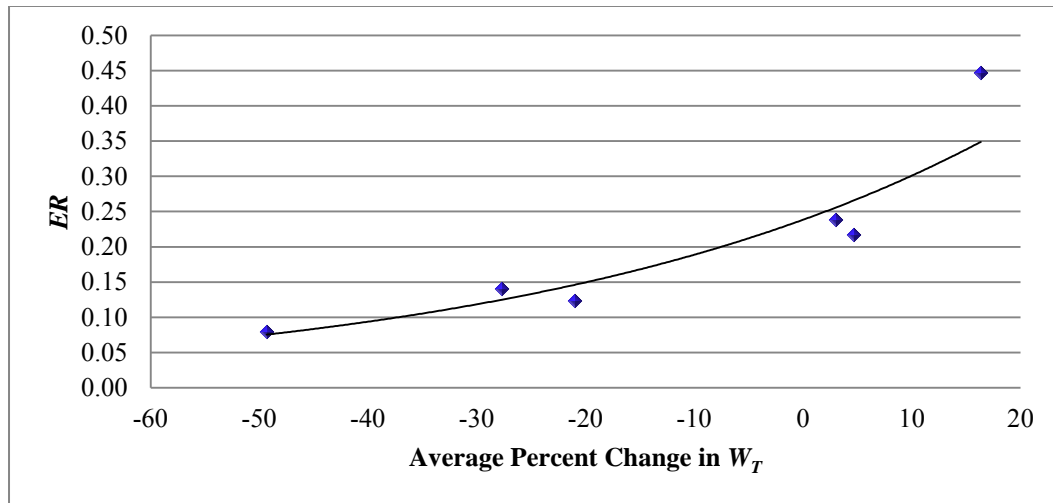
Figure 33. Relationship between *ER* and Average Percent Change in W_T.

Effect of Change in Loading Rate and Testing Temperature

Three loading rates (0.005-mm/s, 0.01-mm/s, and 0.02-mm/s) and three temperatures (10°C, 23°C, and 36°C) were applied to samples in which the film thickness was held constant at 30-μm. Figures 34 and 35 illustrate the force and displacement graphs for asphalt binder ABD with limestone and andesite substrates, respectively. Asphalt binder ABD was chosen as an example because it displayed the greatest change properties when loading rate and temperature were changed.

There was an increase in the total work of fracture with an increase in the displacement rate. The increase in the total work of fracture with increase in displacement rate stemmed from an increase in the maximum failure force and/or an increase in the displacement at failure. Examining Figures 34 and 35, the maximum force increased for asphalt binder ABD as a result of increasing the displacement rate for every temperature and aggregate substrate except andesite at 23°C. Asphalt binder ABD paired with andesite at 23°C experienced a steady decrease in force, but a steady increase in displacement at failure as the displacement rate was increased.

Figure 34. Force and Displacement for Asphalt Binder ABD with Limestone Substrate for Various Loading Rates and Temperatures of (a) 10°C, (b) 23°C, and (c) 36°C.

Figure 35. Force and Displacement for Asphalt Binder ABD with Andesite Substrate for Various Loading Rates and Temperatures of (a) 10°C, (b) 23°C, and (c) 36°C.

When testing temperature was increased and loading rate held constant, the total work of fracture decreased for each asphalt binder and aggregate substrate. The decrease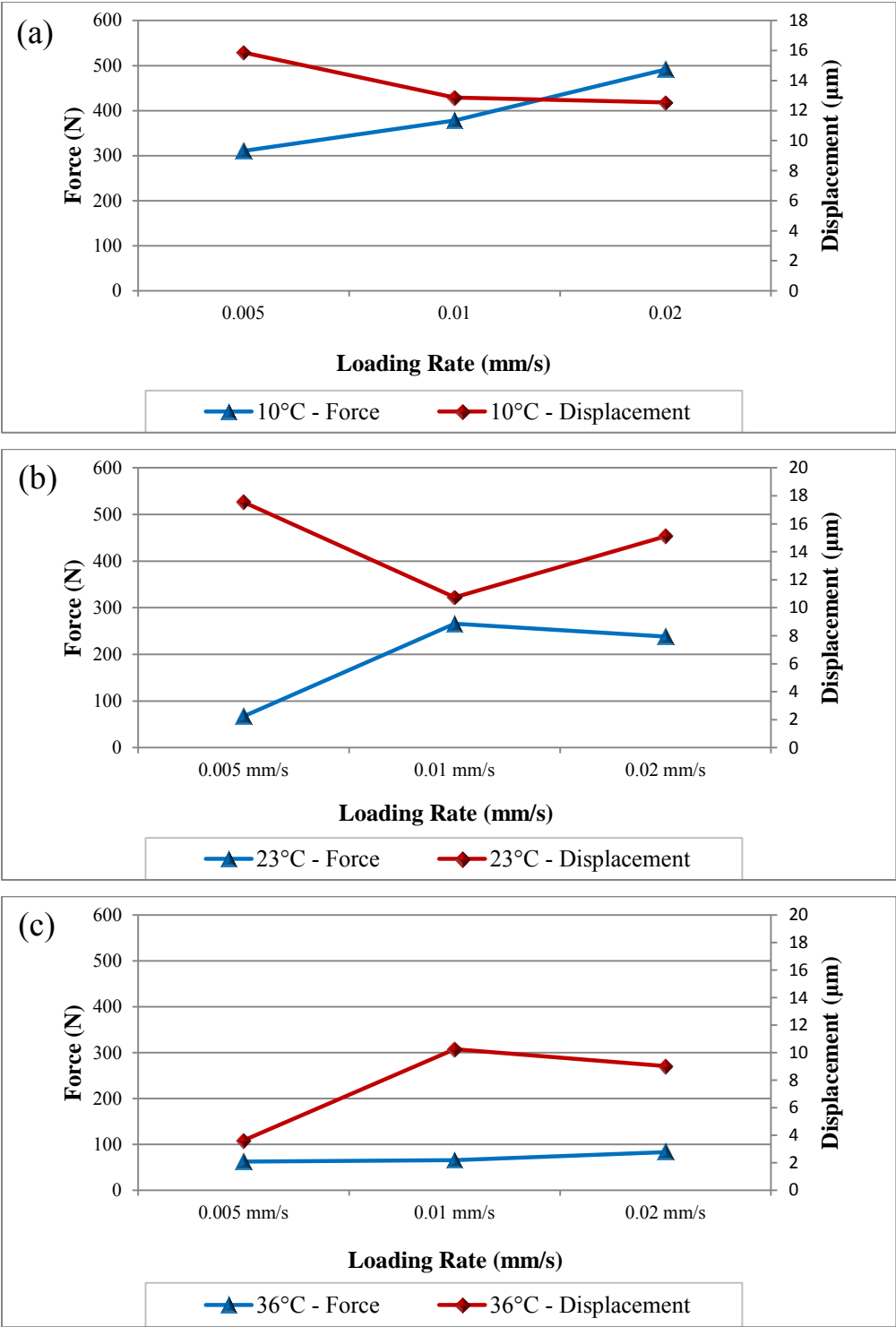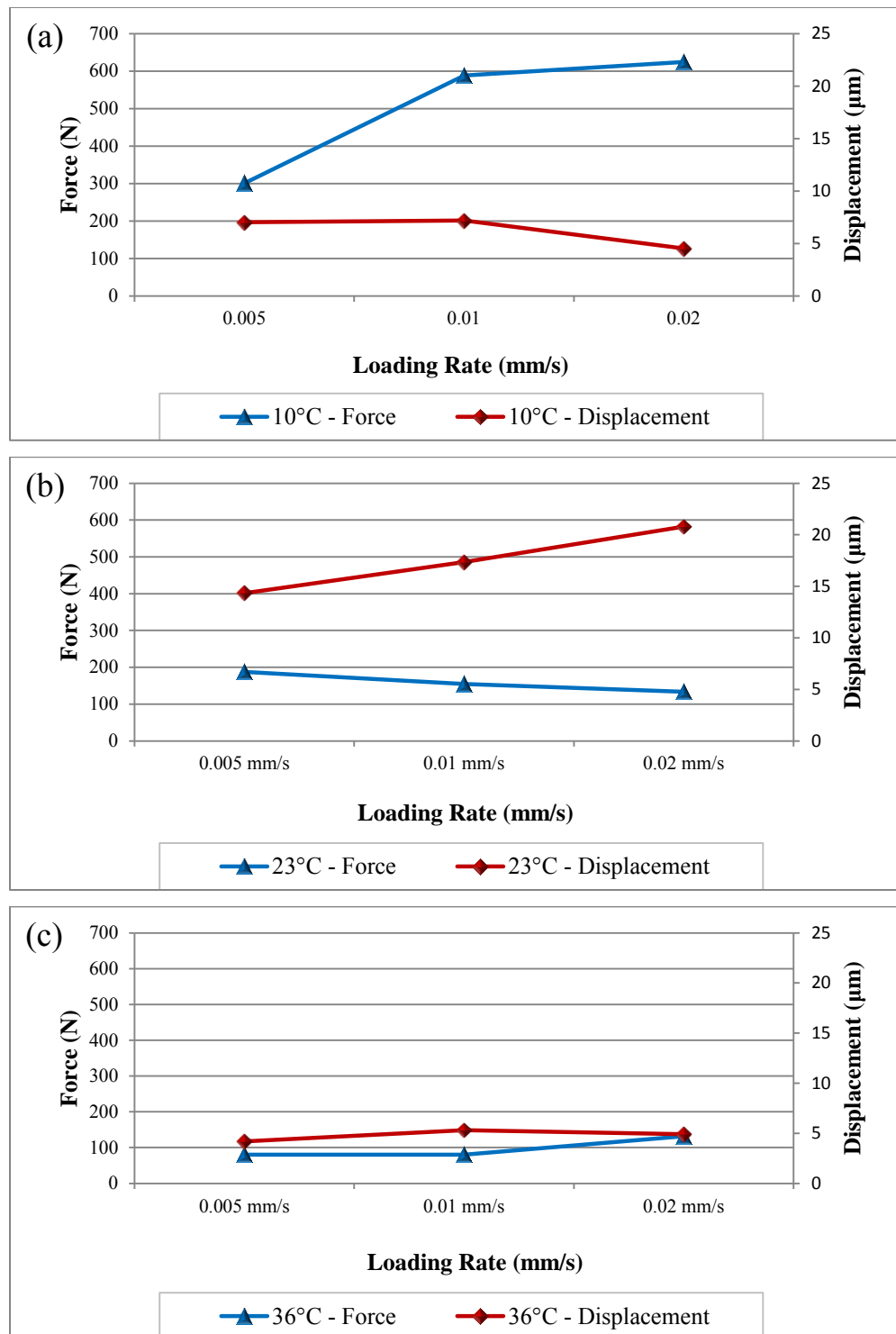 in the total work of fracture was the result of a decrease in the failure force and/or a decrease in the displacement at failure. The decrease in the failure force with the increase in temperature was caused by softening of the asphalt binder. The two aggregate substrates produced different force-displacement profiles (Figures 34 and 35). Limestone substrate resulted in lower failure forces and higher displacements with asphalt binder ABD than andesite for both the 10°C and 36°C tests for all displacement rates; however, higher failure forces and lower displacement were observed for the 23°C tests at 0.01-mm/s and 0.02-mm/s displacement rates.

Figures 36 and 37 reflect the influence of asphalt binder on the total work of fracture for the various temperatures and displacement rates. In agreement with the previous findings, asphalt binder ABD exhibited the largest magnitude of total work of fracture for the standard temperature and displacement rate of 23°C and 0.01-mm/s, respectively. In addition, the magnitude of the total work of fracture for asphalt binder ABD was the greatest at a 10°C testing temperature for all displacement rates and aggregate substrates. When the testing temperature was increased to 36°C, the total work of fracture of asphalt binder ABD greatly decreased. The increase in temperature resulted in a reduction in the total work of fracture by an average of 80% with limestone substrate and 74% with andesite substrate, respectively, when referenced to the 23°C testing temperature. The total work of fracture reduction experienced by asphalt binder ABD was significantly more than asphalt binders AAB and AAD. As seen in Figure 36(c), the total work of fracture for asphalt binder ABD with limestone substrate was very comparable with those of asphalts AAB and AAD, with the total work of fracture for asphalt binder ABD with andesite substrate being only slightly higher than those for asphalts AAB and AAD.
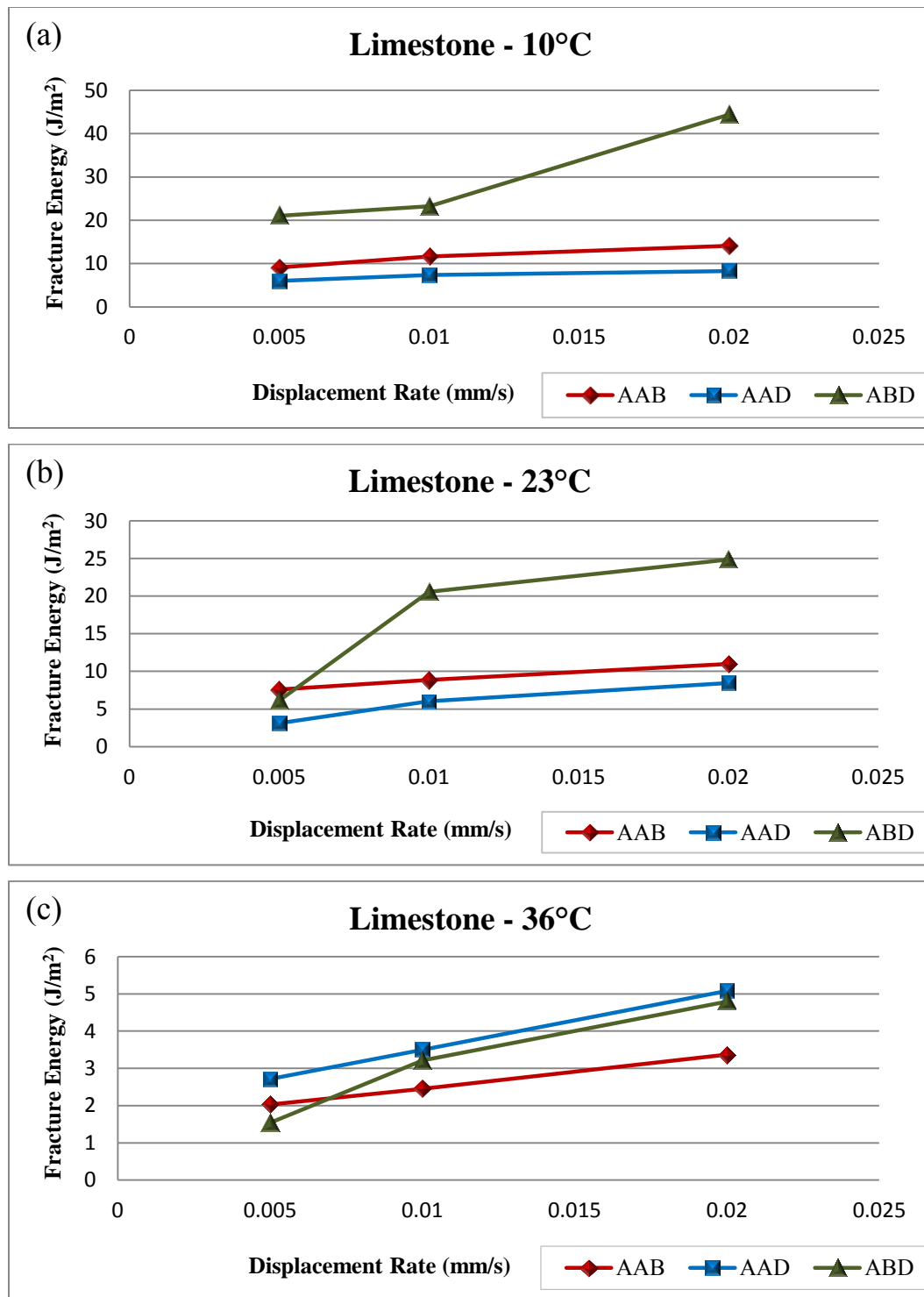
Figure 36. Effect of Change in Loading Rate for Asphalt Binders AAB, AAD, and ABD for Limestone Substrate at Temperatures of (a) 10°C, (b) 23°C, and (c) 36°C.
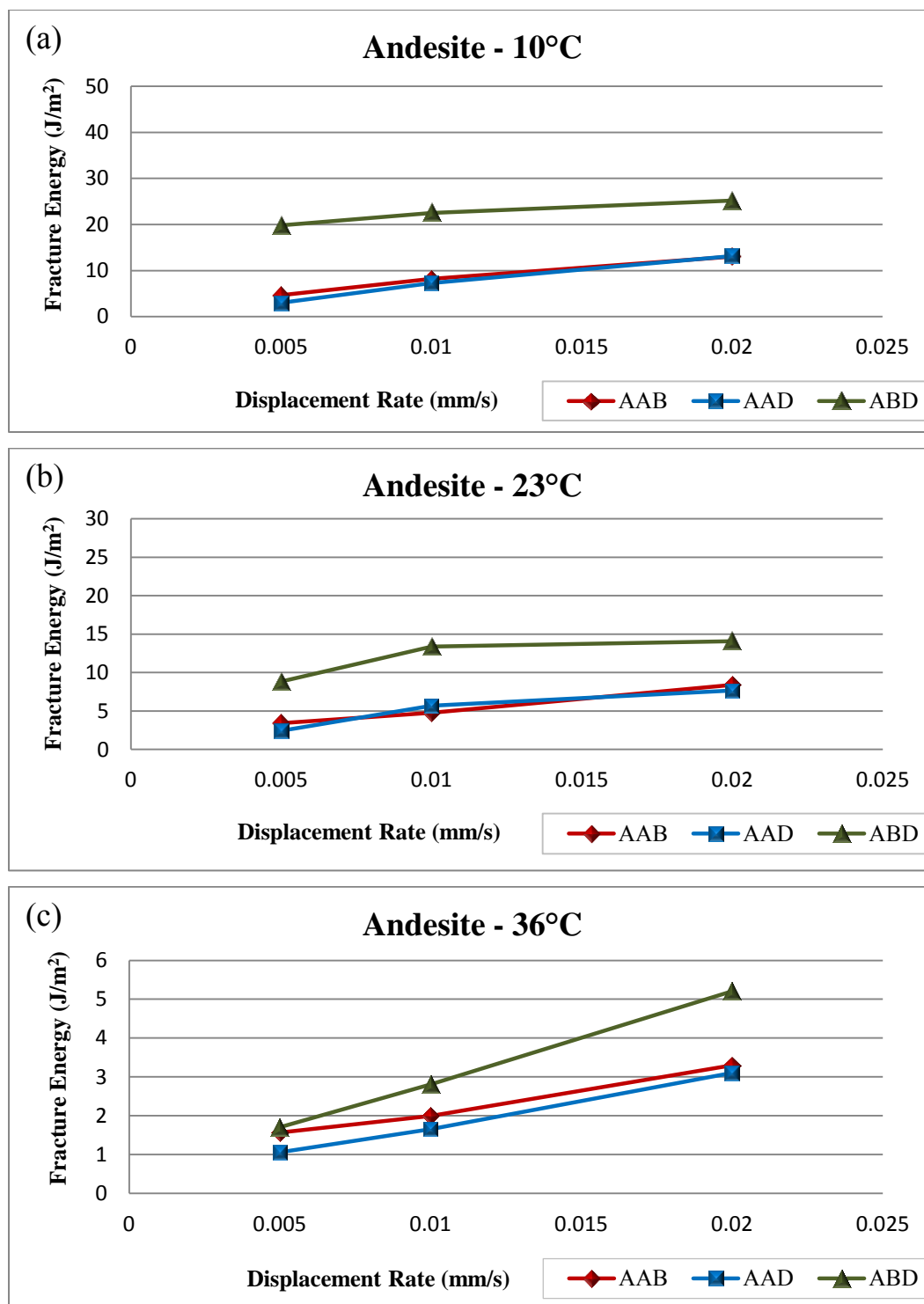
Figure 37. Effect of Change in Loading Rate for Asphalt Binders AAB, AAD, and ABD for Andesite Substrate at Temperatures of (a) 10°C, (b) 23°C, and (c) 36°C.

The importance of the aggregate substrate was recognized by looking at the total work of fracture values at the different temperatures and loading rates (Figures 36 and 37). In the previous section, limestone aggregate was found to yield higher values of total work of fracture than andesite before and after moisture conditioning. Investigating the magnitudes of total work of fracture resulting from changing the displacement rate and/or testing temperature, it was found that 23 of the 27 tests run with the limestone substrate exhibited higher magnitudes of total work of fracture than those run with andesite substrate. Three of four cases in which andesite exhibited a higher total work of fracture occurred when the temperature was 36°C (the highest value tested) and the failure was cohesive. The aggregate substrate should have minimum if any affect on the total work of fracture in these cases.

Fracture Master Curves

The matrix of testing temperatures and displacement rates to which the asphalt binders were subjected allowed the formation of a master curve for each asphalt binder and aggregate substrate. The 10°C and 36°C total work of fracture curves were shifted with respect to the 23°C total work of fracture curve by multiplying the displacement rates by the shift factors, a_T. The shift factors used for the limestone and andesite substrates are shown in Tables 22 and 23, respectively. The shift factors were found using the William, Landel, and Ferry method and were necessary to calculate the temperature modified displacement rate (72). The master curves shown in Figures 38 and 39 allowed the total work of fracture data to be estimated over a large range of displacement rates.

Table 22. Shift Factors (a$_T$) for Asphalt Binders with Limestone Substrate.

Asphalt	Temperature (°C)		
	10	23	36
AAB	2.5	1	0.125
AAD	2	1	0.4
ABD	2	1	0.25
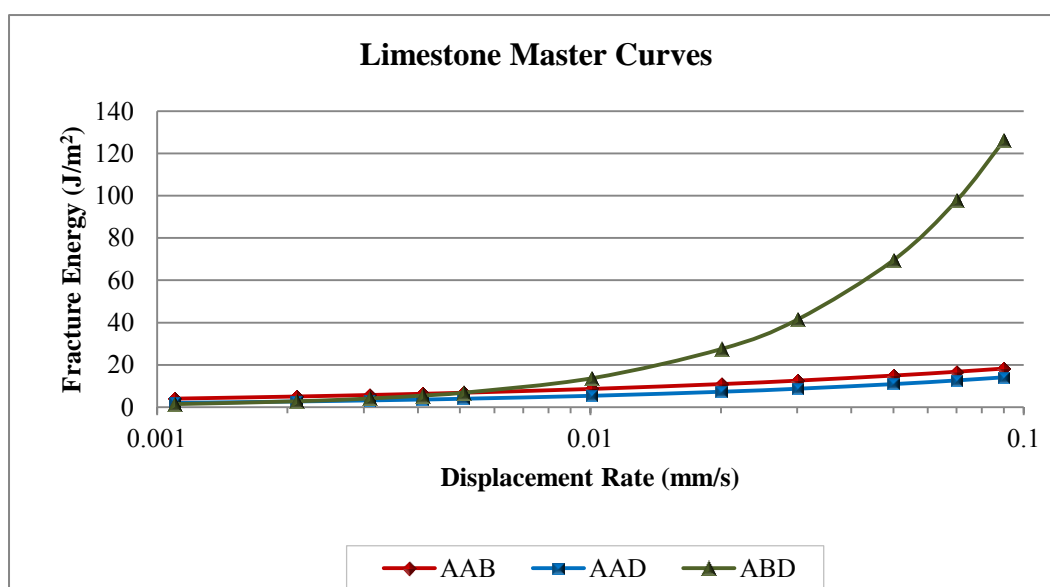
Figure 38. Master Curves for Asphalt Binder AAB, AAD, and ABD with Limestone Substrate.

Table 23. Shift Factors (a$_T$) for Asphalt Binders with Andesite Substrate.

Asphalt	Temperature (°C)		
	10	23	36
AAB	2	1	0.27
AAD	1.7	1	0.3125
ABD	3.25	1	0.1333
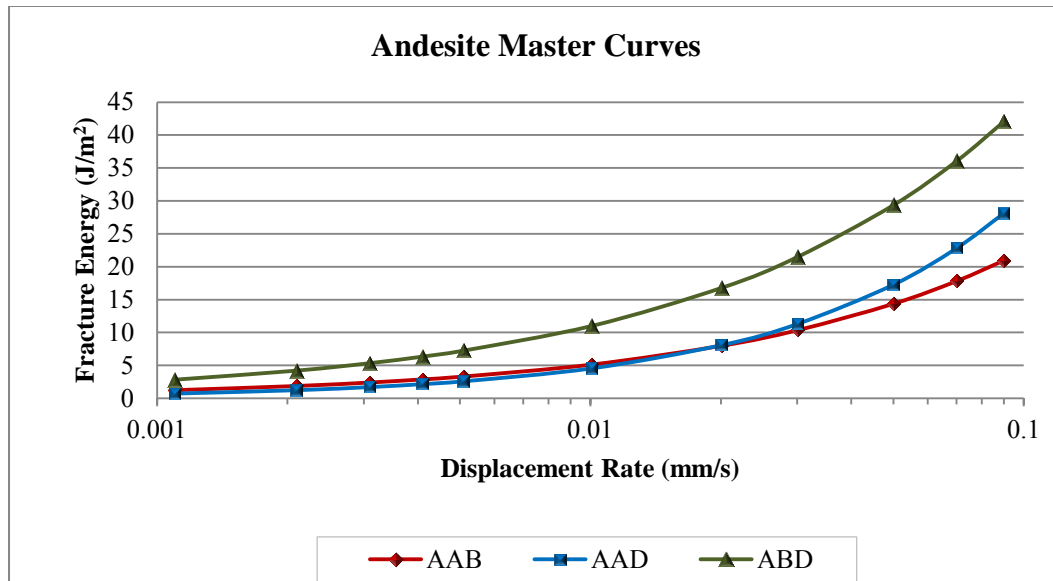
Figure 39. Master Curves for Asphalt Binder AAB, AAD, and ABD with Andesite Substrate.

Relationship between W_T and W_B

As discussed earlier in Chapter II, Equation 13 was developed to predict the total work of fracture for a given viscoelastic material with known bond energy and under various testing conditions. The testing conditions that had the greatest effect on the total work of fracture were temperature, loading rate, film thickness, and the interfacial properties. The experiments conducted in this study resulted in the following observations:

- Increases in film thickness resulted in increases in total work of fracture due to greater dissipation of energy in the bulk of the viscoelastic asphalt binder. The effect of energy dissipation in viscous deformation can be captured by substituting *k* in Equation 13 with the loss modulus. The loss modulus for each asphalt binder was determined using a DSR.

- Increases in loading rate, related to $\dot{a}$, resulted in an increase in the total work of fracture.

- Changes in testing temperature were combined with the loading rate (using term a_T) to formulate master curves (Figures 38 and 39).

In addition to the results listed above, moisture and aggregate type also influenced the total work of fracture. These effects, however, were dependent on the chemical makeup of the asphalt binder and aggregate. Limestone, which has a lower bond energy than andesite, resulted in a higher total work of fracture for two of the three asphalt binders. The authors believe that this was a result of stronger and/or more durable bonds developed between the calcium ions on the surface of the limestone aggregate and certain functionalities in the asphalt binder. In regard to moisture conditioning, limestone resulted in a higher total work of fracture for each asphalt binder and for each conditioning time than andesite. In addition, asphalt binder ABD displayed the largest decrease in total work of fracture due to moisture conditioning, despite having the highest bond energy. These experimental results were accurately predicted using *ER* as described above.

The results obtained in this chapter were compared against the relationship shown in Equation 13 using a linear regression analysis. The linear regression function is displayed in Equation 22, with the regression constants for the two aggregate substrates shown in Table 24.

$$\frac{W_T}{W_B} = A_1 + A_2 a_T + A_3 \dot{a} + A_4 k \tag{22}$$

where, A_1 through A_4 are regression constants, a_T is the shift factor, $\dot{a}$ is the loading rate, and k is the frequency dependent loss modulus at low frequencies. The values of the viscous modulus were determined at frequencies of 0.0679, 0.14, and 0.289-Hz using the DSR. These frequencies were selected since they reflect the slow rate of loading that was used in the pull-off tests.

Table 24. Regression Constants for Linear Regression Model

Substrate	Regression Constants			
	A_1	A_2	A_3	A_4
Limestone	-13.651	59.915	2300.26	61.714
Andesite	-5.482	27.283	2656.97	12.406

Figures 40 and 41 display the relationship between the ratio of measured total work of fracture to measured adhesive bond energy (W_T/W_B) and the ratio of W_T/W_B found using linear regression for limestone and andesite substrate, respectively. The linear regression model shown in Equation 9 proved a good fit to the data (Figures 40 and 41) and displays that there was a strong relationship between the bond energy and the total work of fracture. The R^2 values were found to be 0.634 and 0.864 for limestone and andesite, respectively. The residual scatter in the data was likely caused by errors in the experimental data or limitations in the regression model.
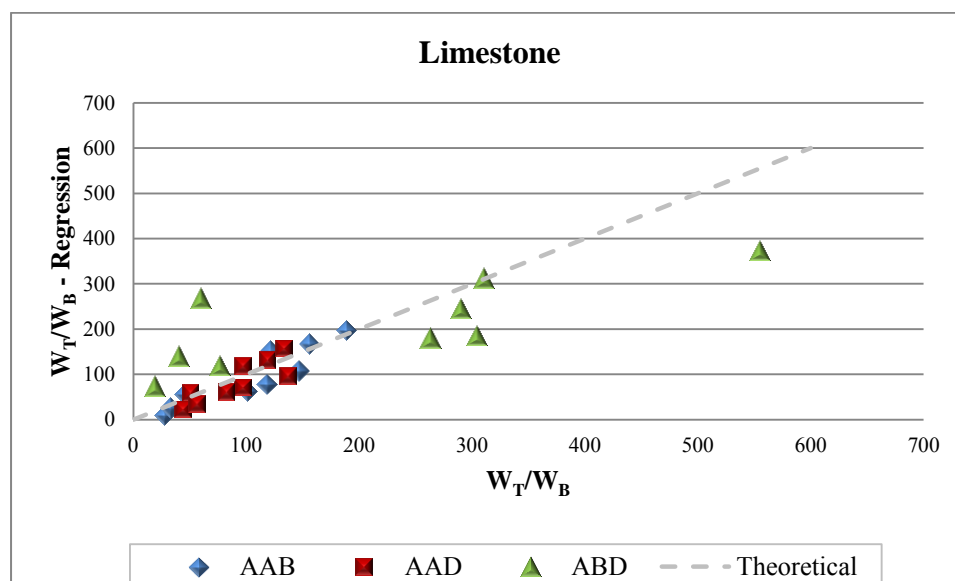
Figure 40. Relationship between Experimental W_T/W_B and W_T/W_B Found Through Regression Analysis for Limestone Substrate.
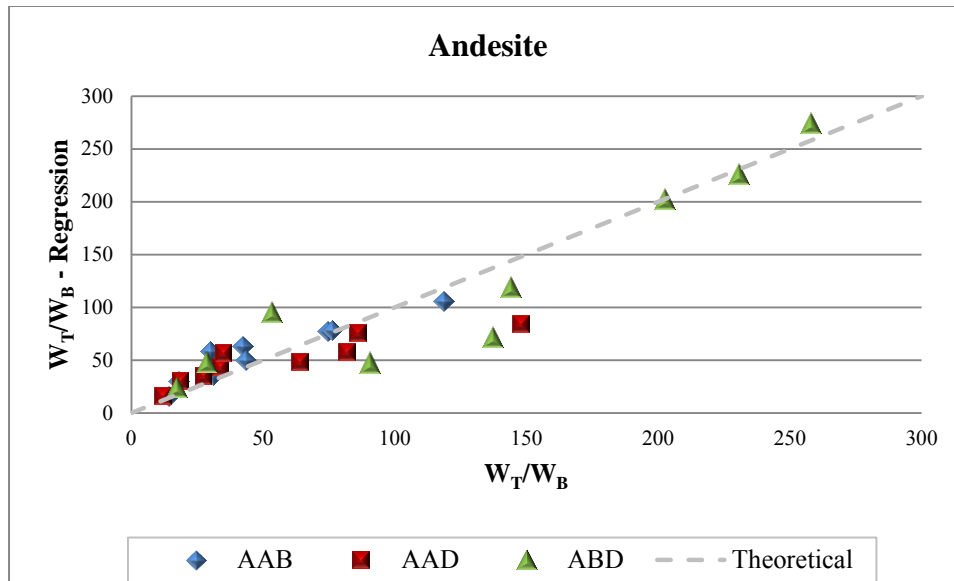
Figure 41. Relationship between Experimental W_T/W_B and W_T/W_B Found Through Regression Analysis for Andesite Substrate.

Summary of Findings

The prime objective of this study was to investigate the relationship between the bond energy and total work of fracture for asphalt binder-aggregate systems. In addition, the loading rate, temperature, film thickness, and moisture content at the interface were varied for different asphalt-aggregate specimens to investigate their influence on the total work of fracture. The primary findings are as follows:

- An increase in film thickness resulted in increases in total work of fracture. Increased film thickness allowed more energy to be dissipated in the bulk of the viscoelastic asphalt binder. This was true in 28 of 30 cases.

- The influence of moisture on the total work of fracture varied for each asphalt-aggregate combination. The total work of fracture for the combination of limestone with asphalt AAB increased upon moisture conditioning while andesite and asphalt ABD combination displayed the largest decrease due to moisture

conditioning. The effect of moisture conditioning on the measured total work of fracture was accurately predicted using the parameter *ER*.

- Both testing temperature and loading rate affected the measured total work of fracture independently of asphalt or aggregate type. Increasing the testing temperature decreased the total work of fracture, and increasing the loading rate increased the total work of fracture for every asphalt binder-aggregate combination tested. This information was combined to formulate master curves for work of fracture for each asphalt binder-aggregate system to predict the total work of fracture for a large range of loading rates.

- The chemical composition of the asphalt binder greatly affects its total work of fracture under various conditions. Asphalt binder ABD exhibited the highest bond energy and highest measured total work of fracture at 10°C and 23°C, but also showed the greatest reduction in total work of fracture due to moisture conditioning and temperature change (10°C to 36°C). Asphalt binder AAB exhibited the lowest bond energy, but showed an increase in total work of fracture due to moisture conditioning and a small decrease in total work of fracture due to changes in temperature (10°C to 36°C). The effects of moisture were accurately predicted by *ER* and surface free energy.

- Aggregate substrate has a substantial effect on the total work of fracture. Limestone substrate performed better than andesite in every test. It resulted in higher total work of fracture across the range of film thicknesses, resulted in a smaller reduction in total work of fracture due to moisture conditioning, and resulted in a smaller reduction in total work of fracture due to increases in temperature. However, limestone exhibited a lower adhesive bond energy as compared to andesite. The authors hypothesize that calcium ions on the surface of the limestone aggregate may have provided the source of a more durable bond with certain functional groups, i.e., carboxylic acids in the asphalt binders used.

- A regression model was developed between bond energy and total work of fracture. The regression model demonstrated a strong relationship between bond

energy and total work of fracture when loading rate, time-temperature shift, and viscous deformation were taken into account. The results support that the bond energy was a very good indicator of performance.

CHAPTER VII

CONCLUSIONS AND RECOMMENDATIONS

Asphalt Modifications and Surface Free Energy

Three types of modifications were investigated. These included, modifications made to the binder by the manufacturer, modification due to addition of liquid anti-strip agents, and modification due to in service oxidative aging of the binder. In addition, the effect pH on the surface free energy components of water due to contact with aggregate particles was studied. Important conclusions related to the effect of each type of modification on the fracture properties and moisture sensitivity of asphalt mixtures based on the changes observed in the energy parameters are as follows:

Asphalt Binders

- Asphalt binders can be ranked based on their cohesive bond energy or any of its surface free energy components. This ranking can be used as a screening tool to compare binders against each other and determine the ones that have the best resistance to fracture and moisture damage when used with aggregates.

- Modifications made to a base asphalt binder by the manufacturer to produce an asphalt binder with a higher PG grade typically increased the work of cohesion indicating better fracture resistance of the modified mixes. These modifications did not change the moisture sensitivity of the asphalt mixture significantly except when TRS was used as a modifier. In this case the acid component of the asphalt binder increased providing a potential improvement in the adhesive bond strength with most types of aggregates. For one of the asphalt binders, addition of SBS also showed improvement in the moisture resistance after aging.

- Addition of liquid anti-strip agents typically reduced the surface free energy and consequently the work of cohesion of the asphalt binders. Upon further examination, it was found that the decrease in the cohesive bond energy of the asphalt binder resulted from a decrease in the non-polar γ^{LW} component of the surface free energy. A reduction in the γ^{LW} component of the surface free energy allows better coating of the aggregate by the asphalt, improving interfacial adhesion and, thus, improving the fracture resistance of the mixture matrix. This can indirectly improve the fracture resistance by promoting better adhesion between the fines and the binder during the mixing and compaction process.

- Use of liquid anti-strip agents either improved or did not significantly change the moisture resistance of the asphalt binder with the selected aggregates (gauged using the parameter *ER*). The liquid anti-strip agents from the two different sources demonstrated different levels of changes in the moisture resistance even with the same asphalt binder and aggregate.

- Aging can have different impacts on different asphalt binders depending on the initial chemistry of the asphalt binder. Furthermore, differences in kinetics of different compounds formed during oxidative aging also influence the chemistry and, consequently, the surface free energy components and performance of different asphalt binders after short- and long-term aging.

- In most cases long-term aging reduced the work of cohesion indicating lower fracture resistance of the aged binder. In the case of one neat binder and one modified binder, the work of cohesion increased after long-term aging. After long-term aging, asphalt binders from one source demonstrated a decrease in the moisture sensitivity, while asphalt binders from the other source demonstrated an increase or no change with the moisture sensitivity with both the aggregates used in this study. It was speculated that the differences in the polar functional groups between the two unaged asphalt binders resulted in different surface properties due to aging.

Contact Water

- No significant changes in the total surface free energy or the acid and base components of surface free energy were observed for the contact water when compared to values obtained using a control sample of distilled water. Within the range of pH that was achieved by exposing distilled water to aggregates in this project, there was no significant correlation between the change in surface free energy components and the pH of the water.

- While the methodology used with the Wilhelmy Plate was able to obtain the relative changes in surface free energy components of pH modified waters, it would not be a viable option if the absolute values were required due to error propagation.

Fracture Energy

The bond energy, W_B, computed using surface free energy measurements and the total work of fracture, W_T, determined from mechanical tests, can be very different in magnitude. In fact, the latter can be several orders of magnitude greater than the former, independently of the type of failure (i.e., cohesive failure within the material or adhesive failure at the interface of adhesive joints). The factors contributing to such differences were explored based on experimental and numerical data reported in the literature and are summarized below.

Stainless Steel Substrate

- During the measurement of W_T, materials dissipate energy due to irreversible processes such as viscous and plastic deformation. These energy contributions make the value of W_T to be larger than W_B. The range of this difference strongly depends on the characteristics of the materials (e.g., time-dependent and yielding properties) and on the experimental conditions at which W_T is measured. In the

case of viscoelastic materials, it has been found that W_T is a function of the rate of loading, temperature, and rate of crack growth.

- The relationship between W_B and W_T in metal-asphalt binder specimens was studied and compared against that reported in the literature. Surface free energies of the substrate and adhesive (i.e., metal and asphalt binder, respectively) were used to compute the cohesive bond energy of three different types of asphalt binders and the adhesive bond energy corresponding to the asphalt binders-metal interface (W_B). Measurements of the total work of fracture (W_T) for the metal-asphalt binder specimens were obtained by means of a pull-off test. The test setup was designed to measure the tensile force and displacement for different film thicknesses of asphalt binders.

- The experimental results showed that as the thickness of the asphalt layer increased, the failure mode transitioned from adhesive to cohesive. Experimental data also showed that an increase in film thickness of the asphalt layer resulted in a decrease in the maximum tensile force at failure, an increase in the total displacement until failure, and an increase in the total work of fracture. In general, the experimental results support the hypothesis that for a given test configuration larger values of bond energy are associated with larger values of total work of fracture.

- The most important conclusion is that even though W_B is not equal in magnitude to W_T, these two values are strongly related. This means that any small modification in the bond energy will have a significant impact on the total work of fracture. In other words, materials with larger values of W_B will naturally show larger values of W_T during mechanical testing.

Aggregate Substrate

- Increases in film thickness resulted in increased total work of fracture. The increased film thickness allowed more energy to be dissipated in the bulk of the

viscoelastic asphalt binder. Only two of the 30 cases did not adhere to this result and are most likely due to errors in the experimental process.

- The influence of moisture on the total work of fracture varied between each asphalt-aggregate combination. The total work of fracture of limestone coupled with asphalt AAB increased due to moisture conditioning while andesite with asphalt ABD displayed the largest decrease due to moisture conditioning. The effect of moisture conditioning on the measured total work of fracture can be estimated accurately using the parameter *ER*.

- Testing temperature and loading rate both affected the measured total work of adhesion independently of asphalt or aggregate type. Increasing the testing temperature decreased the total work of fracture, and increasing the loading rate increased the total work of fracture for every asphalt binder and aggregate type tested. This information was combined to formulate master curves for each asphalt binder and aggregate to predict the total work of fracture for a large range of loading rates.

- The chemical composition of the asphalt binder greatly affects its total work of fracture under various conditions. Asphalt binder ABD had the highest bond energy and had the highest measured total work of fracture at 10°C and 23°C, but also had the greatest reduction in total work of fracture due to moisture conditioning and temperature change (10°C to 36°C). Asphalt binder AAB had the lowest bond energy, but had an increase in total work of fracture due to moisture conditioning and a low decrease in total work of fracture due to changes in temperature (10°C to 36°C).

- The aggregate substrate has a great effect on the total work of fracture. Limestone substrate performed superiorly to andesite in every test. It resulted in higher total work of fracture with changes in film thickness, resulted in lower reduction in total work of fracture due to moisture conditioning, and resulted in lower reduction in total work of fracture due to increases in temperature. However, limestone had a lower adhesive bond energy as compared to andesite.

It is believed lime from the limestone was absorbed into the asphalt binder, resulting in the increased performance.

- The results from this study were validated using a linear regression model based on Equation 21. The regression model demonstrated a strong relationship existed between bond energy and total work of fracture.

Recommendations

The work in this dissertation displayed how surface free energy changes due to different modifications and the validity of using the computed bond energy as a tool to predict the fracture energy or total work of fracture of a asphalt-aggregate combination. The testing platform developed in this research is extremely versatile in the types and geometry of specimens it can test. It is recommended to conduct more experiments in which modified asphalt binders (i.e., different PGs, anti-strip agents, short and long-term aged) or mastics are used. The use of modifications, as compared to unmodified binders, will allow one to determine the effect of binder modification on the total work of fracture. The impact of miller filler and chemically active fillers should be considered as part of the composite film. The authors suggest that the interaction of mineral filler and bitumen may impact the bond between the mastic and the aggregate surface and that the dispersion of mineral filler may toughen the mastic and impact work of fracture. Moreover, the authors recommend developing a test method to determine the effect of temperature on the surface free energy of asphalt binders.

Research is lacking in the area of understanding material interaction of asphalt binder and aggregate. It is recommended to study the interfacial properties using high resolution characterization techniques such as nano-indentation and atomic force microscopy.

REFERENCES

1.   Griffith, A.A. The Phenomena of Rupture and Flow in Solids. *Philosophical Transactions of the Royal Society of London. Series A, Containing Papers of a Mathematical or Physical Character*, Vol. 221, 1921, pp. 163-198.

2.   Schapery, R.A. Correspondence Principles and a Generalized J Integral for Large Deformation and Fracture Analysis of Viscoelastic Media. *International Journal of Fracture*, Vol. 25, No. 3, 1984, pp. 195-223.

3.   Little, D.N., Bhasin, A. and Hefer, A.W. *Using Surface Energy Measurements to Select Materials for Asphalt Pavements*. Final Report 09-37, National Cooperative Highway Research Program, Washington, DC, 2006.

4.   Masad, E., Branco, V.C. and Little, D. *Fatigue Damage: Analysis of Mastic Fatigue Damage Using Stress Controlled and Strain Controlled Test*. Report No. 473630, Texas Transportation Institute in Cooperation with Federal Highway Administration and Western Research Institute, College Station, TX, 2006.

5.   Cheng, D., *Surface Free Energy of Asphalt-Aggregate System and Performance Analysis of Asphalt Concrete Based on Surface Free Energy*. Ph.D Dissertation, Civil Engineering, Texas A&M University, College Station, TX, 2002.

6.   Huang, S.C.H.E., Branthaver, J.F. and Robertson, R.E. *Aggregate Effects on the Asphalt-Aggregate Interaction in the Presence of Water*. 8th Annual Symposium of the International Centre for Aggregate Research, Western Research Institute, Denver, CO, 2000.

7.   Labib, M. *Asphalt-Aggregate Interactions and Mechanisms for Water Stripping*. Preprint American Chemical Society Division of Fuel Chemistry, Vol. 37(3), 1992.

8.   Scott, J.A.N. Adhesion and Disbonding Mechanisms of Asphalt Used in Highway Construction and Maintenance. *Proceedings of the Association of Asphalt Paving Technologists*, Vol. 47, 1978, pp. 19-48.

9.   Yoon, H.H. and Tarrer, A.R. Effect of Aggregate Properties on Stripping. In *Transportation Research Record: Journal of the Transportation Research Board*, No. 1171, Transportation Research Board of the National Academies, Washington, D.C., 1988, pp. 37-43.

10.   Hughes, R.I., Lamb, D.R. and Pordes, O. Adhesion in Bitumen Macadam. *Journal of Applied Chemistry*, Vol. 10, 1960, pp. 433-443.

11.   van Oss, C.J. and Giese, R.F. Influence of the Ph of Water on Its Electron-Acceptivity and Donicity. *The Journal of Adhesion*, Vol. 81, No. 3, 2005, pp. 237-244.

12.   Mittal, K. Adhesion Measurement: Recent Progress, Unsolved Problems, and Prospects. *ASTM Special Technical Publication 640*, 1978, pp. 5-17.

13.   Okamatsu, T., Yasuda, Y. and Ochi, M. Thermodynamic Work of Adhesion and Peel Adhesion Energy of Dimethoxysilyl-Terminated Polypropylene Oxide/Epoxy Resin System Jointed with Polymeric Substrates. *Journal of Applied Polymer Science*, Vol. 80, No. 11, 2001, pp. 1920-1930.

14.   van Oss, C., Chaudhury, M. and Good, R. Monopolar Surfaces. *Advances in Colloid and Interface Science*, Vol. 28, 1987, pp. 35-64.

15.   Miller, C., *Adhesion and the Surface Energy Components of Natural Minerals and Aggregates*. M.S., Geology and Geophyics, Texas A&M University, College Station, TX, 2010.

16.   Bhasin, A., Masad, E., Little, D. and Lytton, R. Limits on Adhesive Bond Energy for Improved Resistance of Hot Mix Asphalt to Moisture Damage. In *Transportation Research Record: Journal of the Transportation Research Board*, No. 1970, Transportation Research Board of the National Academies, Washington, D.C., 2006, pp. 3-13.

17.   Lytton, R.L., Masad, E., Zollinger, C., Bulut, R. and Little, D. *Measurements of Surface Energy and Its Relationship with Moisture Damage*. Publication FHWA/TX-05/0-4524-2, Texas Transportation Institute, 2005.

18.   Masad, E., Zollinger, C., Bulut, R., Little, D. and Lytton, R. Characterization of Hma Moisture Damage Using Surface Energy and Fracture Properties. *Journal of the Association of Asphalt Paving Technologists*, Vol. 75, 2006, pp. 713 - 748.

19.   Orowan, E. Notch Brittleness and the Strength of Metals. *Transactions of the Institute of Engineers and Shipbuilders in Scotland*, Vol. 89, 1945, pp. 165-215.

20.   Irwin, G.R. *Handbook of Physics, Vol. 6*. Springer Verlag, Berlin, 1958.

21.   Gent, A.N. and Kinloch, A.J. Adhesion of Viscoelastic Materials to Rigid Substrates 111. Energy Criterion for Failure. *Journal of Polymer Science: Part A-2*, Vol. 9, 1971, pp. 659-669.

22. Gent, A.N. and Schultz, J. Effect of Wetting Liquids on the Strength of Adhesion of Viscoelastic Materials. *The Journal of Adhesion*, Vol. 3, No. 4, 1972, pp. 281-294.

23. Andrews, E.H. and Kinloch, A.J. Mechanics of Adhesive Failure. 11. *Proceedings of the Royal Society of London, Series A*, Vol. 332, No. 1590, 1973, pp. 401-414.

24. Xu, D.B., Hui, C.Y. and Kramer, E.J. Interface Fracture and Viscoelastic Deformation in Finite Size Specimens. *Journal of Applied Physics*, Vol. 72, No. 8, 1992, pp. 3305-3316.

25. Shull, K.R., Ahn, D., Chen, W.L., Flanigan, C.M. and Crosby, A.J. Axisymmetric Adhesion Tests of Soft Materials. *Macromolecular Chemistry and Physics*, 199, No. 4, 1998, pp. 489-511.

26. Seshadri, M., Saigal, S., Jagota, A. and Bennison, S.J. Scaling of Fracture Energy in Tensile Debonding of Viscoelastic Films. *Journal of Applied Physics*, Vol. 101, No. 9, 2007, pp. 093504-093504-8.

27. Kaelble, D.H. A Relationship between the Fracture Mechanics and Surface Energetics Failure Criteria. *Journal of Applied Polymer Science*, Vol. 18, No. 6, 1974, pp. 1869-1889.

28. Jokl, M.L., Vitek, V. and McMahon, C.J. A Microscopic Theory of Brittle Fracture in Deformable Solids: A Relation between Ideal Work to Fracture and Plastic Work. *Acta Metallurgica*, Vol. 28, 1980, pp. 1479-1488.

29. Wei, Y. and Hutchinson, J.W. Interface Strength, Work of Adhesion and Plasticity in the Peel Test. *International Journal of Fracture*, Vol. 93, No. 1, 1998, pp. 315-333.

30. Volinsky, A.A., Moody, N.R. and Gerberich, W.W. Interfacial Toughness Measurements for Thin Films on Substrates. *Acta Materialia*, Vol. 50, 2002, pp. 441-466.

31. Sharon, E., Gross, S.P. and Fineberg, J. Energy Dissipation in Dynamic Fracture. *Physical Review Letters*, Vol. 76, No. 12, 1996, pp. 2117-2120.

32. Miller, O., Freund, L.B. and Needleman, A. Energy Dissipation in Dynamic Fracture of Brittle Materials. *Modelling and Simulation in Materials Science and Engineering*, Vol. 7, No. 4, 1999, pp. 573-586.

33. Fineberg, J., Sharon, E. and Cohen, G. Crack Front Waves in Dynamic Fracture. *International Journal of Fracture*, Vol. 121, 2003, pp. 55-69.

34. Zhang, Z.J., Paulino, G.H. and Celes, W. Extrinsic Cohesive Modelling of Dynamic Fracture and Microbranching Instability in Brittle Materials. *International Journal for Numerical Methods in Engineering*, Vol. 72, No. 8, 2007, pp. 893-923.

35. Penn, L.S. and Defex, E. Relation between Work of Adhesion and Work of Fracture for Simple Interfaces. *Journal of Materials Science*, Vol. 37, 2002, pp. 505-513.

36. Zosel, A. Adhesion and Tack of Polymers: Influence of Mechanical Properties and Surface Tensions. *Colloid & Polymer Science*, Vol. 263, No. 7, 1985, pp. 541-553.

37. Kawashita, L.F., Moore, D.R. and Williams, J.G. *A Protocol for Determination of Adhesive Fracture Toughness of Flexible Laminates by Peel Testing: Mandrel Peel Method*. Imperial College, London, UK, 2005.

38. Moore, D.R. and Williams, J.G. *A Protocol for Determination of the Adhesive Fracture Toughness of Flexible Laminates by Peel Testing: Fixed Arm and T-Peel Methods*. Imperial College, London, UK, 2007.

39. Kim, J., Kim, K.S. and Kim, Y.H. Mechanical Effects in Peel Adhesion Test. *Journal of Adhesion Science and Technology*, Vol. 3, 1989, pp. 175-187.

40. Kinloch, A., Lau, C. and Williams, J. The Peeling of Flexible Laminates. *International Journal of Fracture*, Vol. 66, 1994, pp. 45-70.

41. Hadavinia, H., Kawashita, L., Kinloch, A.J., Moore, D.R. and Williams, J.G. A Numerical Analysis of the Elastic-Plastic Peel Test. *Engineering Fracture Mechanics*, Vol. 73, No. 16, 2006, pp. 2324-2335.

42. Aubrey, D.W. and Ginosatis, S. Peel Adhesion Behaviour of Carboxylic Elastomers. *The Journal of Adhesion*, Vol. 12, No. 3, 1981, pp. 189-198.

43. Charmeau, J.Y., Gerin, P.A., Vovelle, L., Schirrer, R. and Holl, Y. Adhesion of Latex Films. Part Iii. Surfactant Effects at Various Peel Rates. *Journal of Adhesion Science and Technology*, Vol. 13, No. 2, 1999, pp. 203-215.

44. Tsai, K.H. and Kim, K.S. Stick-Slip in the Thin Film Peel Test - I. The 90° Peel Test. *International Journal of Solids and Structures*, Vol. 30, No. 13, 1993, pp. 1789-1806.

45. Chuang, H.K., Chiu, C. and Paniagua, R. Avery Adhesive Test Yields More Performance Data Than Traditional Probe. *Adhesives Age*, Vol. 40, No. 10, 1997, pp. 18-23.

46. Lakrout, H., Sergot, P. and Creton, C. Direct Observation of Cavitation and Fibrillation in a Probe Tack Experiment on Model Acrylic Pressure-Sensitive-Adhesives. *The Journal of Adhesion*, Vol. 69, No. 3, 1999, pp. 307-359.

47. Shull, K.R. and Creton, C. Deformation Behavior of Thin, Compliant Layers under Tensile Loading Conditions. *Journal of Polymer Science, Part B, Polymer Physics*, Vol. 42, No. 22, 2004, pp. 4023-4043.

48. Zosel, A. Adhesive Failure and Deformation Behaviour of Polymers. *The Journal of Adhesion*, Vol. 30, No. 1, 1989, pp. 135-149.

49. Creton, C. and Lakrout, H. Micromechanics of Flat-Probe Adhesion Tests of Soft Viscoelastic Polymer Films. *Journal of Polymer Science: Part B: Polymer Physics*, Vol. 38, 2000, pp. 965-979.

50. Marek, C.R. and Herrin, M. Tensile Behavior and Failure Characteristics of Asphalt Cements in Thin Films. *Proceedings of the Association of Asphalt Paving Technologists*, 1958, pp. 386-421.

51. Vassiliev, N., Davison, R. and Glover, C. Development of a Stirred Airflow Test Procedure for Short-Term Aging of Asphaltic Materials. In *Transportation Research Record: Journal of the Transportation Research Board*, No. 1810, Transportation Research Board of the National Academies, Washington, D.C., 2002, pp. 25-32.

52. Hefer, A.W., Bhasin, A. and Little, D.N. Bitumen Surface Energy Characterization Using a Contact Angle Approach. *Journal of Materials in Civil Engineering*, Vol. 18, No. 6, 2006, pp. 759-767.

53. Bhasin, A. and Little, D.N. Characterization of Aggregate Surface Energy Using the Universal Sorption Device. *Journal of Materials in Civil Engineering*, Vol. 19, No. 8, 2007, pp. 634-641.

54. Robertson, R., Branthaver, J., Harnsberger, P., Petersen, J., Dorrence, S., McKay, J., Turner, T., Pauli, A., Huang, S. and Huh, J. *Fundamental Properties of Asphalts and Modified Asphalts, Volume I: Interpretive Report*. FHWA-RD-99-212, Western Research Institute and Federal Highway Administration, McLean, VA, 2001.

55. Petersen, J.C. and Harnsberger, P.M. Asphalt Aging: Dual Oxidation Mechanism and Its Interrelationships with Asphalt Composition and Oxidative Age Hardening. In *Transportation Research Record: Journal of the Transportation Research Board*, No. 1638, Transportation Research Board of the National Academies, Washington, D.C., 1998, pp. 47-55.

56. Lucic, S., Kovacevic, V. and Hace, D. Mechanical Properties of Adhesive Thin Films. *International Journal of Adhesion and Adhesives*, Vol. 18, No. 2, 1998, pp. 115-123.

57. Bhasin, A., Howson, J.E., Masad, E., Little, D.N. and Lytton, R.L. Effect of Modification Procceses on Bond Energy of Asphalt Binders. In *Transportation Research Record: Journal of the Transportation Research Board*, No. 1988, Transportation Research Board of the National Academies, Washington, D.C., 2007, pp. 29-37.

58. Song, B. and Springer, J. Determination of Interfacial Tension from the Profile of a Pendant Drop Using Computer-Aided Image Processing: 1. Theoretical. *Journal of Colloid and Interface Science*, Vol. 184, 1996, pp. 64-76.

59. Song, B. and Springer, J. Determination of Interfacial Tension from the Profile of a Pendant Drop Using Computer-Aided Image Processing: 2. Experimental. *Journal of Colloid and Interface Science*, Vol. 184, 1996, pp. 77-91.

60. Harvey, J.A.F. and Cebon, D. Failure Mechanisms in Viscoelastic Films. *Journal of Materials Science*, Vol. 38, No. 5, 2003, pp. 1021-1032.

61. Harvey, J.A.F. and Cebon, D. Fracture Tests on Bitumen Films. *Journal of Materials in Civil Engineering*, Vol. 17, 2005, pp. 99-107.

62. Cho, D.W., Bahia, H.U. and Kamel, N.I. Critical Evaluation of Use of the Procedure of Superpave Volumetric Mixture Design for Modified Binders. In *Transportation Research Record: Journal of the Transportation Research Board*, No. 1929, Transportation Research Board of the National Academies, Washington, D.C., 2005, pp. 114-125.

63. Kanitpong, K. and Bahia, H. Relating Adhesion and Cohesion of Asphalts to the Effect of Moisture on Laboratory Performance of Asphalt Mixtures. In *Transportation Research Record: Journal of the Transportation Research Board*, No. 1901, Transportation Research Board of the National Academies, Washington, D.C., 2005, pp. 33-43.

64. Copeland, A.R., Youtcheff, J. and Shenoy, A. Moisture Sensitivity of Modified Asphalt Binders: Factors Influencing Bond Strength. In *Transportation Research Record: Journal of the Transportation Research Board*, No. 1998, Transportation Research Board of the National Academies, Washington, D.C., 2007, pp. 18-28.

65. Bhasin, A., *Development of Methods to Quantify Bitumen-Aggregate Adhesion and Loss of Adhesion Due to Water*. PhD Dissertation, Civil Engineering, Texas A&M University, College Station, TX, 2006.

66. Hallab, N.J., Bundy, K.J., O'Connor, K., Moses, R.L. and Jacobs, J.J. Evaluation of Metallic and Polymeric Biomaterial Surface Energy and Surface Roughness Characteristics for Directed Cell Adhesion. *Tissue Engineering*, Vol. 7, No. 1, 2001, pp. 55-71.

67. Marasteanu, M.O., *Critical Evaluation of Models for the Characterization of Asphalt Cement Rheological Master Curves*. Ph.D Dissertation, Civil Engineering, Pennsylvania State University, College Park, 1995.

68. Lesueur, D. and Little, D. Effect of Hydrated Lime on Rheology, Fracture, and Aging of Bitumen. In *Transportation Research Record: Journal of the Transportation Research Board*, No. 1661, Transportation Research Board of the National Academies, Washington, D.C., 1999, pp. 93-105.

69. Little, D. and Petersen, J. Unique Effects of Hydrated Lime Filler on the Performance-Related Properties of Asphalt Cements: Physical and Chemical Interactions Revisited. *Journal of Materials in Civil Engineering*, Vol. 17, No. 2, 2005, pp. 207-218.

70. Little, D. and Epps, J. *The Benefits of Hydrated Lime in Hot Mix Asphalt*. Prepared for National Lime Association, College Station, TX, 2001.

71. Hoffman, P., van Veldhuizen, M., Noor, H. and Smits, R., *Hydroxide in Filler*. Netherlands Pavement Consultants, Utrecht, Netherlands, 1998.

72. Ferry, J.D. *Viscoelastic Properties of Polymers*. John Wiley & Sons Inc., New York, 1980.

VITA

Jonathan Embrey Howson, E.I.T.

Permanent Address:
CE/TTI Bldg. Room 503B
3135 TAMU
College Station, TX 77843-3135

EDUCATION

Ph.D., Civil Engineering, Texas A&M University, August 2011
Materials and Pavements Engineering Emphasis

M.E., Civil Engineering, Texas A&M University, December 2007
Materials and Pavements Engineering Emphasis

B.S., Civil Engineering, Texas A&M University, May 2005
General Emphasis

WORK HISTORY

2011-   Senior Research Associate
               Texas Transportation Institute, College Station, TX

2010-2011   Teaching Assistant
               Texas A&M University, College Station, TX

2010-2010   Graduate Research Assistant
               Texas A&M University at Qatar, Doha, Qatar

2005-2010   Graduate Research Assistant
               Texas Transportation Institute, College Station, TX

2004-2005   Undergraduate Assistant
               Texas Transportation Institute, College Station, TX

2004-2004   Materials Engineering Internship
               Texas A&M University, College Station, TX